Quickbird Satellite in-orbit Modulation Transfer Function (MTF) Measurement Using Edge, Pulse and Impulse Methods for Summer 2003

By

Dennis Helder, Taeyoung Choi, Manjunath Rangaswamy

Electrical Engineering and Computer Science Department

South Dakota State University

August, 2005

Quickbird Satellite in-orbit Modulation Transfer Function (MTF) Measurement Using Edge, Pulse and Impulse Methods for Summer 2003

By

Dennis Helder, Taeyoung Choi, Manjunath Rangaswamy

Electrical Engineering and Computer Science Department

South Dakota State University

August, 2005

Table of Contents

List of Tables

List of Figures

1. Introduction

The spatial characteristics of an imaging system cannot be expressed by a single number or simple statement. However, the Modulation Transfer Function (MTF) is one approach to measure the spatial quality of an imaging system. Basically, MTF is the normalized spatial frequency response of an imaging system.

The frequency response of the system can be evaluated by applying an impulse input. The resulting impulse response is termed the Point Spread function (PSF). This function is a measure of the amount of blurring present in the imaging system and is itself a useful measure of spatial quality. An underlying assumption is that the imaging system is linear and shift-independent. The Fourier transform of the PSF is called the Optical Transfer Function (OTF) and the normalized magnitude of the OTF is the MTF.

In addition to using an impulse input, a knife-edge in technique has also been used in this project. The sharp edge exercises an imaging system at all spatial frequencies. The profile of an edge response from an imaging system is called an Edge Spread Function (ESF). Differentiation of the ESF results in a one-dimensional version of the Point Spread

Function (PSF). Finally, MTF can be calculated through use of Fourier transform of the PSF as stated previously.

Every image includes noise in some degree which makes MTF of PSF estimation more difficult. To avoid the noise effects, many MTF estimation approaches use smooth numerical models. Historically, Gaussian models [1] and Fermi functions [2] were applied to reduce the random noise in the output profiles.

The pulse-input method was used to measure the MTF of the Landsat Thematic Mapper (TM) [3] using 8^{th} order even functions over the San Mateo Bridge in San Francisco, California. Because the bridge width was smaller than the 30-meter ground sample distance (GSD) of the TM, the Nyquist frequency was located before the first zero-crossing point of the sinc function from the Fourier transformation of the bridge pulse. To avoid the zero-crossing points in the frequency domain from a pulse, the pulse width should be less than the width of two pixels (or 2 GSD's), but the short extent of the pulse results in a poor signal-to-noise ratio. Similarly, for a high-resolution satellite imaging system such as Quickbird, the input pulse width was critical because of the zero crossing points and noise present in the background area. It is important, therefore, that the width

of the input pulse be appropriately sized. Finally, the MTF was calculated by taking ratio between Fourier transform of output and Fourier transform of input.

Regardless of whether the edge, pulse and impulse target method is used, the orientation of the targets is critical in order to obtain uniformly spaced sub-pixel data points. When the orientation is incorrect, sample data points tend to be located in clusters that result in poor reconstruction of the edge or pulse profiles. Thus, a compromise orientation must be selected so that all spectral bands can be accommodated.

This report continues by outlining the objectives in Section 2, procedures followed in Section 3, descriptions of the field campaigns in Section 4, results in Section 5, and a brief summary in Section 6.

2. Objectives

The NASA Science Data Purchase (SDP) specifies the spatial quality of Quickbird imagery by placing a lower bound on the MTF at the Nyquist frequency. Spatial quality associated with the panchromatic band should produce an MTF of at least 0.09 at the Nyquist frequency. Also, the multispectral bands should have an MTF of at least 0.20 at Nyquist.

This work has concentrated on measuring the value at Nyquist frequency according to the specification. In addition, spatial domain analysis was also performed using Full-Width at Half-Maximum (FWHM) values from the estimated point spread functions. FWHM is suggested as a spatial domain figure of merit. Lastly, MTF values at Nyquist measured previously in 2002 were compared to values obtain from 2003 estimates contained in this report, to detect possible temporal changes.

3. Experimental Procedures

3.1. Basics Concepts of MTF Estimators

A newly developed impulse method algorithm was applied on 2002 and 2004 IKONOS and QuickBird imagery. A set of 20 convex mirrors was developed as a phased array to obtain an over-sampled data set of a point source. By fitting a two-dimensional Gaussian model to the data from each mirror, locations of each point source can be determined as accurately as 0.05 GSD. Once the mirror locations are determined, data grids from the mirrors are aligned using the estimated peak locations as a common origin. Then, a Gaussian model is applied to the accumulated data points to calculate a final two-dimensional PSF estimate. In Figure 3.1, a Fourier Transform is applied to the PSF and normalized to obtain the corresponding MTF in the 'x' and

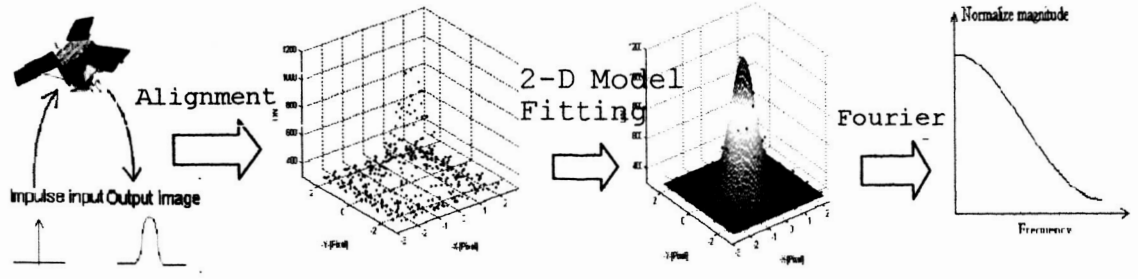

Figure 3.1 Impulse method procedures

'y' directions. One significant advantage of this method is that it can potentially provide a full two-dimensional estimate of the PSF.

The edge method was applied using a sharp edge target--the NASA Stennis tarps. Procedures for PSF/MTF estimation include edge detection, sub-pixel interpolation of the detected edge profiles to obtain the over-sampled Edge Spread Function (ESF), differentiation of the ESF to obtain the 1-D PSF, discrete Fourier transformation of the PSF to obtain the Optical Transfer Function (OTF), and normalization of the OTF magnitude by the DC component value to calculate the MTF. The procedure flow is illustrated in Figure 3.2.

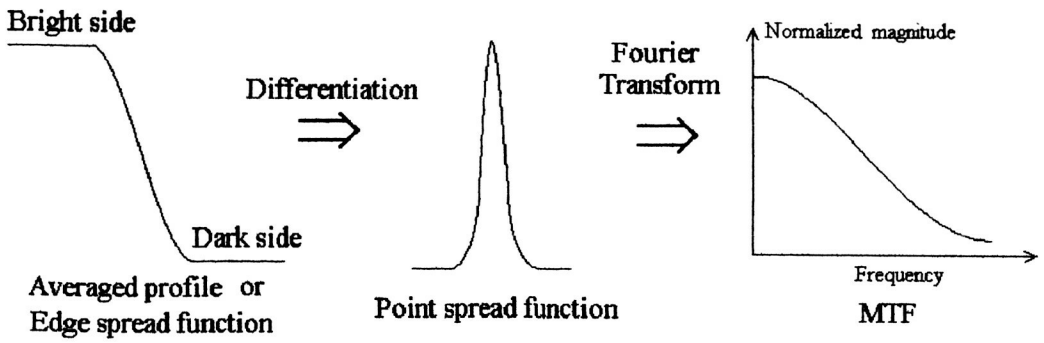

Figure 3.2. Edge method procedures.

The pulse method, typically applied to multispectral band data due to its lower spatial resolution, uses slightly different steps to obtain the MTF. The edge detection and interpolation steps applied to a pulse target are identical to the edge method. Instead of the ESF as in the edge method, the interpolated data produce the system's pulse response function (PRF). Finally, the MTF is calculated as a ratio of the Fourier transform of the PRF to an ideal rectangular pulse whose width is the same as the ground-based the pulse target as shown in Figure 3.3.

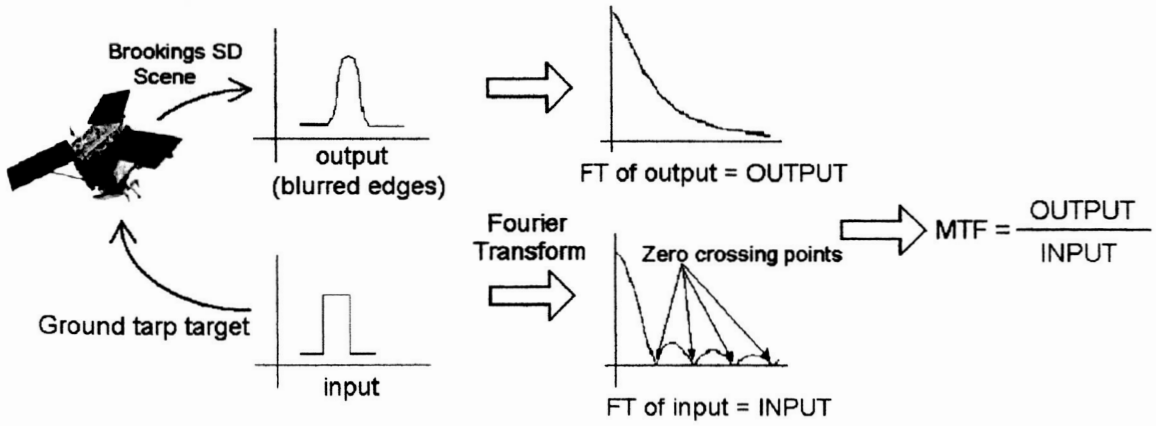

Figure 3.3. Pulse method.

3.2. Impulse Method

3.2.1. Peak Position Estimation and Alignment

For a set of point source data, the estimated mean position, and standard deviation in the cross-track and

along-track directions, along with the peak pixel value, are given as initial values to the MATLAB function 'fminsearch'. According to MATLAB documentation, "fminsearch finds the minimum of a scalar function of several variables, starting at an initial estimate. This is generally referred to as unconstrained nonlinear optimization" [4]. Successful use of the 'fminsearch' function requires initial estimates of mean and standard deviation in cross-track and along-track directions, peak DN value, and bias to be approximately equal to their respective true values. The initial peak value was chosen as the DN value of the brightest pixel of each individual mirror image. The initial peak location in the cross-track was the pixel location of the brightest pixel in the X direction in that image. The initial cross-track standard deviation was visually estimated from the data. The initial peak location and standard deviation in the along-track direction were similarly approximated. The bias was approximated by averaging the uniform region around the mirror data. These parameters along with a reference to the function to be minimized were passed into 'fminsearch', which returned the estimated model parameters for a two-dimensional Gaussian curve.

3.2.2. Alignment of Point Sources and Least Square Error Gaussian Surface

Once model estimates of peak location are obtained from all of the available point source data sets, the point source data sets were aligned such that the estimated model peak locations occurred at (0,0) as shown in the example two-dimensional plot of Figure 3.4. In this example, the data sets were noiseless and were limited to a 3x3 window.

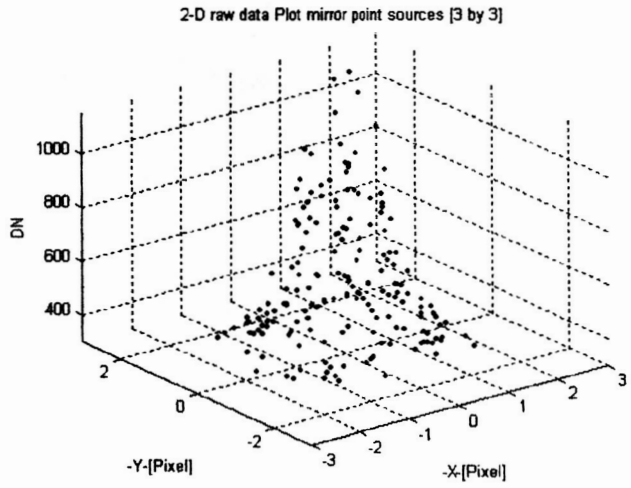

Figure 3.4 An example of aligned point source data.

To the aligned point source data, a least square error two-dimensional Gaussian model was fitted as shown in the example of Figure 3.5(a). Again, the MATLAB function fminsearch, described in Section 3.2.1, was used to fit the

model. The model was initially estimated from the data points within a 3x3 window; the model was later extended to include data within a 5x5 window in order to obtain a wider representation of the Gaussian surface, as shown in Figure 3.5 (a). The data in the extended area from 3x3 to 5x5 window was effectively a 'bias' that was not used in the calculation of model parameters. The resulting Gaussian surface is the estimated two-dimensional PSF of the point source data and the parameters (x-mean, y-mean, x-stdev, y-stdev) are the estimated model parameters. Figure 3.5 (b) represents the 1-D PSF obtained by slicing through the peak of 2-D PSF in the cross-track (X) direction and similarly, Figure 3.9 (c) represents the sliced 1-D PSF in the along-track (Y) direction. These plots give a better view of the model fit to the data.

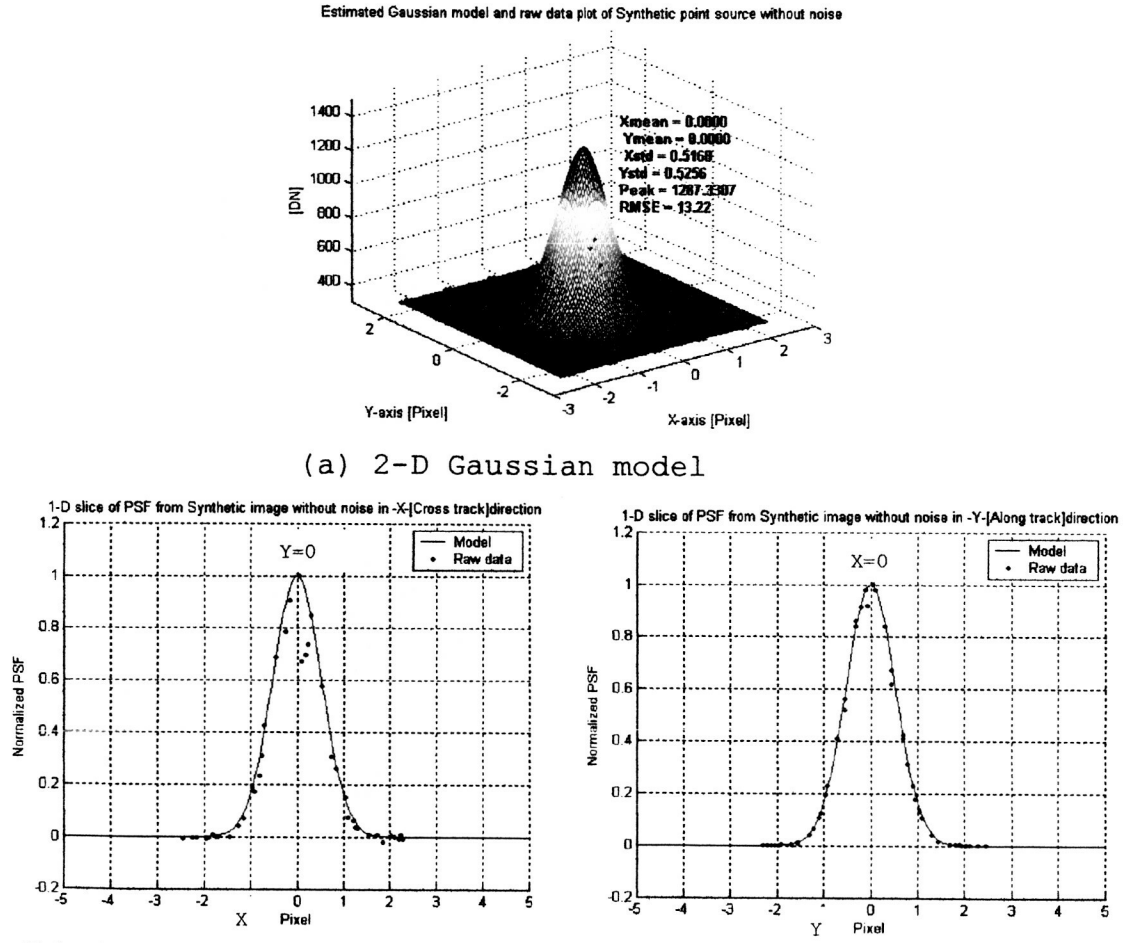

(a) 2-D Gaussian model

(b) 1-D slice in X direction (c) 1-D slice in Y direction

Figure 3.5 Estimated model PSF of synthetic point source.

3.2.3. FWHM and MTF Calculations

To obtain an estimate for the overall FWHM, the two-dimensional PSF was sliced into 1-D PSFs through the peak in the cross- and along-track directions. Each 1-D PSF slice was then normalized such that the peak value is 1.0. The

FWHM value can be calculated by measuring the width of the PSF model at an amplitude of 0.5.

Finally, Fourier transformation was applied to the sliced 1-D PSF in the cross-track direction. The resulting transfer function was then normalized by the DC term to obtain the cross-track MTF. Similarly, along-track MTF was obtained from the sliced 1-D PSF in the along-track direction.

3.3. Edge and Pulse Method

3.3.1. Edge Detection

Edge detection is one of the most crucial steps in the edge and pulse MTF estimation methods. The initial MTF research at South Dakota State University (SDSU) implemented edge detection as a simple polynomial fitting process; however, target angle estimation error was ±0.2 degrees as shown in the previous generic sensor modeling report [5]. As a worst case, the angle error lowered the MTF value at Nyquist about 0.08 from the true value. As a solution of the angle estimation problem, a parametric edge detection method based on Fermi functions was developed and implemented. Initial MTF estimates of edge targets using

the non-parametric edge detection method did not seem to account for asymmetric overshoots and undershoots observed in the edge response. The overall ESF was observed to be similar in appearance to the standard Fermi function [2]

$$f(x) = \frac{a}{\exp\left[\frac{(x-b)}{c} - 1\right]} + d \qquad (3.1)$$

In Equation 3.1, the parameter 'a' is a scale factor, 'b' is the symmetry point (corresponding to the edge location), 'c' represents the transition rate (essentially the 'slope' of the edge transition), and 'd' is a bias level. Using the MATLAB fminsearch function, sub-pixel edge locations were calculated for each profile by finding parameters with minimum squared error. The critical value for accurate edge detection was found to be the symmetry point 'b'.

Most ESF's with MTF Compensation (IKONOS imagery) observed in practice have not been found to be well behaved around the edge inflection point due to the asymmetric undershoots and overshoots in response. A summation of Fermi functions resulted in a better approximation of the ESF than

the previous cubic polynomial fitting technique reducing the error level from 1.5 degree to 0.2 degree.

3.3.2. Modified Savitzky-Golay (MSG) Interpolation

As discussed in the previous sensor modeling report [5], sliding-window interpolation tended to produce improved MTF estimates from the non-uniformly sampled edge data as compared to straight cubic spline interpolation. The resulting MTF estimates were still found to be too low, however, most likely due to the first order fit. The concept behind Savitzky-Golay filtering appeared to be very similar to the sliding-window method, but used higher-order polynomial fitting. Unfortunately, the initial detected edge locations were not uniformly distributed, as the Savitzky-Golay method traditionally requires. Using the initial concept, modifications to the traditional Savitzky-Golay filtering process were developed and implemented that would account for the non-uniformly distributed data. The MATLAB function 'fminsearch' was used to fit a quadratic function to the data points within the moving window, as shown in Figure 3.6(a) (the fit is represented by the black line within the light blue area of the window). The 4th

order polynomial was evaluated at the midpoint of the window width to obtain the output value. As with the sliding-window method, the window was then shifted 0.05 pixels to the right (Figure 3.6(b)), and a new model was fitted to the data points within the new window location. The process was repeated across the profile. Finally, an overall profile was obtained from the evaluated points at each sub-pixel location.

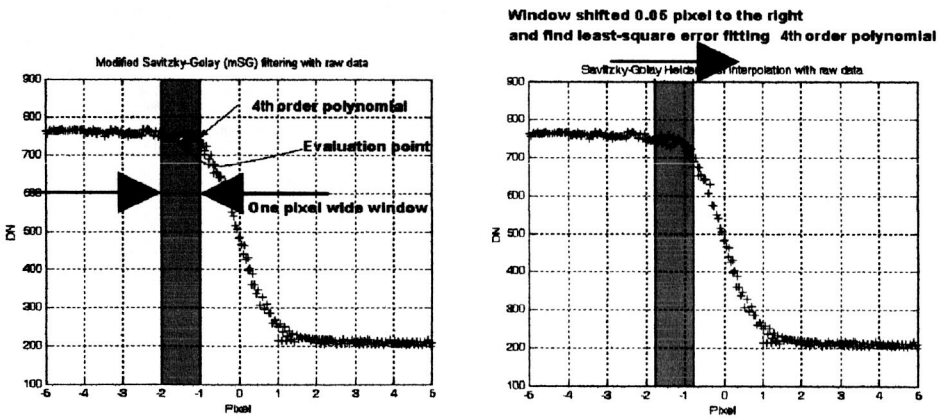

(a) 4th Order Fit **(b) Sliding Window**

Figure 3.6. Modified Savitzky-Golay (mSG) filtering with 1-pixel window and 4th order Polynomial Fitting.

3.3.3. Edge Method MTF Calculation

Once an interpolated ESF profile was obtained, it was numerically differentiated to obtain the Line Spread Function (LSF). As with the differentiation used in the edge detection step, the derivative was approximated by a simple difference between adjacent ESF values:

$$LSF(n) \approx ESF(n) - ESF(n+1) \tag{3.2}$$

Since differentiation is a high-pass filtering operation, edges and high-frequency noise components are amplified, resulting in a decreased signal-to-noise-ratio (SNR). To preserve the SNR of the original edge data, a smoothing filter should be applied to the ESF after the differentiation without damping high frequency components. In [6], for example, smoothing was implemented through convolution of the ESF with a box-car filter. Unfortunately, smoothing tends to degrade the resulting MTF estimate due to the attenuation of the high frequency components and blurring of edges. This difficulty was addressed in the process developed at SDSU by applying a standard 4th-order Savitzky-Golay filter to the LSF profile. Application of

the standard filter was possible because the LSF was obtained from a uniformly sampled ESF profile generated from the previous MSG interpolation step.

The LSF profile was trimmed to reduce the noise present in the uniform areas adjacent to the edge. Both end points were carefully selected to minimize frequency leakage effects due to DN differences between the end points. In all cases, the length of the trimmed LSF was 200 sub-pixel points or 10 full pixels.

A discrete Fourier transform was applied to the trimmed LSF to obtain an estimate of the OTF. The MTF was then obtained from normalizing the OTF magnitude by the magnitude of the DC component. The Nyquist frequency by definition is 0.5 cycles/pixel; its location was calculated from the length of the initial data vector, N, and the interpolated sub-pixel resolution.

3.3.4. Pulse Method MTF Calculation

The same modified Savitzky-Golay filtering techniques used in the edge method were applied in the pulse method. In the edge detection step, the left edges of the SDSU pulse target were used because they were carefully aligned with a

transit. The PRF profile was also trimmed to a 10-pixel-wide window to reduce noise in the areas adjacent to the pulse. Then the Fourier transform was applied to both the input and output pulse data. The MTF was calculated from the normalized ratio of the output transform magnitude to the input transform magnitude. Again, the normalization was performed relative to the magnitude of the DC component.

3.3.5. SNR

SNR is commonly defined as the ratio of the mean value of a signal to its standard deviation:

$$SNR = \frac{\mu}{\sigma} \qquad (2.3)$$

SNR has been found to be a critical factor for accurate PSF and MTF estimation [5]. As presented in this report, SNR for edge and pulse profiles was calculated as shown in Figures 3.7(a) and (b). With edge profiles, the mean value was defined as the difference between the mean DN value of the bright and dark areas; the overall standard deviation was defined as the average standard deviation of the bright and dark areas (excluding the edge transition region). With pulse and impulse profiles, the mean signal value was defined as the difference between the peak DN value and the

mean background DN value; the overall standard deviation was defined as the standard deviation of the background area (excluding the pulse or impulse).

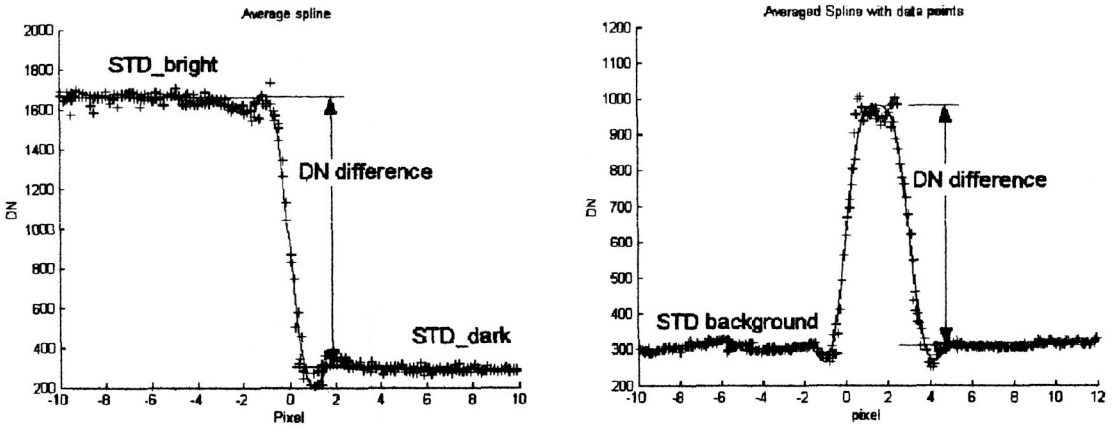

(a) Edge target (b) Pulse and Impulse target

Figure 3.7. Signal-to-Noise ratio for edge, pulse and impulse targets

4. Field Campaign

4.1. Tarp Site

The target site is a large open grassy area that is relatively flat located next to the 3M plant in Brookings, SD. This 150m by 250m target site has been maintained jointly by SDSU and 3M, and is oriented at an angle 6 degrees east of true North. All the targets, i.e, edge, pulse, and point source targets were deployed as shown in the diagram of Figure 4.1 within this target area.

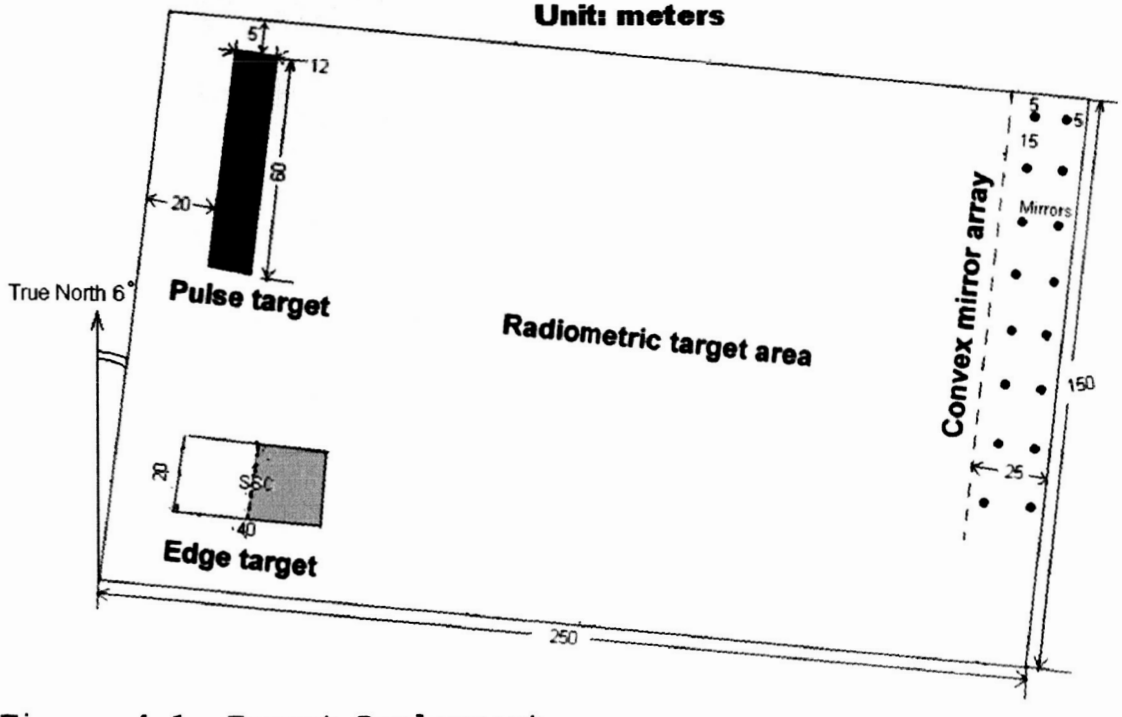

Figure 4.1. Target Deployment.

4.2. Blue Tarp Target

On each collection day, six blue tarps were laid out in a 2 by 3 pattern covering an area of 9m by 60m. The 60m length extended from North to South as shown in Figure 4.2. Tarp 1 and tarp 2 (T1 and T2 in Figure 4.2) were selected as reference tarps. To obtain 6° target angle referenced from the image (true north) grid, targets were aligned by transit at an angle of 8° east from magnetic north to get as straight an edge as possible. In addition, all seams were aligned by transit to maintain straight edges. The tarp angle was critical to obtain uniformly distributed sub-pixel edge locations.

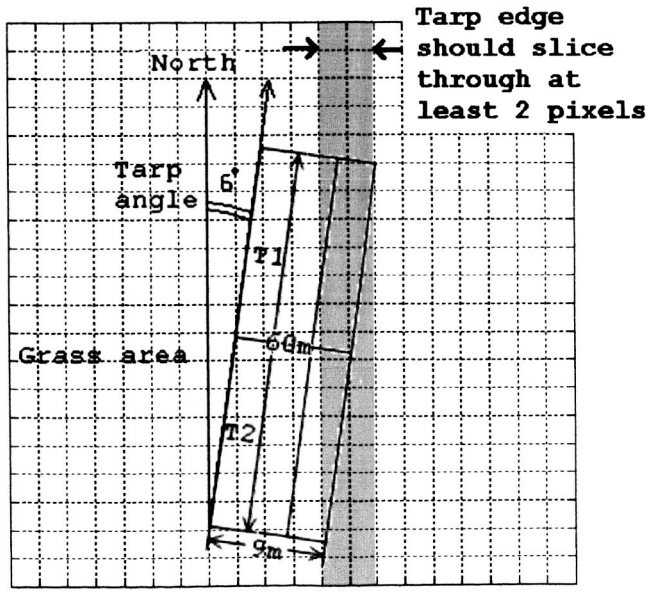

Figure 4.2. Blue tarp target layout.

A hypothetical edge spread function (ESF) is shown in Figure 4.3. In the figure, the right side is the tarp region and the left side is grass. All pixel-sampling points are shown dotted on angled grids. The dashed lines indicate the phasing of the pixel sampling locations as the knife-edge location changes with each row of pixels. The horizontal axis is scaled in units of pixels, which corresponds to one GSD in the output image. The vertical axis, in units of digital numbers (DN), represents the value at each pixel

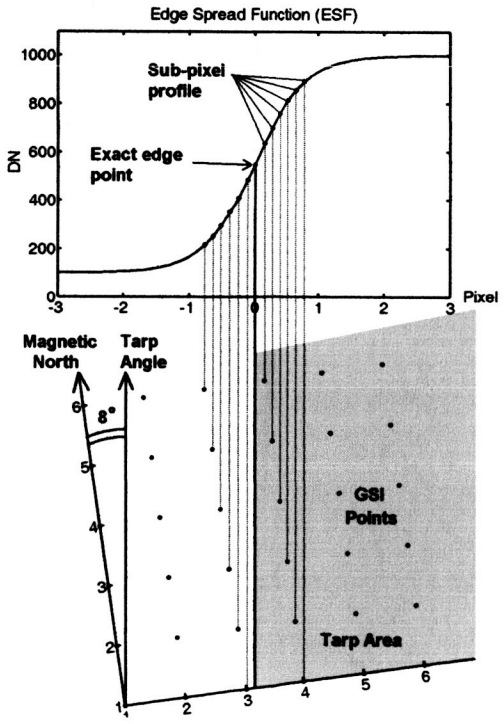

Figure 4.3. Edge Spread Function (ESF) projection from angled Ground Sample Interval (GSI) point.

location. The output edge function is then sampled at sub-pixel resolution. As the orientation of the angle changes, the resolution varies also, becoming either coarser or finer. Optimal angles exist that place the sub-pixel sample locations on a uniform grid.

4.3. Stennis Tarp Target

The Stennis MTL target consists of a series of 9 panels—one set of four 5m by 20m black canvas panels with a known reflectance of 3.6%, one set of four 5m by 20m white canvas panels with a known reflectance of 52.1%, and a transition panel with both black and white strips. Each panel was covered with an acrylic-silicone pigment to provide a radiometrically flat response between 420 nm and 1050 nm. An example deployment at the Brookings site is shown in Figure 4.4. This target was only available on September 15, 2003. The view is along the transition panel seam looking to the south.

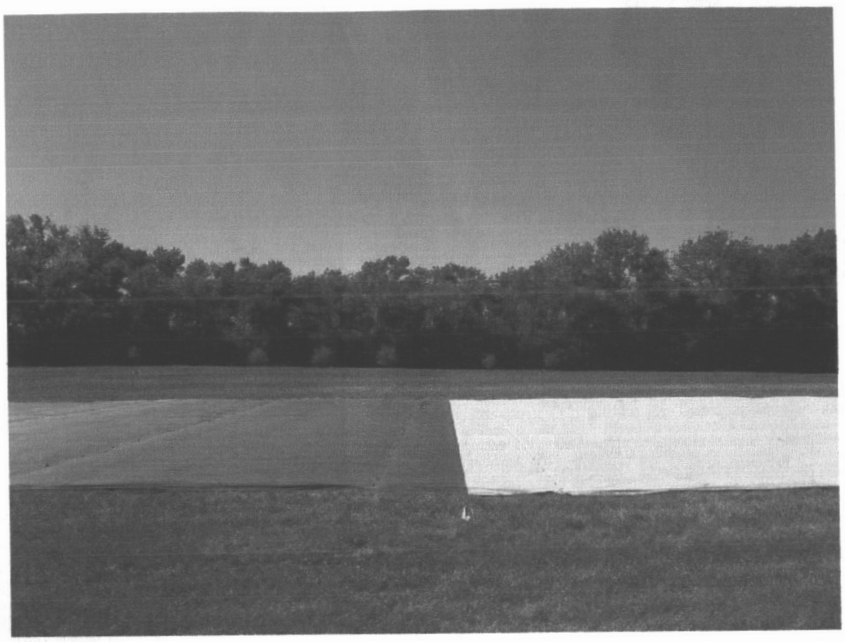

Figure 4.4. Stennis tarp target on a uniform grass area on September 15, 2003.

4.4. Impulse Target

A set of twenty convex mirrors was placed in two columns (10 mirrors in each column) at the northeast end of the target site in a uniform grassy area. Twenty mirrors were chosen in order to have enough data points to reconstruct the PSF. Cost of mirrors and site space were the main constraints for using 20 mirrors. The physical layout of the mirror placement is as shown in Figure 4.5. Mirror 1 of the first column of convex mirrors was placed at a distance of 5 meters from the east edge of the target site.

The corresponding row was inclined at a calculated angle of 10° from south towards west. The subsequent nine mirrors of the first column were spaced at a uniform distance of 8.67 meters and inclined along the same 10° angle. Similarly, a second column of ten convex mirrors were placed 8 meters from the first column. The angle (10°) and distance (8.67 meters) between the mirrors were calculated so as to obtain the desired uniform distribution of mirror samples over one pixel.

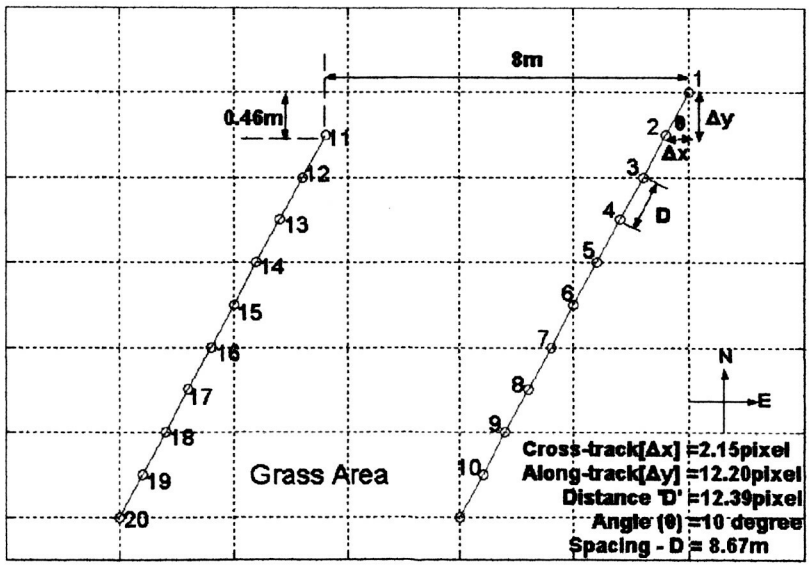

Figure 4.5. Physical layout of Convex Mirror Array.

5. Results

5.1. Scene Information

In 2003, there were three field campaigns: August 23, September 13, and October 21. On each collection date image products with two different types of resampling were available: cubic convolution (CC) and MTF interpolation. In addition, an orthorectified and full scene product with CC resampling was obtained from the August 23 overpass; but those scenes were ordered to perform geometry analysis. Table 5.1 shows the processing information for the 2003 Quickbird images used in this analysis.

Table 5.1. 2003 QuickBird image information.

Acquisition Date	Order number	Resampling Kernel & (Note)
8/23/2003	88500	CC
	88508	CC (orthorectified)
	75234	MTF (full)
9/15/2003	88502	CC
	76412	MTF
10/21/2003	83586	CC
	104274	MTF

5.2. Visual Differences Between CC and MTF Resampled Products

As shown in Table 5.1, Digital Globe provided CC and MTF resampling interpolation options. Figures 5.1(a) and (b) show the September 15 Quickbird images of the Stennis target processed with CC and MTF interpolation. The images in Figure 5.1(b) with MTF interpolation exhibit sharper edges with evident noise components in the grass area as compared to the corresponding CC image in Figure 5.1(a); this is to be expected, given that MTF interpolation is expected to provide more of a high-pass filtering emphasis. Edges in the CC resampled image of Figures 5.1(a) appear smoother than the corresponding edges in the MTF resampled images in Figures 5.1(b), especially in the transition region between the white and black panels.

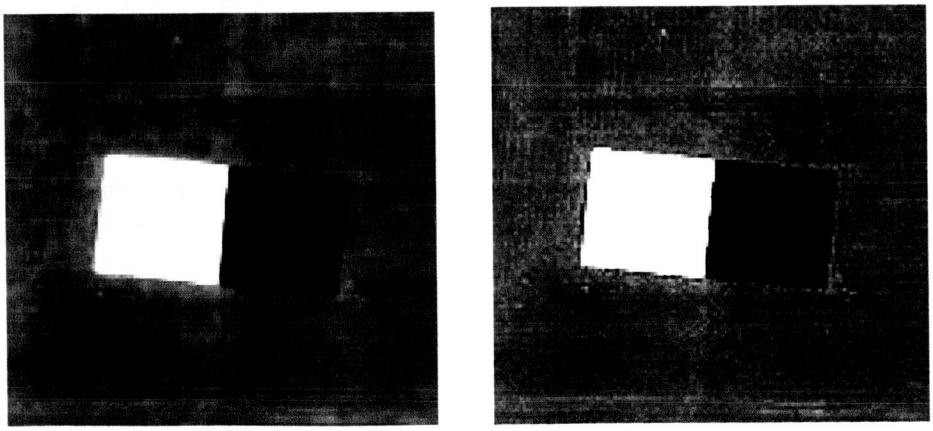

(a) CC interpolation (b) MTF interpolation

Figure 5.1. Stennis tarp target of Quickbird images on September 15, 2003.

5.3. Quickbird Panchromatic Band MTF Results from Edge Target

As stated previously, there was a total of three Quickbird overpasses of the Brookings test site during the 2003 season. The Stennis MTL target was available only on the September 15, 2003 overpass. Table 5.2 and the overplots in Figures 5.2(a) and (b) show the results obtained from applying the edge method to the September 15, 2003 images. The difference between the CC and MTF interpolation methods is apparent in the MTF overplot of Figure 5.2(b); the MTF resampled scene exhibits a significant enhancement in system frequency response, with MTF estimates at Nyquist at least three times greater than the estimates obtained from the CC resampled scenes.

Table 5.2. Panchromatic band results from Stennis tarp

Date	Interpolation method	FWHM	SNR	MTF
9/15/2003	CC	1.3943	110.4	0.1511
9/15/2003	MTF	1.0348	57.2	0.4746

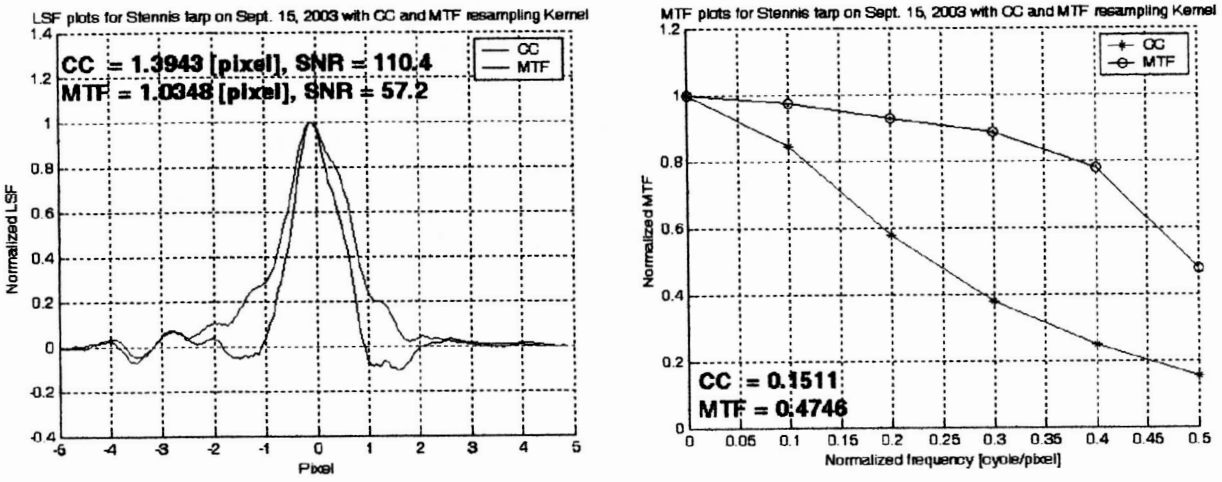

(a) LSF overplot (b) MTF overplot

Figure 5.2. Stennis tarp target of Quickbird images on September 15, 2003.

Overall, the edge method analysis of the Stennis target provided reliable estimates, as indicated by the SNR value of 110 (SNR greater than 100 is desired) with the CC interpolation method. The MTF values at Nyquist met the minimum SDP specification of 0.09 for the panchromatic band with CC resampling.

5.4. GSD Change of 2003 Quickbird Images Versus Nyquist Stability

During the year 2002, all the collections were processed by Digital Globe to have a 0.7 meter GSD in the panchromatic band and a 2.8 meter GSD in the multispectral bands. In 2003, all Quickbird data was resampled to a 2.4

meter multispectral GSD. The pulse target was designed and deployed based on 2.8-meter multispectral band GSD. But when it comes to the pulse method, the pulse width value compared to the GSD becomes critical. When the pulse width is divided by the multispectral band GSD, the result is unit of pixels. The blue tarp width was 8.83 meters, leading to 3.15 pixels with a 2.8 m GSD or 3.68 pixels with a 2.4 m GSD. Because of this GSD change from 2.8 m to 2.4 m in 2003, the Nyquist frequency point moved closer to the second zero-crossing point. As a result, estimates of the most critical Nyquist frequency point became unstable due to its close proximity to the second zero-crossing point as shown in Figure 5.3. This GSD change became an important problem when estimated MTF plots were compared from 2002 and 2003.

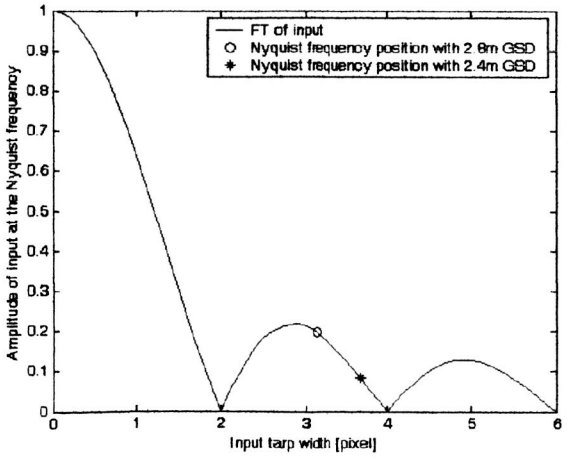

Figure 5.3. Nyquist frequency position on the input sinc function based on tarp width.

5.5. Quickbird Multispectral Bands MTF Results

As discussed in the previous section, the GSD of the pulse target used for year 2002 was 2.8 meters compared to the 2.4 meter GSD for year 2003 scenes. Since the width of 8.83 meters was optimized for a 2.8 meter GSD, the sudden change of GSD to 2.4 meters caused instability of the MTF estimation; additional details on the physical dimensions and pulse method processing plots of this layout are given in Appendix A. Table 5.3 and Figures 5.9(a) and (b) present the results obtained from an analysis of blue band images of the target for the three collects of 2003. The blue band was chosen because it exhibited the largest SNR estimates of all the multispectral bands.

Table 5.3. 2003 Quickbird blue band results

Date	Interpolation method	PRF FWHM	SNR	MTF
8/23/2003	CC	3.6432	73.8	0.3660
	MTF	3.5471	61.1	0.6670
9/15/2003	CC	3.6624	75.1	0.2866
	MTF	3.6076	72.1	0.4229
10/21/2003	CC	3.6862	70.6	0.2244
	MTF	3.6902	62.5	0.2763

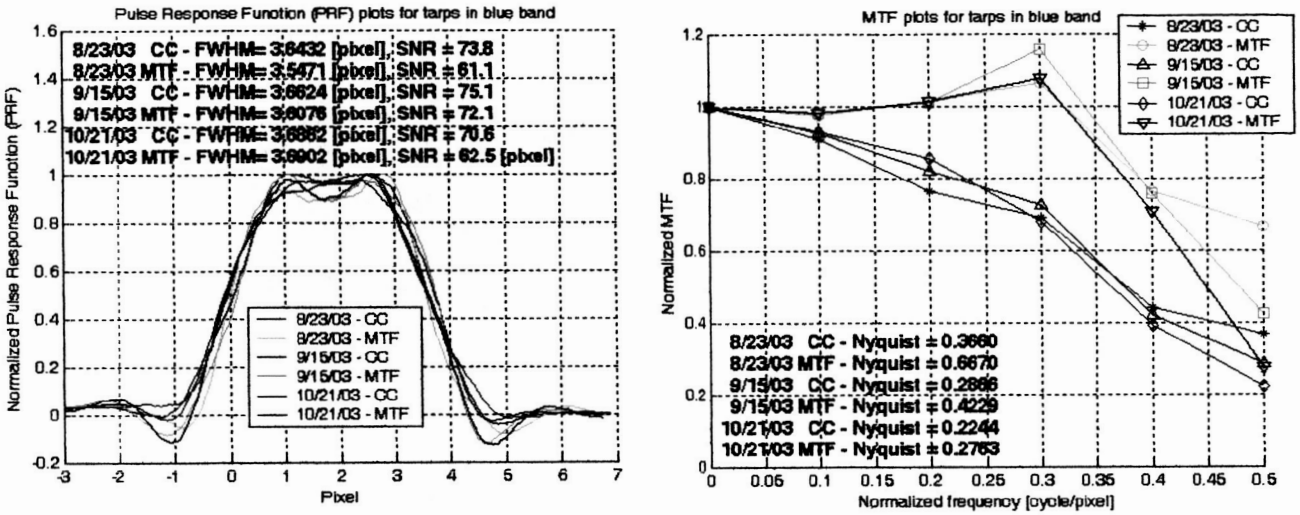

(a) PRF overplot (b) MTF overplot

Figure 5.4. PRF and MTF overplots for the blue tarp target in the blue multispectral band.

As expected, the CC interpolation method produced smoother pulse response function (PRF) profiles than with the MTF interpolation PRF in Figure 5.4(a). Even more, the PRF from MTF interpolation shows over and under shoots along both sides of the pulse, as well as ringing with the pulse. Consequently, the sharper edge transition resulted in larger MTF values at the Nyquist frequency in Table 5.3, and higher MTF in general at all frequencies as shown in the overplot of Figure 5.4(b). The scenes processed with CC resampling consistently yielded MTF estimates of around 0.3 and the scenes processed with MTF resampling yielded MTF estimates approximately twice those of the CC resampled scenes. Due

to lower SNR and the resampling of the data to 2.4m, MTF at Nyquist estimates for the MTF resampled images show poor repeatability. Also, MTF resampling produced abnormally high system frequency response at the 0.3 cycle/pixel point. This is expected due to the normal nature of this type of resampling. The accompanying generic sensor modeling report discusses this problem, and suggests it may possibly be caused by ground measurement errors on pulse width and the input step pulse parameter fed into the Matlab program.

The results of green and NIR bands are shown in the following tables and figures. Detailed processing plots are included in Appendix B. The results from the red band were not considered in this analysis.

Table 5.4. 2003 Quickbird green band results

Date	Interpolation method	PRF FWHM	SNR	MTF
8/23/2003	CC	3.6430	33.5	0.3350
	MTF	3.5811	24.1	0.6147
9/15/2003	CC	3.6766	31.5	0.2765
	MTF	3.6270	29.2	0.4036
10/21/2003	CC	3.7000	34.4	0.2231
	MTF	3.7485	29.1	0.2859

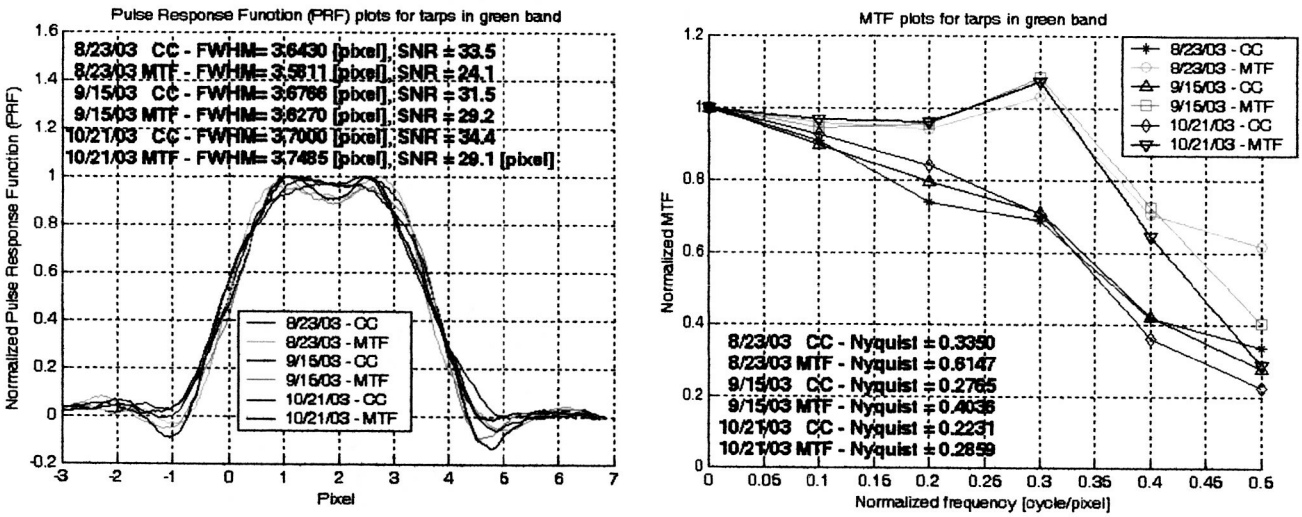

(a) PRF overplot

(b) MTF overplot

Figure 5.5. PRF and MTF overplots for blue tarp target in green band.

Table 5.5. 2003 Quickbird NIR band results

Date	Interpolation method	PRF FWHM	SNR	MTF
8/23/2003	CC	3.6806	14.8	0.2415
	MTF	3.6034	14.3	0.4850
9/15/2003	CC	3.7121	19.9	0.2384
	MTF	3.6499	18.6	0.3688
10/21/2003	CC	3.8290	15.0	0.1067
	MTF	3.8408	15.8	0.1583

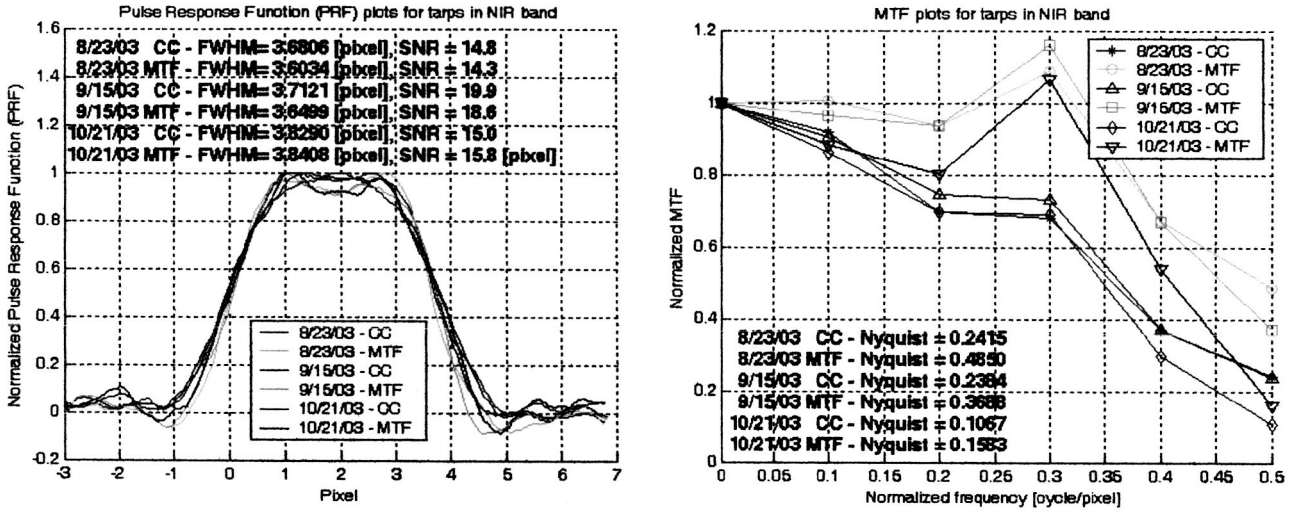

(a) PRF overplot (b) MTF overplot

Figure 5.6. PRF and MTF overplots for blue tarp target in NIR band.

5.6. Comparisons Between 2002 and 2003 Results

5.6.1. Panchromatic Band Comparison

During the summer of 2002, the Stennis tarp target was deployed on July 20, August 25, and September 7. Only CC interpolated scenes were analyzed in this comparison because of MTFC interpolated data sets produced unstable results due to the high pass filtering nature of this resampling kernel. Table 5.6 and the overplots in Figures 5.7(a) and (b) show

the results obtained from applying the edge method to the three 2002 scenes and one 2003 scene in pixel units. Even though the FWHM from the 2003 data is smaller than 2002 values, the MTF plot profile was lower, especially from 0.2 to 0.4 frequencies, as shown in Figure 5.7 (b).

Table 5.6. 2002 and 2003 panchromatic band result comparison with Stennis tarp target

Date	Interpolation method	FWHM [Pixel]	SNR	MTF [Cycle/Pixel]
7/20/02	CC	1.4560	100.1	0.1599
8/25/02	CC	1.4355	100.5	0.1639
9/7/02	CC	1.4523	141.3	0.1824
9/15/2003	CC	1.3943	110.4	0.1511

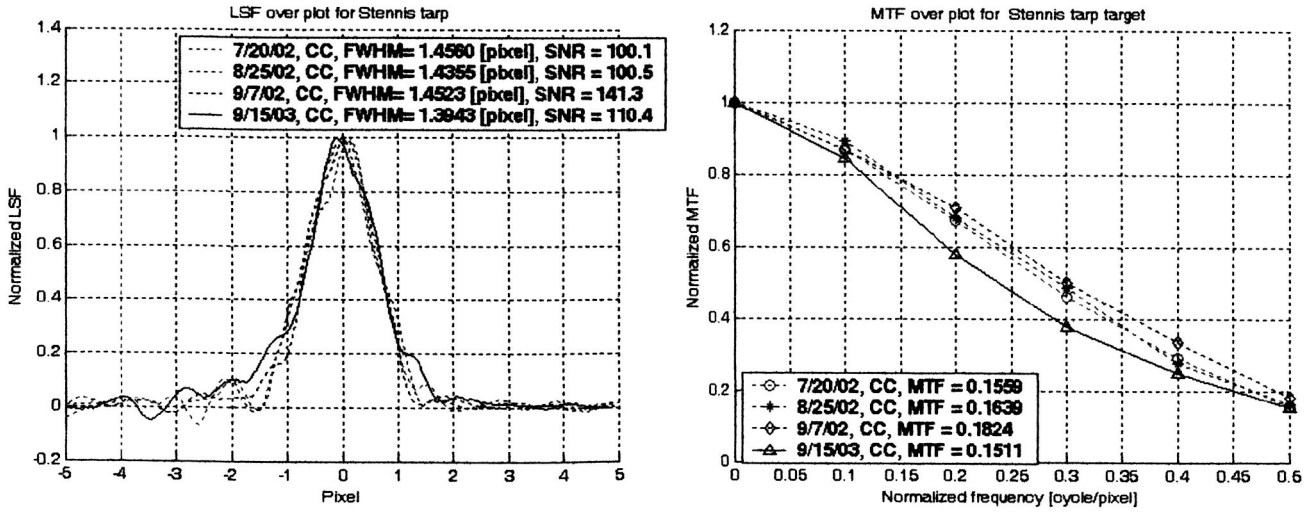

(a) LSF overplot (b) MTF overplot

Figure 5.7. Results from Stennis tarp target of Quickbird images from 2002 to 2003 in pixel unit.

The GSD change had an impact on MTF comparisons because the normalized scale in pixel units doesn't account for the change in GSD. Figure 5.7 should be rescaled in an 'absolute' unit between the two years such as meters. Figure 5.8(a) shows the LSF overplot scaled to meters. The 2003 FWHM was approximately 0.2 meters less than the average FWHM value from 2002. Figure 5.8 shows MTF estimates for 2002 and 2003 based on absolute units of cycles per meter. The corresponding Nyquist frequencies due to sampling rates are also shown. There is very little difference in MTF estimates between the two years. From the shape of the PSF

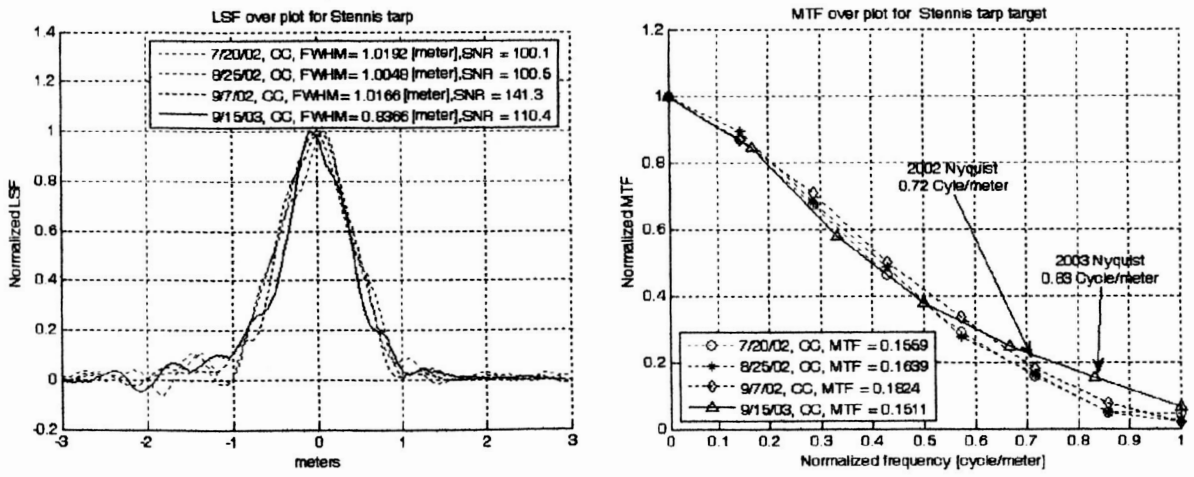

(a) LSF overplot (b) MTF overplot

Figure 5.8. Results from Stennis tarp target of Quickbird images from 2002 to 2003 in panchromatic band with meter unit.

and MTF plots, there is no compelling evidence that the Quickbird imaging system's spatial resolution degraded from 2002 to 2003.

Additionally, edge method analysis using the Stennis target provided reliable estimates, as indicated by consistent SNR values greater than 100. The MTF values at Nyquist met the minimum SDP specification of 0.09 for the panchromatic band.

5.6.2. Blue Band Comparison

The width of the pulse target used in the June 27, 2002 dual overpass (IKONOS and Quickbird sensors) was 12 meters, consistent with the width used for the IKONOS multispectral band MTF analysis. Since this width was subsequently found not to be optimal for QuickBird multispectral MTF analysis (due to the closeness of the Nyquist frequency location to a zero-crossing point and the resulting instability of the MTF estimate), for following overpasses the SDSU target was deployed as a 9m wide pulse in a 2 by 3 pattern. In 2003, since sensor GSD was changed without notice, this resulted in larger FWHM values as shown in Table 5.7 and Figure 5.9(a).

The scenes processed with CC resampling yielded MTF estimates with a mean of 0.31 and standard deviation of 0.05. At the frequencies of 0.3 and 0.4 cycles per pixel, many 2002 data points showed significantly more scatter than

Table 5.7. 2002 and 2003 blue band result comparison with blue tarp target

Date	Interpolation method	FWHM	SNR	MTF
6/27/02	CC	4.1680	57.7	0.3227
7/20/02	CC	3.1525	62.2	0.3333
8/25/02	CC	3.2059	93.5	0.3238
9/7/02	CC	3.2102	95.8	0.3687
8/23/03	CC	3.6432	73.8	0.3660
9/15/03	CC	3.6624	75.1	0.2866
10/21/03	CC	3.6862	70.6	0.2244

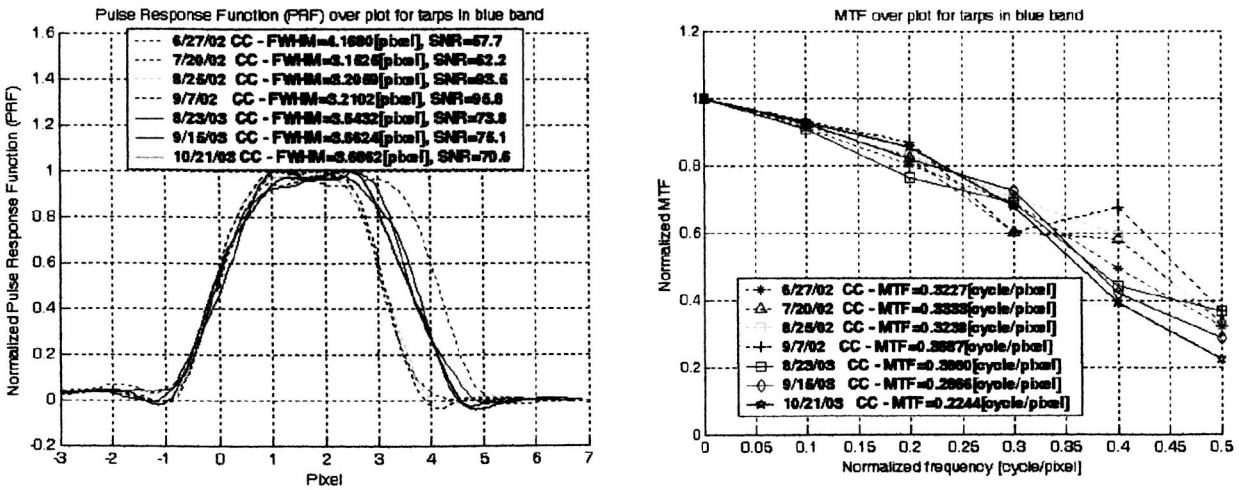

(a) LSF overplot (b) MTF overplot

Figure 5.9. Results from blue tarp target of Quickbird images from 2002 to 2003 in pixel unit.

the 2003 MTF data points. The reason for this is caused by width estimation error described in the sensor modeling report. Error detection and correction for this analysis is also reported in the sensor modeling report.

Figure 5.9 was based on pixel units which doesn't describe the GSD change from 2.8 meters to 2.4 meters from 2002 to 2003. Figure 5.10 shows LSF and MTF overplots in meters, which contains exactly the same information but provides a rescaled 'x' axis based on the specific GSD in each year. Nyquist frequency for the 2.8 meter GSD was 0.18 cycle/meter in 2002 and the Nyquist frequency for the 2.6 meter GSD was 0.21 cycle/meter in 2003. These two Nyquist frequencies are indicated as green and magenta dash lines in

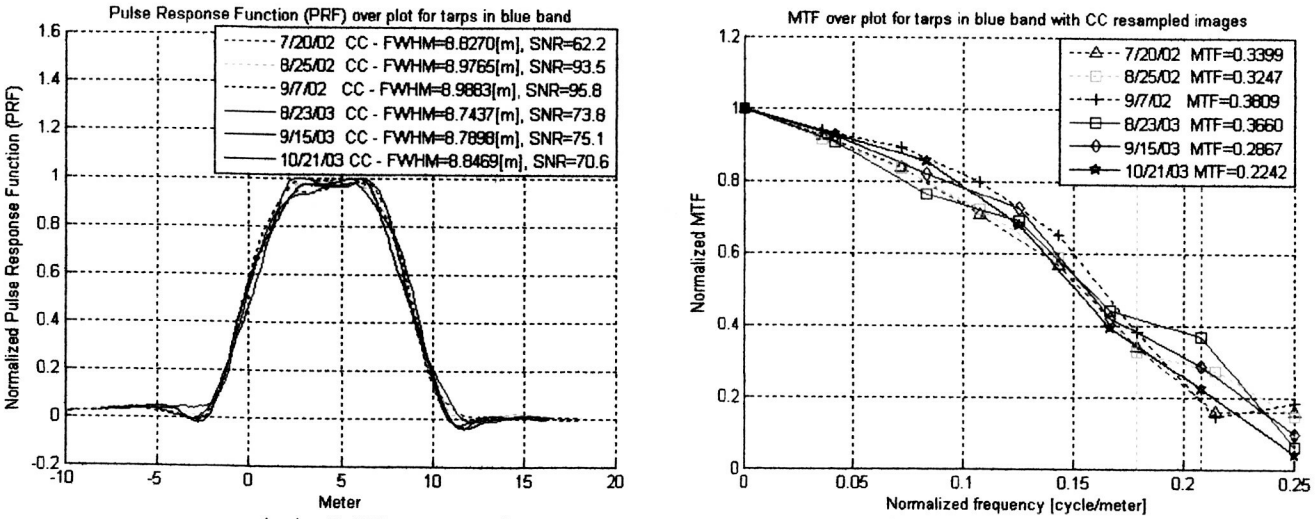

(a) LSF overplot (b) MTF overplot

Figure 5.10. Results from Stennis tarp target of Quickbird images from 2002 to 2003 in blue band.

Figure 5.10(b). Repeatability of the tarp width was less than 10 centimeters over the six campaigns in 2002 and 2003 which is shown in Figure 5.10(a). The MTF over plot trend was very consistent over the two years and and supports the conclusion that there is little or no evident spatial degradation in the blue band from 2002 to 2003.

To address the deformation in the shape of the MTF estimate, pulse width error was corrected as shown in Table 5.8 and Figure 5.11. Only 2002 tarp width error correction was possible because of the GSD change in 2003. The tarp width needs to be approximately 3-pixels wide to predict the MTF behavior caused by width measurement error. The deformation at 0.3 cycles/pixel was caused by tarp measurement error. From simulation results, a smaller than true estimate of the tarp width will cause a lower MTF value at 0.3 cycles/pixel with the three-pixel tarp input. The tarp width was increased until it showed the most reasonably shaped curve. Through this error detection method, we could correct tarp width error down to about the 1 cm level. Interestingly, although this error is very pronounced at 0.3 and 0.4 cycle per pixel, it is quite small at Nyquist.

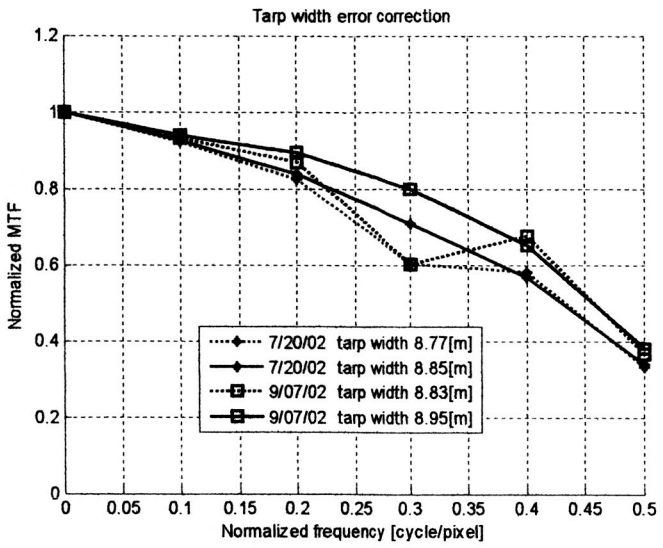

Figure 5.11. MTF after tarp width correction.

Table 5.8. Tarp width correction from MTF plot deformation

Date	Original Tarp width	New Tarp width	Original MTF	New MTF
7/20/02	8.77	8.85	0.3333	0.3399
9/7/02	8.83	8.95	0.3687	0.3809

5.7. QuickBird Panchromatic Band MTF Results from Impulse Target

5.7.1. Data Sets

Three Brookings, SD scenes were used for MTF estimation. The first image was acquired on August 23, 2003 from the Quickbird sensor, the second scene was taken on September 15, and the third scene was acquired on October 21, 2003. Only Quickbird panchromatic band images were used in this work. In the multispectral band, the DN values of the point sources were as low as 560, which is comparably close to the

DN value of the background (330) and hence reconstruction of the PSF was not feasible.

5.7.2. Phasing Of Point Sources

In order to get the uniform sample distribution shown in Figure 5.12 (b), mirror 1 was designated to be the reference mirror (located at (0, 0)). One important factor was to verify the spacing between two mirrors (D) was at least 5 GSDs (3.5m) apart in order to allow enough grass area between mirrors to avoid overlapping of mirror PSF responses. Another important aspect was that the fractional pixel distances in the cross-track (Δx) and along-track (Δy) directions should be increments of 0.2 and 0.25 GSDs respectively, to obtain the desired uniform distribution. By a number of trials, it was found that 1.25 GSDs and 10.2 GSDs were the appropriate cross-track and along-track distances. These values resulted in an angle of 7 degrees.

$$\tan\theta = \frac{\Delta x}{\Delta y}$$

$$\theta = \tan^{-1}\frac{\Delta x}{\Delta y}$$

$$\theta = \tan^{-1}\frac{1.25}{10.2}$$

$$\theta = 7^{o}$$

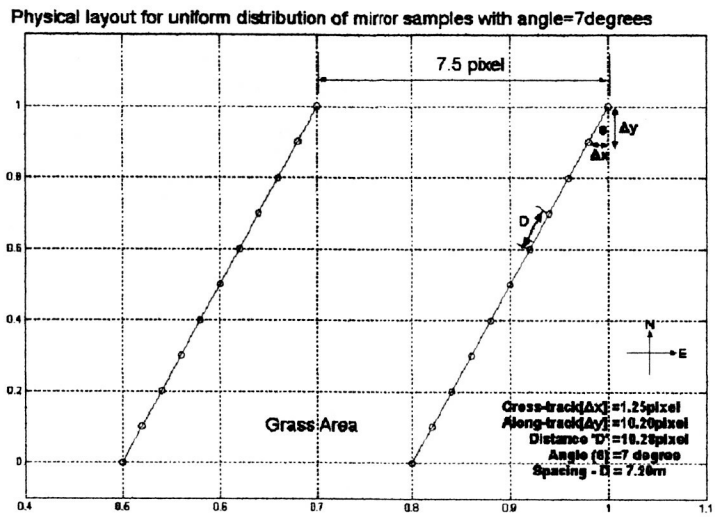

(a) Final convex mirror layout of summer 2003

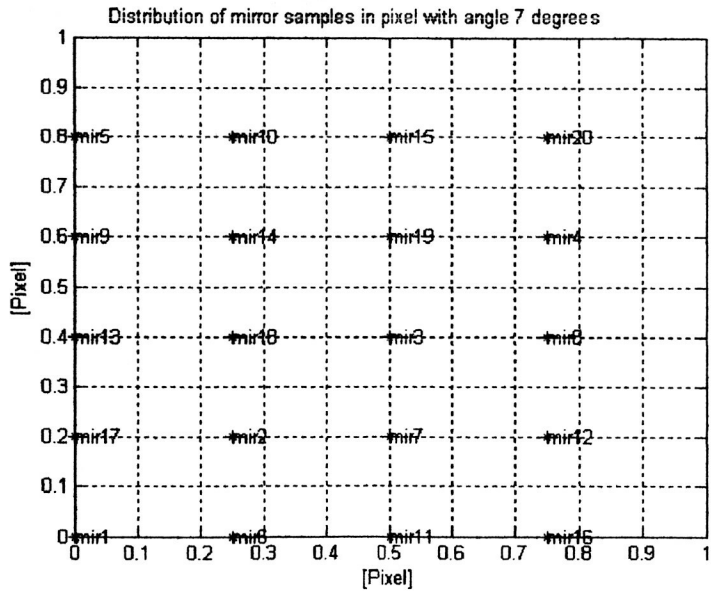

(b) Distribution in one pixel

Figure 5.12 Sampling distribution of mirrors based on ground measurement on summer 2003.

5.7.2.1 Two-dimensional Gaussian Model Fit

The location of the PSF peak for each mirror was determined from the extracted mirror data using a parametric two-dimensional Gaussian model. The mirror data were then aligned to a common reference at the pixel coordinates (0, 0). The two-dimensional Gaussian model was applied again to estimate the overall PSF of the imaging system. Finally, a Fourier transform was applied to the estimated PSF and normalized to obtain the MTF.

5.7.2.2 Peak Position Estimation of Mirror Responses

Figure 5.13 (a), (b) and (c) show examples of extracted images of mirror data from the August 23, September 15, and October 21 scenes. Visually from these images, it can be seen that some of the mirrors from August 23 appear to be darker than in September and October. This unequal response is believed to be due to the haze present in the atmosphere on August 23.

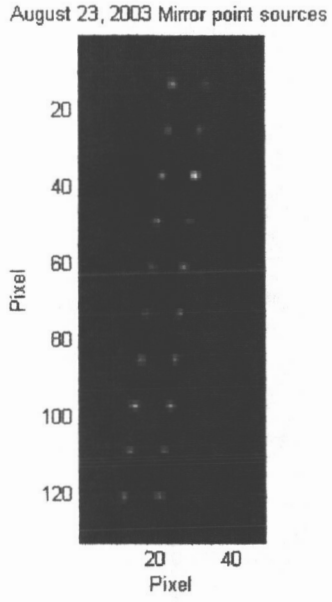

(a) 20 Mirror data from August 23, 2003 Quickbird Image

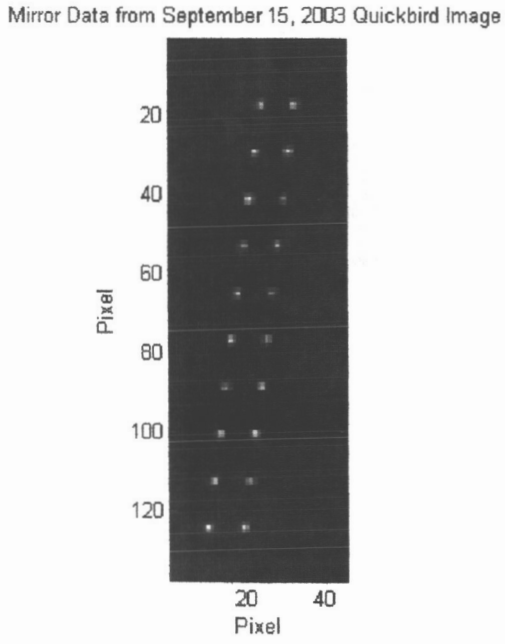

(b) 20 Mirror data from September 15, 2003 Quickbird Image

Figure 5.13. Mirror Images from Summer 2003 Quickbird Sensor.

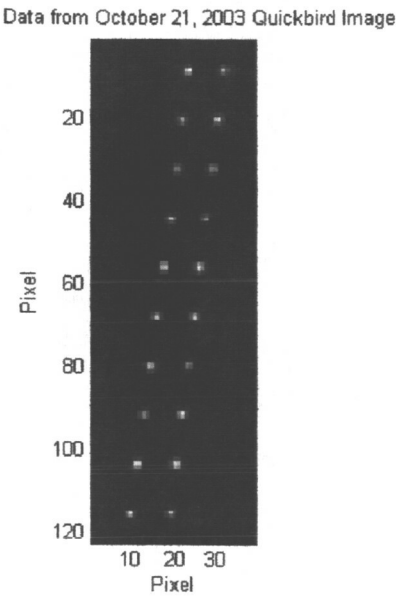

(c) 20 Mirror data from October 21, 2003 Quickbird Image

Figure 5.13. Mirror Images from Summer 2003 Quickbird Sensor.

A two-dimensional Gaussian model was applied to the individual mirror responses of August, September and October Quickbird data to estimate the peak position and their corresponding peak DN values. Examples of some of the mirror data, and the 2D Gaussian model used to estimate their peak positions, are given in Appendix C.

5.7.3 Comparison of Mirror Sample Distribution

The actual and estimated sub-pixel positions of the August 23, 2003 mirror point sources are shown in Figure

5.14(a) [in pixels] and (b) [in meters]. The positional errors are calculated and listed in Table 5.9.

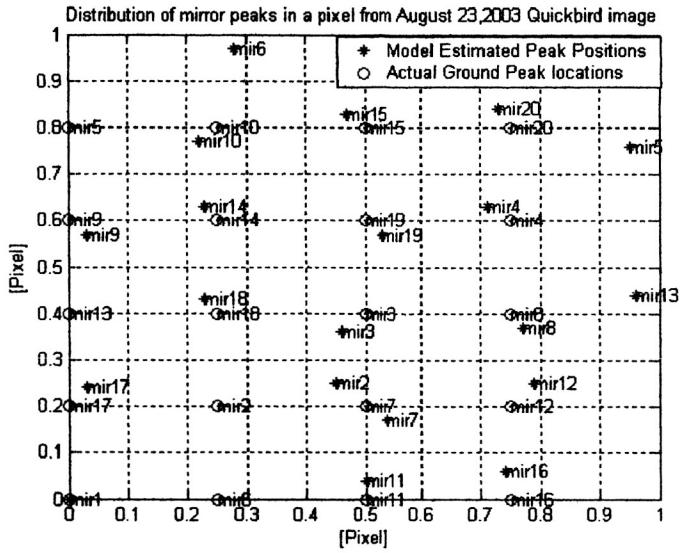

(a) Distribution of Mirror Peak location in 1 pixel

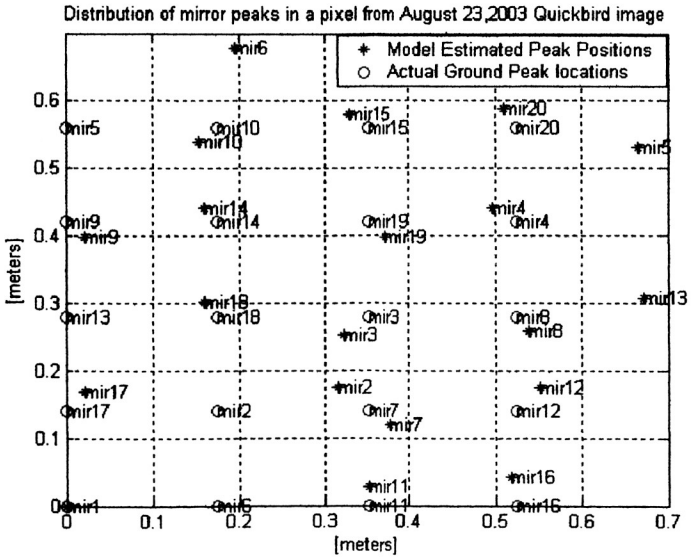

(b) Distribution of Mirror Peak location in 1 GSD (0.7m)

Figure 5.14 Distribution of ground based and estimated mirror peak locations of August 23, 2003 Quickbird image.

The measurements are relative to mirror 1, i.e., taking mirror 1 as the reference location. The error ranges from 0 to 12cm in the cross-track and 0 to 4cm in the along-track direction. These differences might be caused by various sources of error such as the background and flexibility of the convex mirrors. The RMSE of all twenty mirrors is 3.31cm and 2.31cm in the cross-track and along-track direction, respectively. It is evident that the positional errors of mirrors 2 and 5 are high compared to other mirrors. This increase in offset is may be caused by manual errors in mirror placement in along-track and cross-track directions. The unevenness of the ground underneath the mirrors is also an error source.

With the September 15 data set, the RMSE for all twenty mirrors was 2.48cm and 1.94cm in cross- and along-track directions, respectively. Mirrors 2 and 5 have greater positional offset as compared to other mirrors, which is similar to the August 23 result. Again, positional offsets may be due to the flexibility of the mirrors, uneven background, and improper mirror placement.

Table 5.9 Difference between the ground and estimated peak positions of the mirrors from Aug 23, 2003 Quickbird data.

Mirror #	Positional Errors [cm] Cross-track direction	Positional Errors [cm] Along-track direction
1	0.00	0.00
2	12.00	3.00
3	-2.40	-2.40
4	-2.40	1.80
5	4.00	-2.40
6	1.80	3.60
7	2.40	-1.80
8	1.20	-1.80
9	1.80	-1.80
10	-1.80	-1.80
11	0.00	2.40
12	2.40	3.00
13	2.40	2.40
14	-1.20	1.80
15	-1.80	1.80
16	-0.60	3.60
17	1.80	2.40
18	-1.20	1.80
19	1.80	-1.80
20	-1.20	2.40
RMSE	3.31	2.31

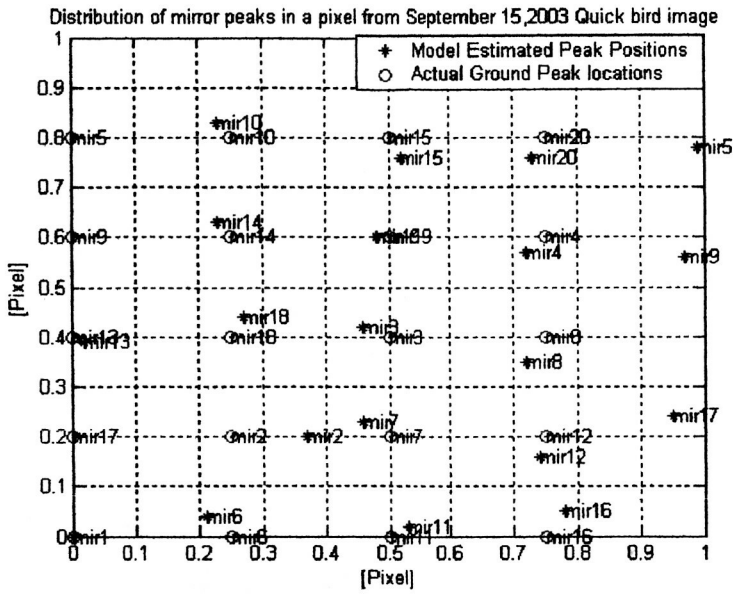

(a) Distribution of Mirror Peak location in 1 pixel

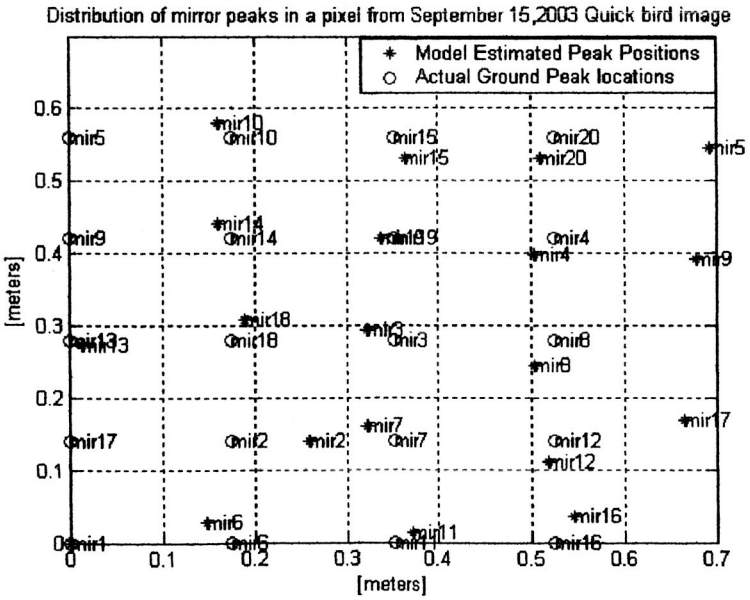

(b) Distribution of Mirror Peak location in 1 GSD (0.7m)

Figure 5.15 Distribution of ground based and estimated mirror peak locations of September 15,2003 Quickbird image.

Table 5.10 Difference between the ground and estimated peak position of the mirrors from Sept 15, 2003 Quickbird data.

Mirror #	Positional Errors [cm] Cross-track direction	Positional Errors [cm] Along-track direction
1	0	0
2	7.2	0
3	-2.4	1.2
4	-1.8	-1.8
5	3.6	-1.2
6	-2.4	2.4
7	-2.4	1.8
8	-1.8	-3
9	3	-2.4
10	-1.2	1.8
11	1.8	1.2
12	-0.6	-2.4
13	1.2	-0.6
14	-1.2	1.8
15	1.2	-2.4
16	1.8	3
17	3	2.4
18	1.2	2.4
19	-1.2	0
20	-1.2	-2.4
RMSE	2.48	1.94

Similarly, the sub-pixel position plots of October 21, 2003 mirrors and their actual ground positions are shown in Figure 5.16(a) in pixels and (b) in meters. The red asterisks represent the model estimated peak locations and blue circle the actual ground positions. All 20 mirror positional errors are calculated and listed in Table 5.11. The errors vary from 0 to 2.4cm in the cross-track direction and 0 to 2.4cm in the along-track direction. RMSE for all twenty mirrors is 1.2cm and 1.37cm in cross- and along-track directions respectively. Mirrors 2 and 16 have greater positional offset as compared to other mirrors.

The error on August 25 is greater than September 15 and October 21, 2003. This might be due to the layer of haze in the atmosphere during the satellite overpass on August 23, 2003.

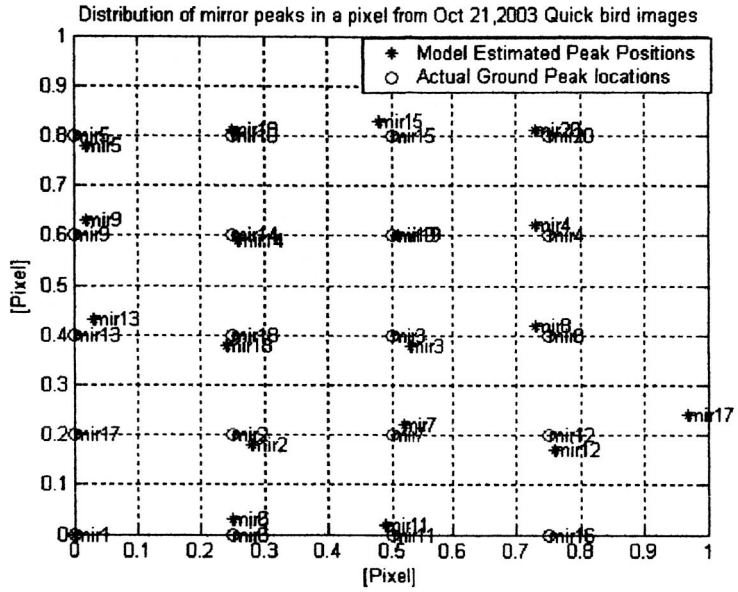

(a) Distribution of Mirror Peak location in 1 pixel

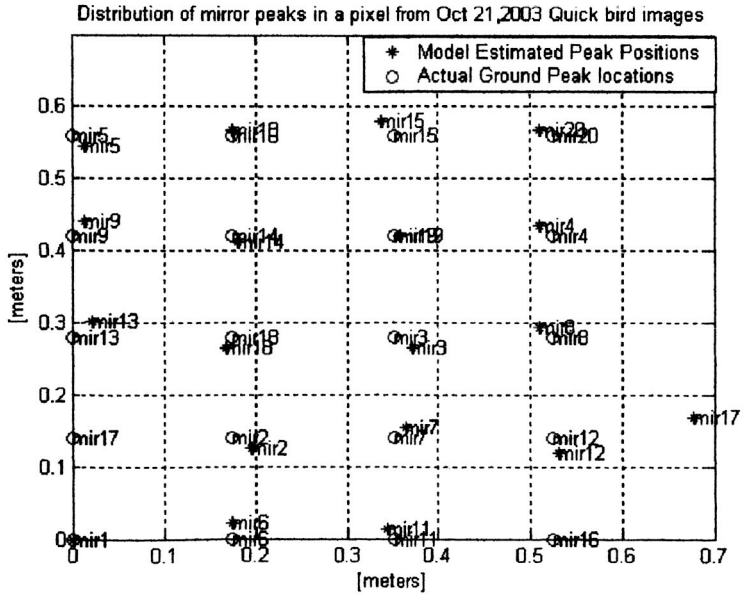

(b) Distribution of Mirror Peak location in 1 GSD (0.7m)

Figure 5.16 Distribution of ground based and estimated mirror peak locations of October 21, 2003 Quickbird image.

Table 5.11 Difference between the ground and estimated peak positions of the mirrors from Oct 21, 2003 Quickbird data.

Mirror #	Positional Errors [cm] Cross-track direction	Positional Errors [cm] Along-track direction
1	0	0
2	1.8	-1.2
3	1.8	-1.2
4	-1.2	1.2
5	1.2	-1.2
6	0	1.8
7	1.2	1.2
8	-1.2	1.2
9	1.2	1.8
10	0	0.6
11	-0.6	1.2
12	0.6	-1.8
13	1.8	1.8
14	0.6	-0.6
15	-1.2	1.8
16	-2.4	1.8
17	1.2	2.4
18	-0.6	-1.2
19	0.6	0
20	-1.2	0.6
RMSE	1.20	1.37

5.8 Alignment and Least Square Error Gaussian Surface

After the estimates of peak location were obtained for all mirrors on all three days, the mirror data were then aligned and a 2D Gaussian model was fitted to the data to obtain an estimate of the oversampled PSF of the mirror responses as shown in Figure 5.17(a-d).

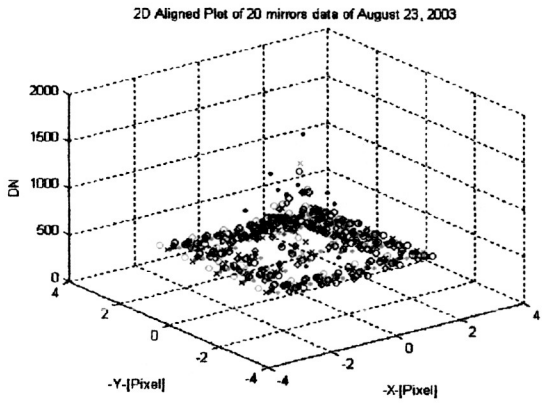

(a)August 23, Aligned Data

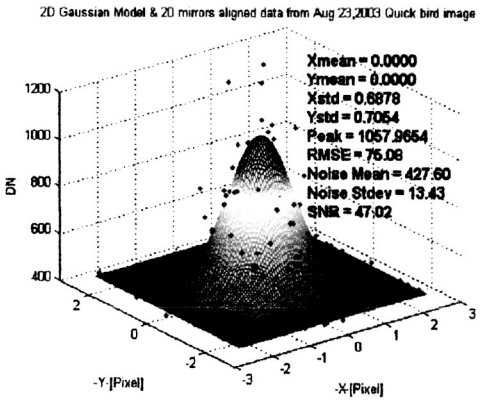

(b)August 23, 2D PSF

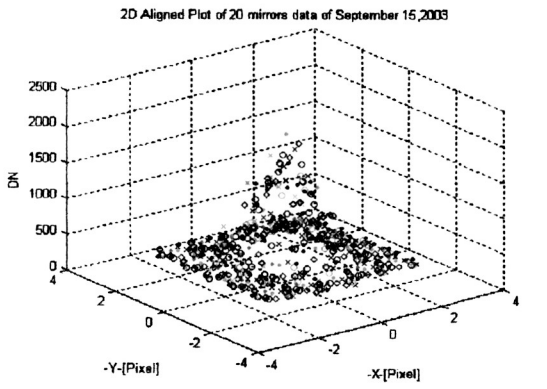

(c)September 15, Aligned Data

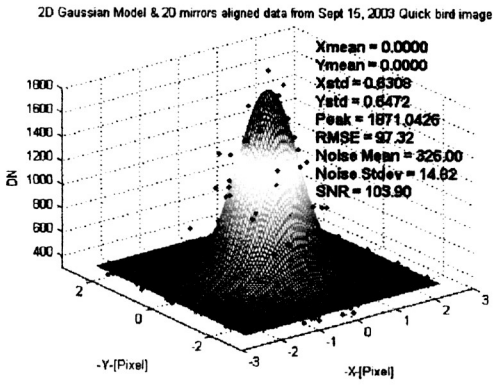

(d)September 15, 2D PSF

Figure 5.17 Least Square Error Gaussian Surface fit for aligned mirror data of August 23, September 15, and October 21 2003 Quickbird images.

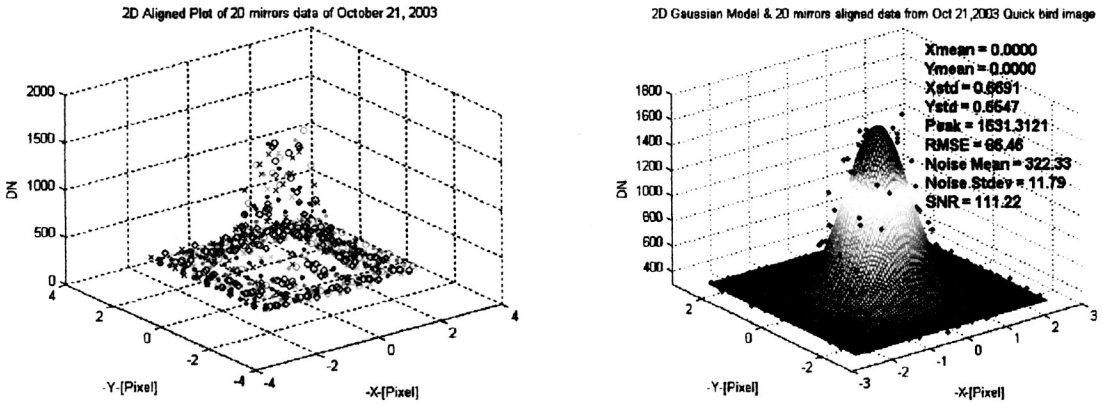

(e) October 21, Aligned Data (f) October 21, 2D PSF

Figure 5.17 Least Square Error Gaussian Surface fit for aligned mirror data of August 23, September 15, and October 21 2003 Quickbird images.

A two-dimensional Gaussian model was applied to the aligned August 25 and September 7 mirror data to estimate net PSF in along and cross-track, using the MATLAB 'fminsearch' function described previously. Detailed plots of all the mirror data, and the 2D Gaussian model used to estimate their peak positions, are given in Appendix C.

Figure 5.17 (a) and (b) display the aligned mirror data and least square error Gaussian surface of August 23 respectively. In the Gaussian fit plots, the peak position on both days is at the center (0,0). The 'Xstd' and 'Ystd' are Gaussian function standard deviation values, which represent cross and along track direction blurring. The

error between the model and the actual data, is given by the RMSE. The mean DN value of the grass background is named as 'NoiseMean' in the plot which is followed by its own standard deviation value. Finally, the SNR value is calculated by dividing the Gaussian model peak value 'Peak' by background mean 'NoiseMean'.

Overall, the peak signal level (DN values) of all the mirror data on August 23 is very low as compared to September and October. However, this might be due to the thick layer of haze present in the atmosphere on that date and is consitent with the larger peak location error on August 23 as shown in Table 5.12. The wider random distributions of estimated mirror peak locations will contribute to increase blurring the 20 mirror aligned profile. Consequently, the peak values from September 15 and October 21 were 77 and 54.4 percent higher than the peak value from August 23 when peak values were compared from information in Figure 5.17.

Table 5.12. Comparison of estimated mirror errors in cross-track and along-track directions in August 23, Sept 15, and Oct 21, 2003.

Date	Aug 23, 2003	Sept 15, 2003	Oct 21, 2003
RMSE [cm] Cross-track	3.31	2.49	1.20
Mean [cm] Along-track	2.31	1.94	1.37

5.9 Results of Mirror FWHM and MTF Estimation

The estimated two-dimensional PSF was sliced into 1D PSFs through the peak in the cross-track and along-track directions. Figure 5.18 shows the PSF overplots of August 23, September 15, and October 21 in the cross-track direction. The FWHM value of Aug 23 result is greater than Sept 15 and Oct 21 data as shown in Table 5.13. This suggests that the blurring on August 23 data was greater than the other two days as discussed in the previous section.

Table 5.13 Comparison of FWHM from Aug, Sept, Oct, 2003 Quickbird mirror data.

Mirror data	Full-Width at Half-Maximum Measurement	
Overpass Date	Cross-track [Pixel]	Along-track [Pixel]
August 23, 2003	1.796	1.764
September 15, 2003	1.566	1.610
October 21, 2003	1.666	1.647

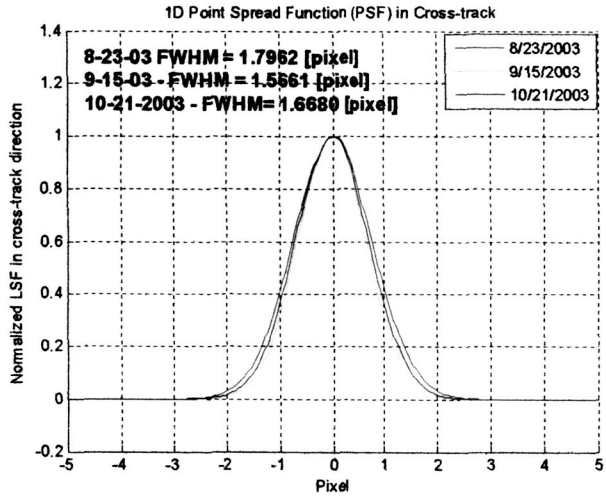

Figure 5.18. PSF plots of Aug 23, Sept 15 and Oct 21, 2003 in Cross-track.

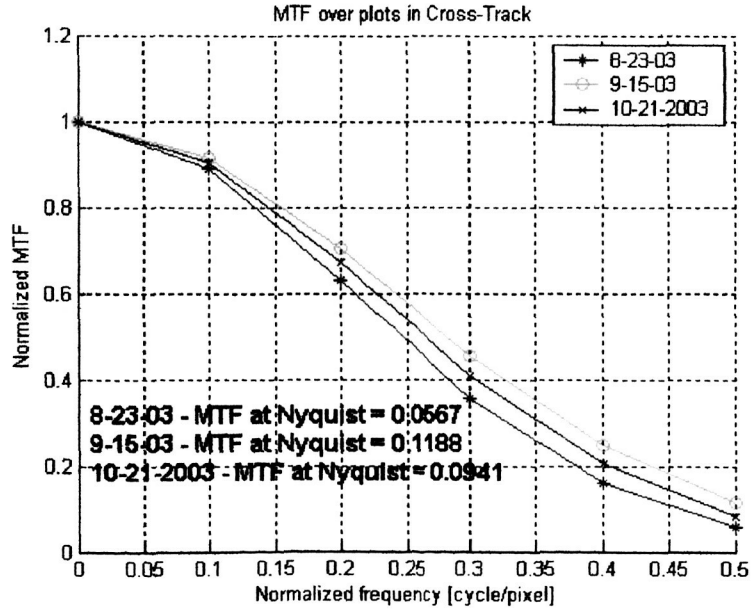

Figure 5.19. MTF Plots of Aug 23, Sept 15 and Oct 21, 2003 in Cross-track.

Figure 5.19 shows the MTF over plots of Aug 23 (blue), Sept 7(green), Oct 21(red), 2003 in the cross-track direction. Similarly Figure 5.20 and 5.21 show the FWHM and MTF plots in along-track direction. Table 5.14 compares MTF values at the Nyquist frequency. These result indicate fairly consist PSF and MTF estimates on all three dates. The August results indicate additional blurring that is probably atmospheric and deployment related rather than an indication of degraded sensor responses. Also, additional blurring in the along-track direction is expected due to satellite motion. This cannot be observed, however, in these results.

A comparison can be made better FWHM estimates in the cross-track direction between the Stennis tarp result (FWHM=1.29 pixels) and the mirrors where the FWHM = 1.57 pixels. It is pleasing to note a relative difference between the two estimates of 13%. Since the mirrors based approach is still considered to 'experimental' in nature, this level of consistency suggests continual exploration of the mirror target method. Based on the SNR values from Figure 5.17, October 21 most likely produced the most reliable result, since SNR was maximized and greater than 100. The SDP specification was met.

Table 5.14 Comparison of MTF from Aug, Sept, Oct, 2003 and Aug 25, Sept 7, 2002 Quickbird mirror data.

Mirror data	Modulation Transfer Function values [MTF] @ Nyquist	
Overpass Date	Cross-track [Pixel]	Along-track [Pixel]
August 23, 2003	0.06	0.06
September 15, 2003	0.12	0.10
October 21, 2003	0.09	0.09

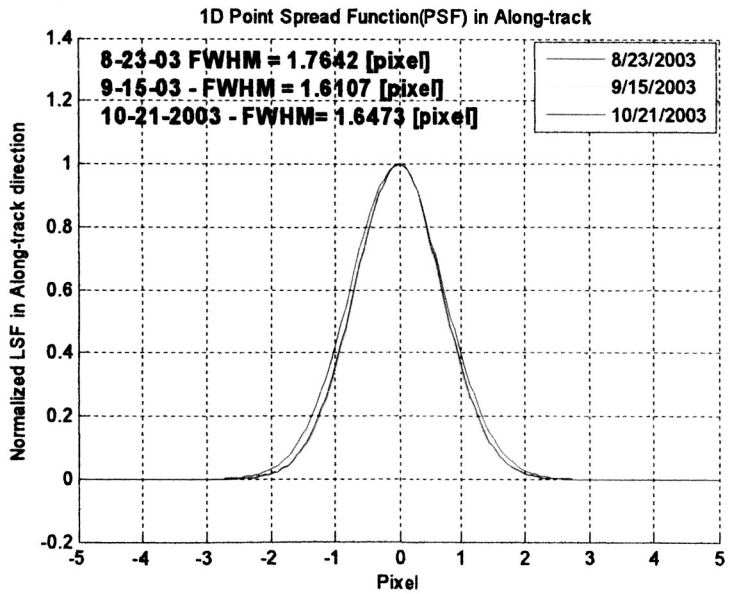

Figure 5.20. PSF plots of Aug 23, Sept 15 and Oct 21, 2003 in Along-track.

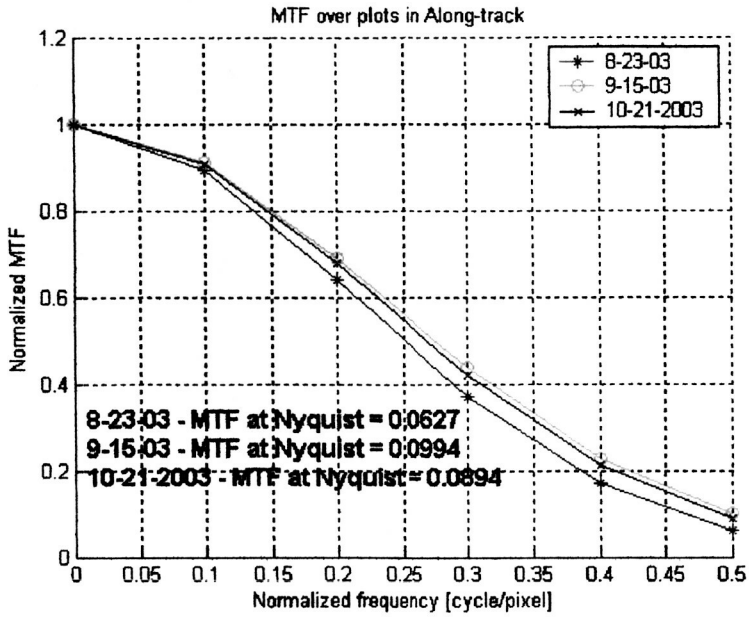

Figure 5.21 MTF Plots of Aug 23, Sept 15 and Oct 21, 2003 in Along-track.

6. Conclusions

The Stennis tarp target again provided an excellent edge target for the panchromatic band. SNR values from the uniform edge target on September 15, 2003 exceeded the minimum confidence level of 100 with the cubic convolution (CC) resampled product. The MTF value at Nyquist was 0.15 which was higher than the SDP specification with a margin of 0.06. However the MTF resampled product provided a lower SNR value of 57.2 because the noise was amplified by the nature of MTF kernel. The MTF value at Nyquist was approximately three times higher than the MTF value from the CC resampled image with a margin of 0.38. From these two MTF results, the Quickbird panchromatic band spatial quality met the SDP specification.

A set of blue tarps formed a ground step pulse for the multispectral bands. As a representative multispectral band, the blue band MTF values at Nyquist were used for specification comparison since it produced SNR at least two times higher than the other bands. Although the blue band SNR values were approximately 30 percent less than the desired SNR, the MTF values at Nyquist were 0.36, 0.28 and 0.22 with the SDP specification set at 0.20. It is

reasonable to assume that the spatial quality of the multispectral bands met the SDP specification.

Lastly, the mirror target provided a 2-D PSF and MTF estimate that was consistent with panchromatic band results obtained from the Stennis tarp target. Although still considered to be experimental, this approach continues to show good potential for becoming a reliable spatial quality estimates procedure for high spatial resolution imaging systems.

References

[1] V. Kaftandjian, Y. M. Zhu, G, Roziere, G. Peix and D.Babot, "A Comparison ofthe Ball, Wire, Edge, and Bar/Space Pattern Techniques for Modulation Transfer Funtion Measurements of Linear X-Ray Dectectors," Journal of X-Ray Science and Technology, Vol. 6, 1996,Page 205-221.

[2] Alexis P. Tzannes, Jonathan M. Mooney, "Measurement of the modulation transfer function of infrared cameras," Optical Engineering, Vol. 34 No. 6, June 1995.

[3] Robert Schowengerdt, Remote Sensing models and methods for image processing Academic Press 2nd Edition, 1997, Page 78~83.

[4] *Optimization Toolbox For Use with MATLAB - User's Guide.* Nattick, MA: The Mathworks, Inc., web site: www.mathworks.com, Online PDF version, pp. 4-54 - 4-57, June 2001.

[5] Dennis Helder, Taeyoung Choi, "Generic Sensor Modeling" NASA Stennis report from SDSU, 2003.

[6] P. B. Greer and T. van Doorn, "Evaluation of an algorithm for the assessement of the MTF using an edge method," Med. Phys., Vol. 27, No. 9, Sept 2000, page 2048~2059

APPENDIX A

Physical Layout of Tarp Target

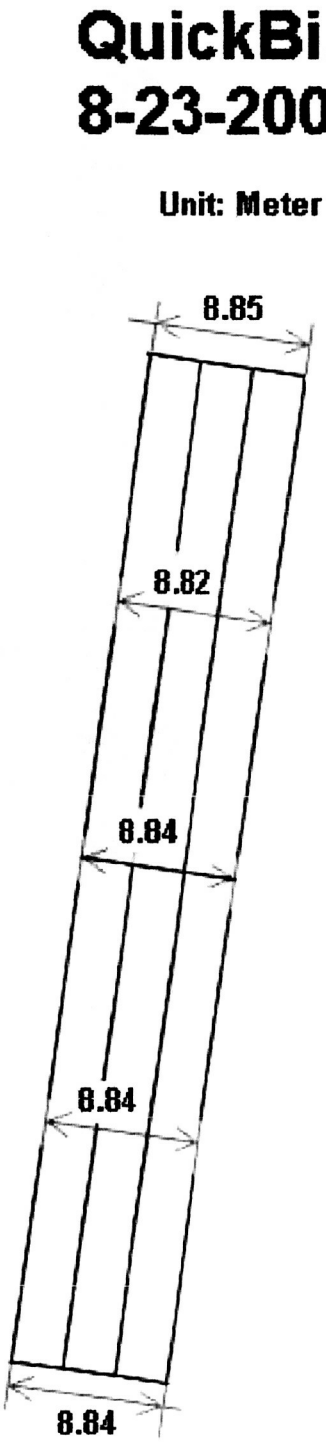

Figure A.1 Quickbird field campaign on Aug. 23, 2003.

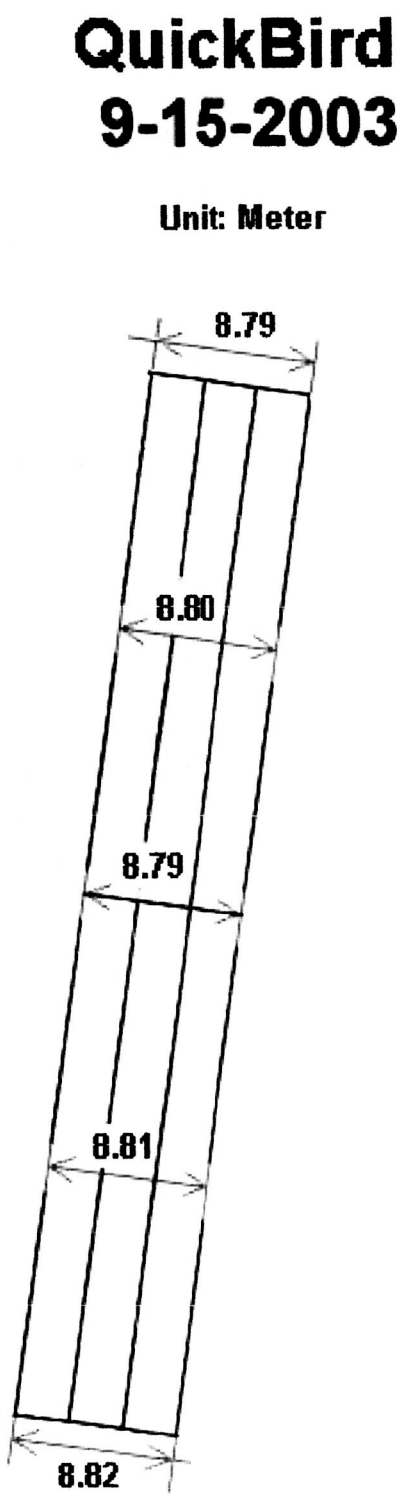

Figure A.2 Quickbird field campaign on Sept. 15, 2003.

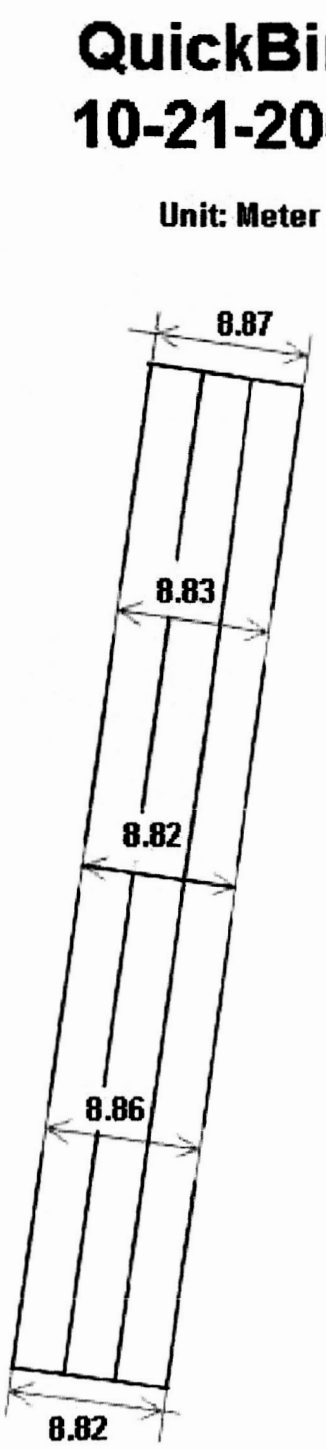

Figure A.3 Quickbird field campaign on October 21, 2003.

APPENDIX B

Edge and Pulse method MTF Procedure plots:

Brookings South Dakota

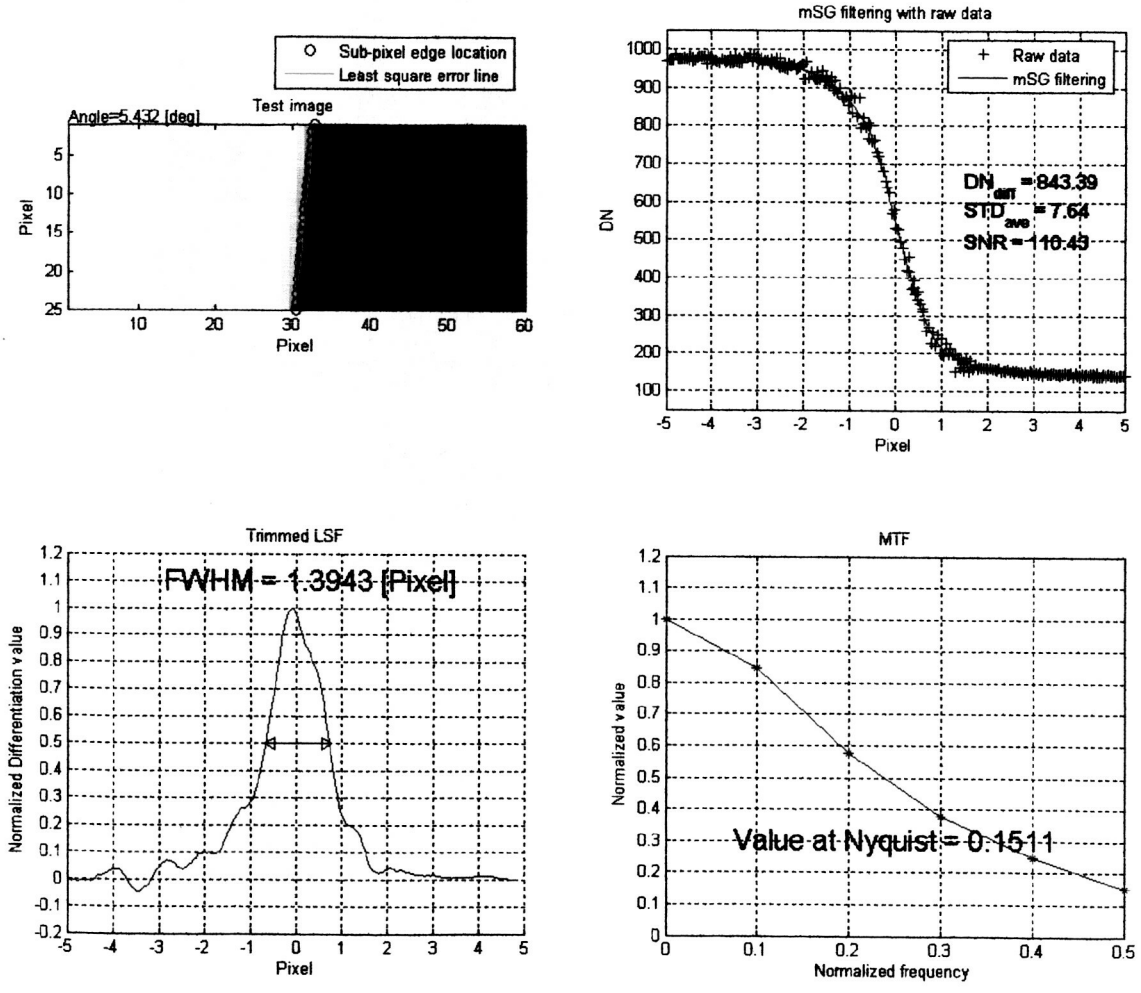

Figure B.1 Quickbird Stennis tarp target in panchromatic band on September 15, 2005 with cubic convolution interpolation.

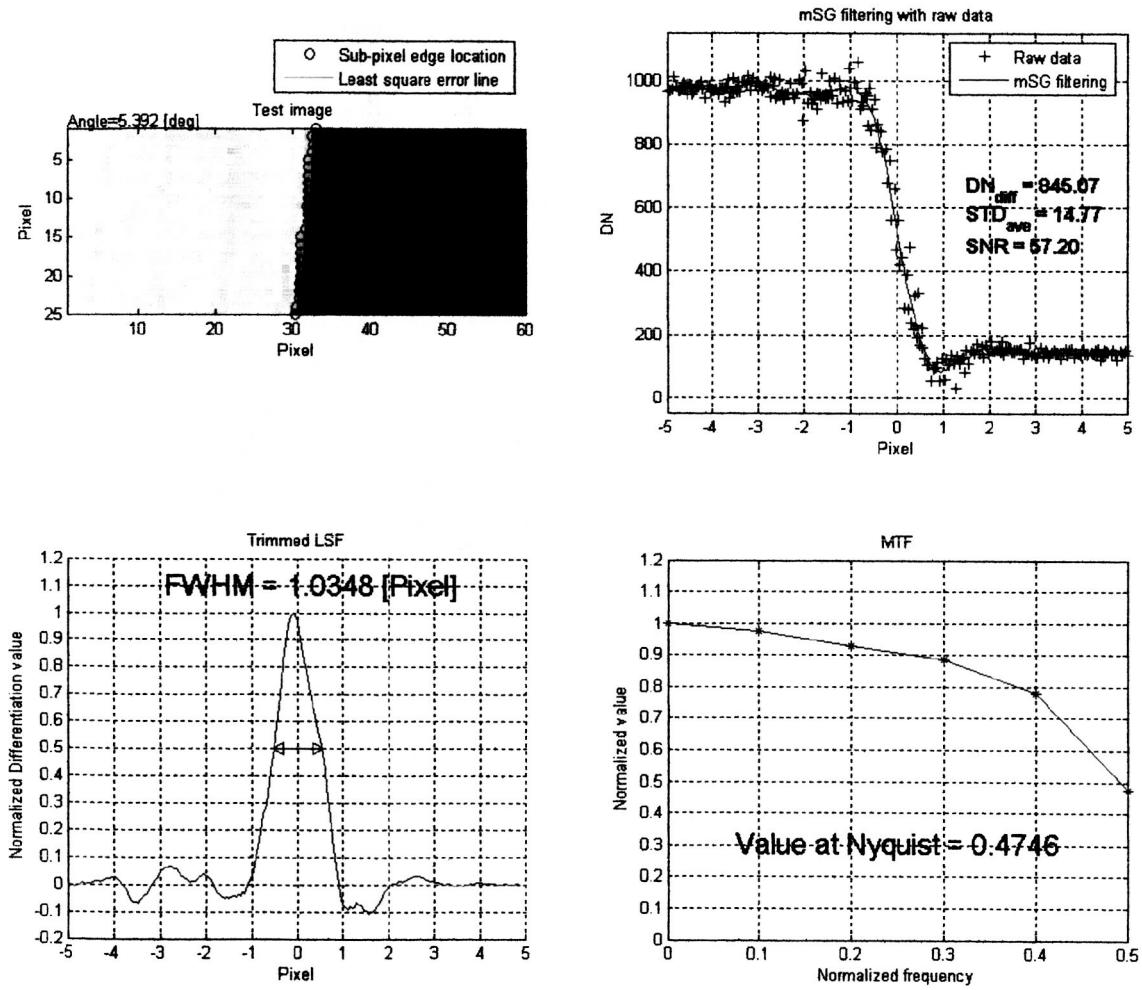

Figure B.2 Quickbird Stennis tarp target in panchromatic band on September 15, 2005 with MTF interpolation.

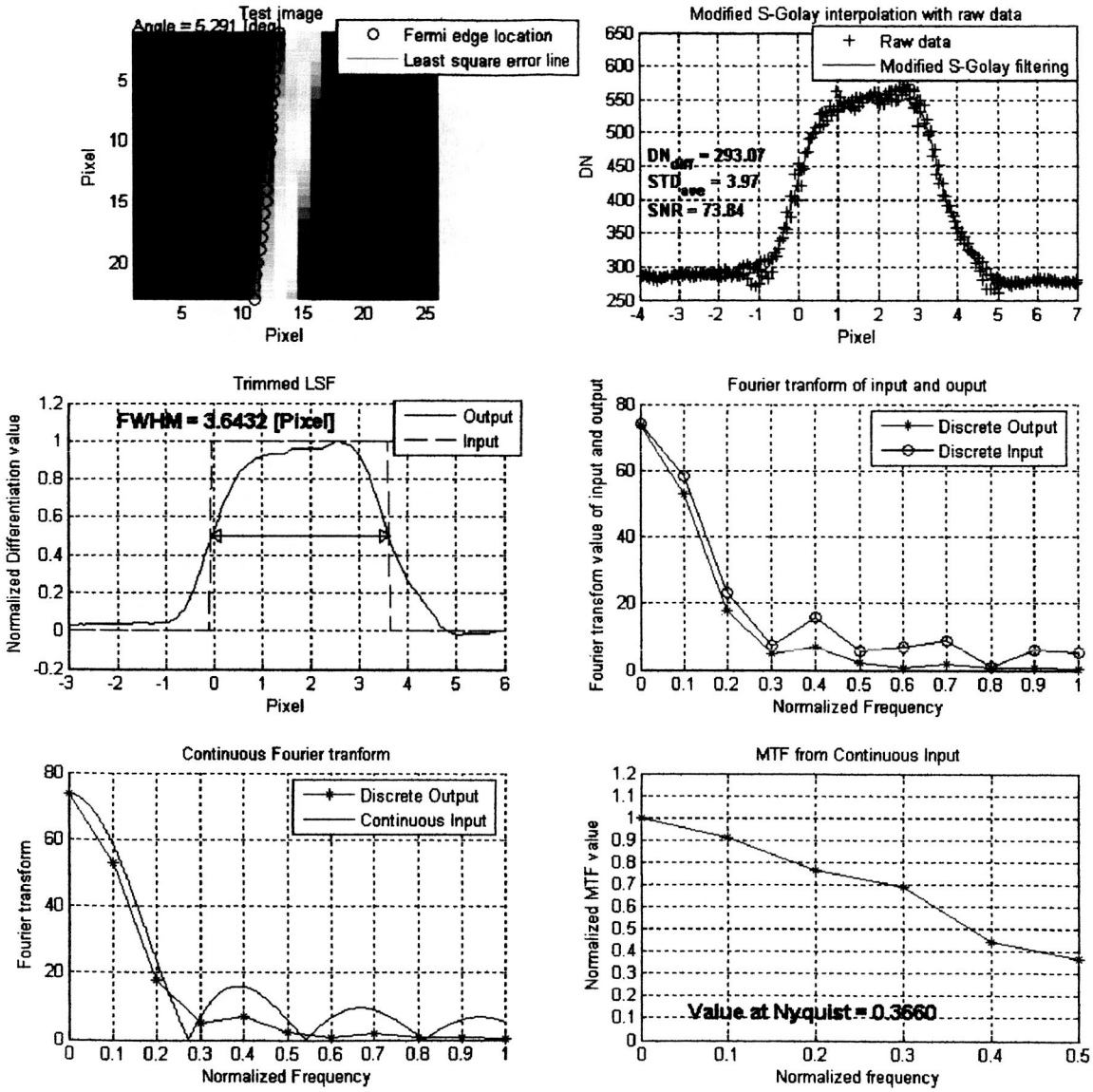

Figure B.3 Quickbird blue tarp target in blue band on August 23, 2003 with cubic convolution interpolation.

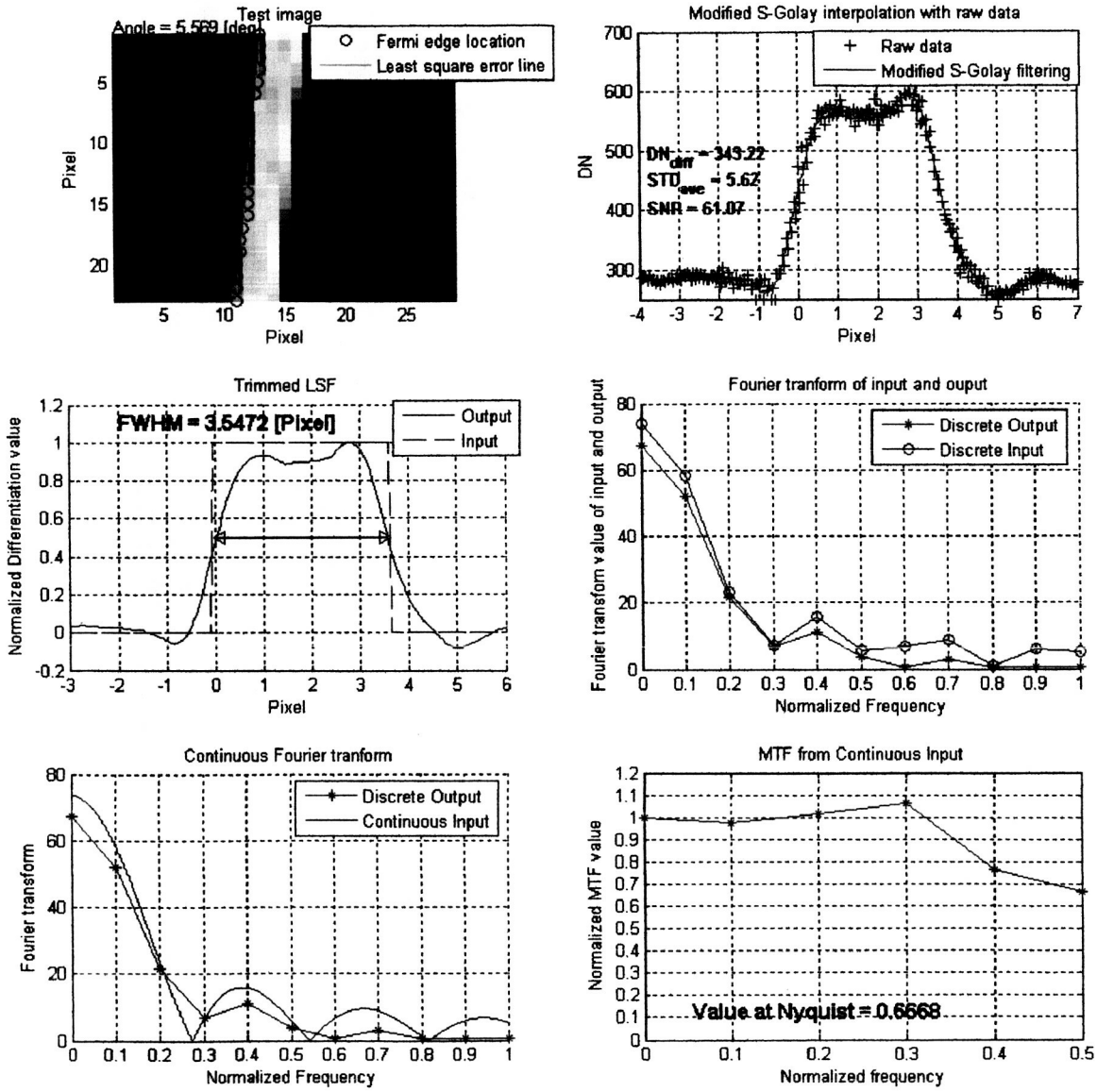

Figure B.4 Quickbird blue tarp target in blue band on August 23, 2003 with MTF interpolation.

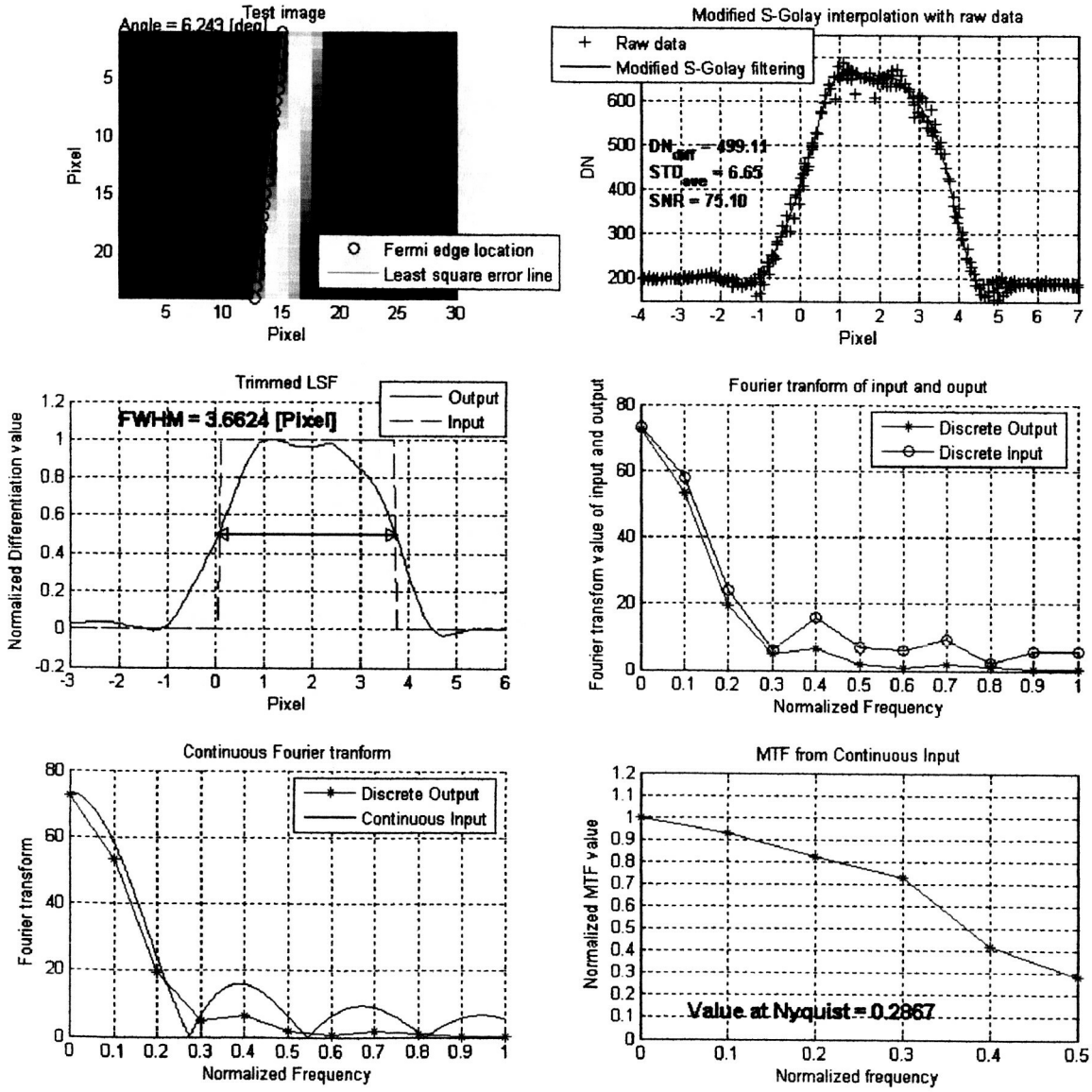

Figure B.5 Quickbird blue tarp target in blue band on September 15, 2003 with cubic convolution interpolation.

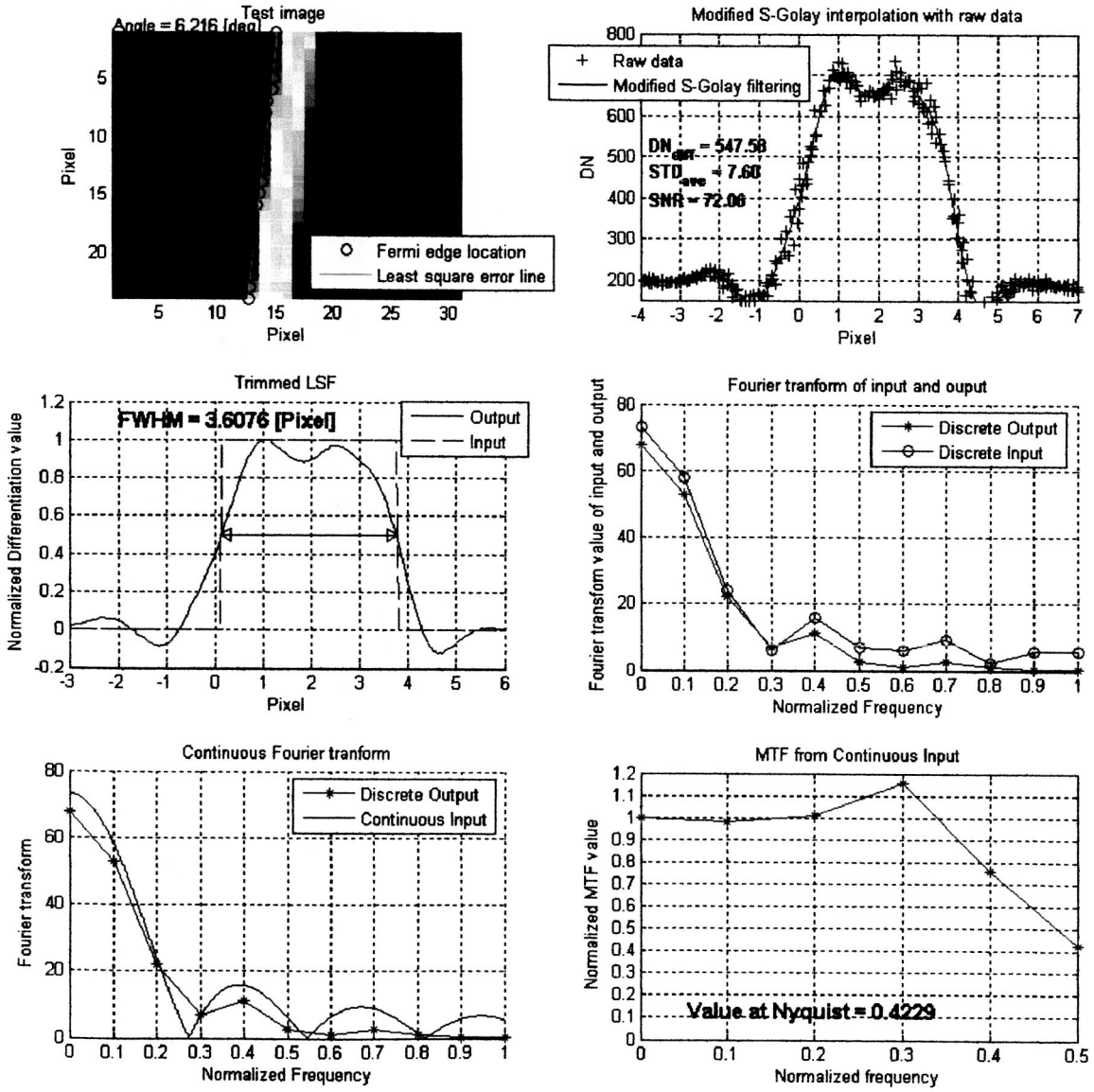

Figure B.6 Quickbird blue tarp target in blue band on September 15, 2003 with MTF interpolation.

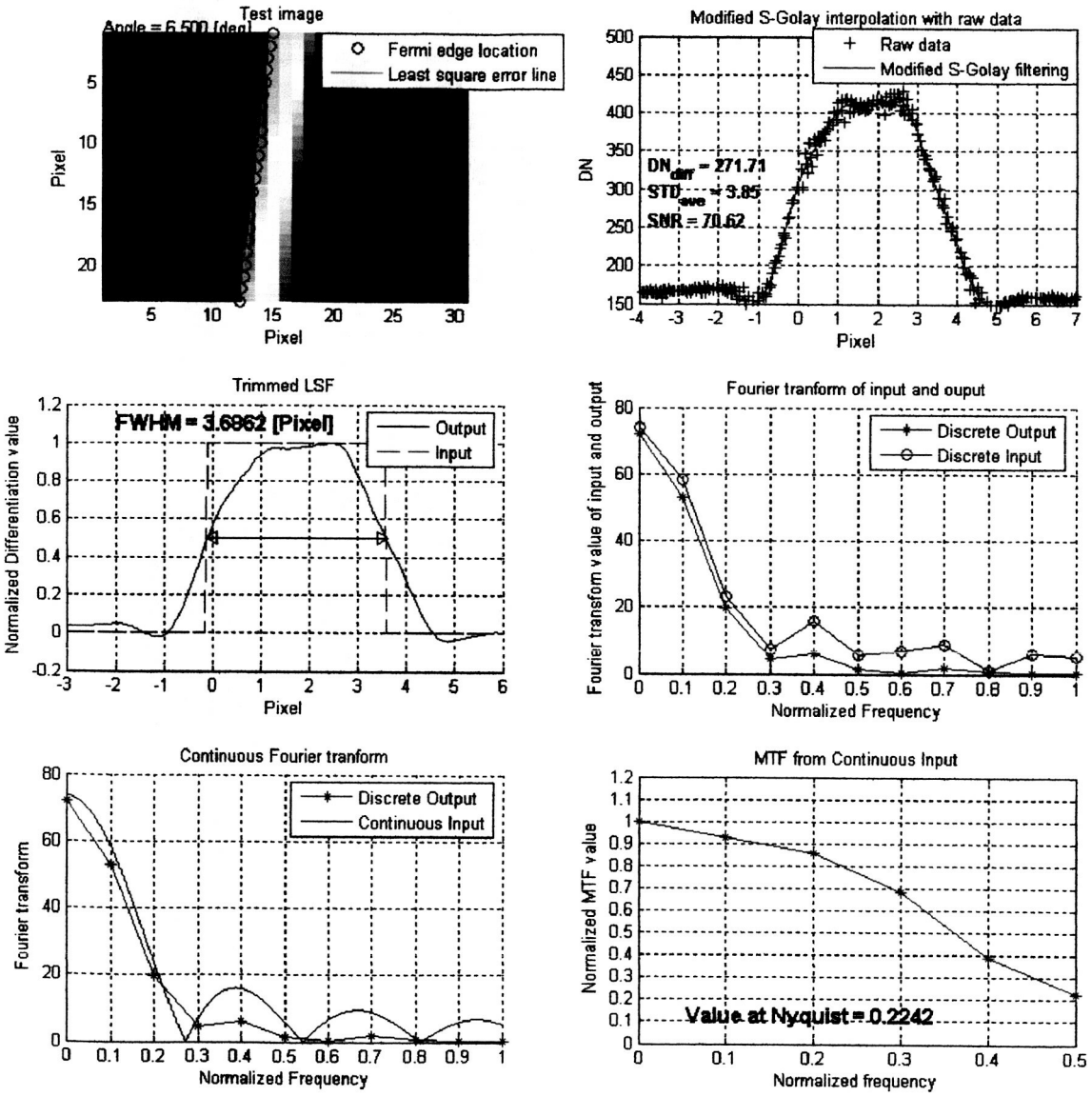

Figure B.7 Quickbird blue tarp target in blue band on October 21, 2003 with cubic convolution interpolation.

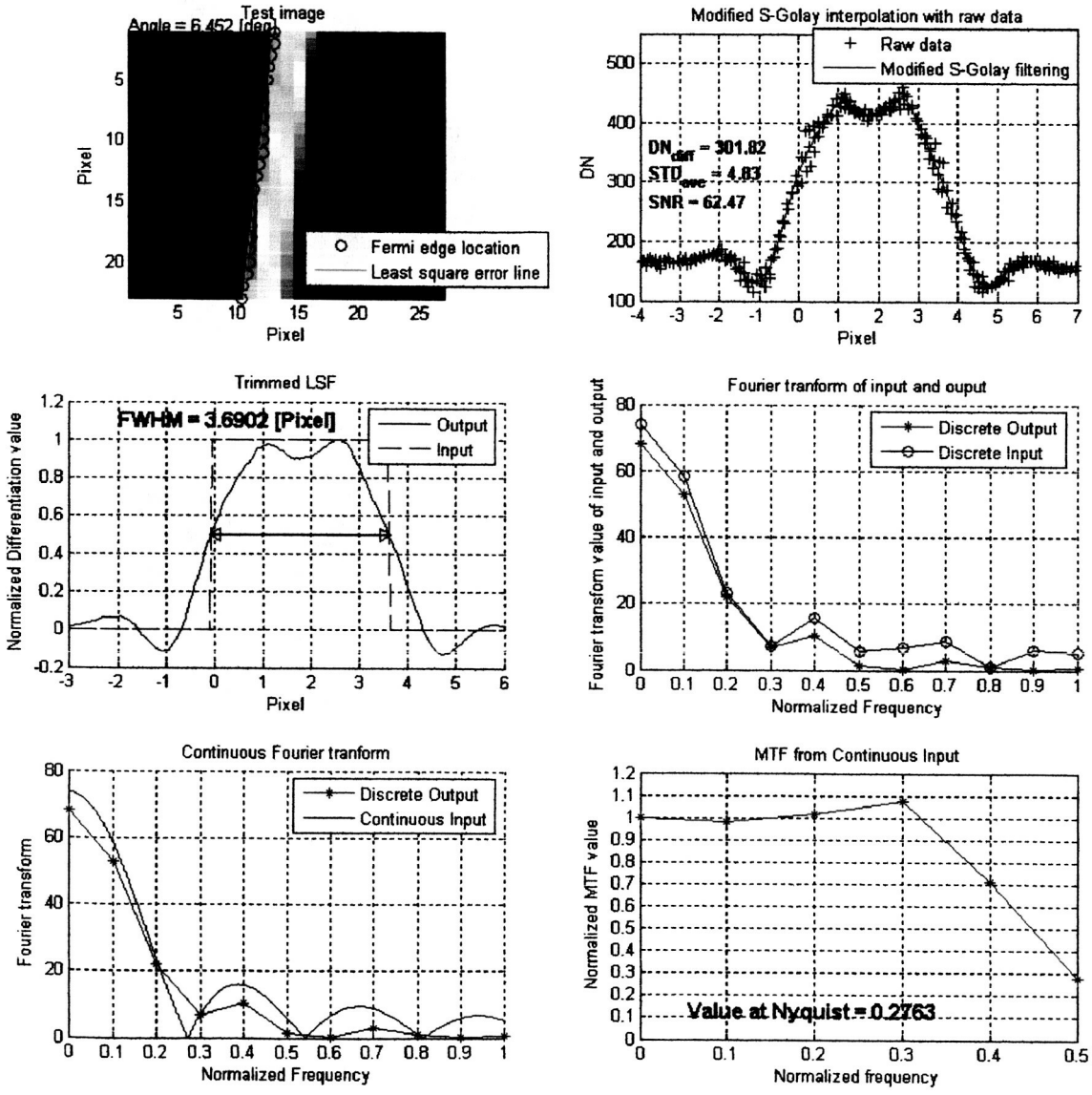

Figure B.8 Quickbird blue tarp target in blue band on October 21, 2003 with MTF interpolation.

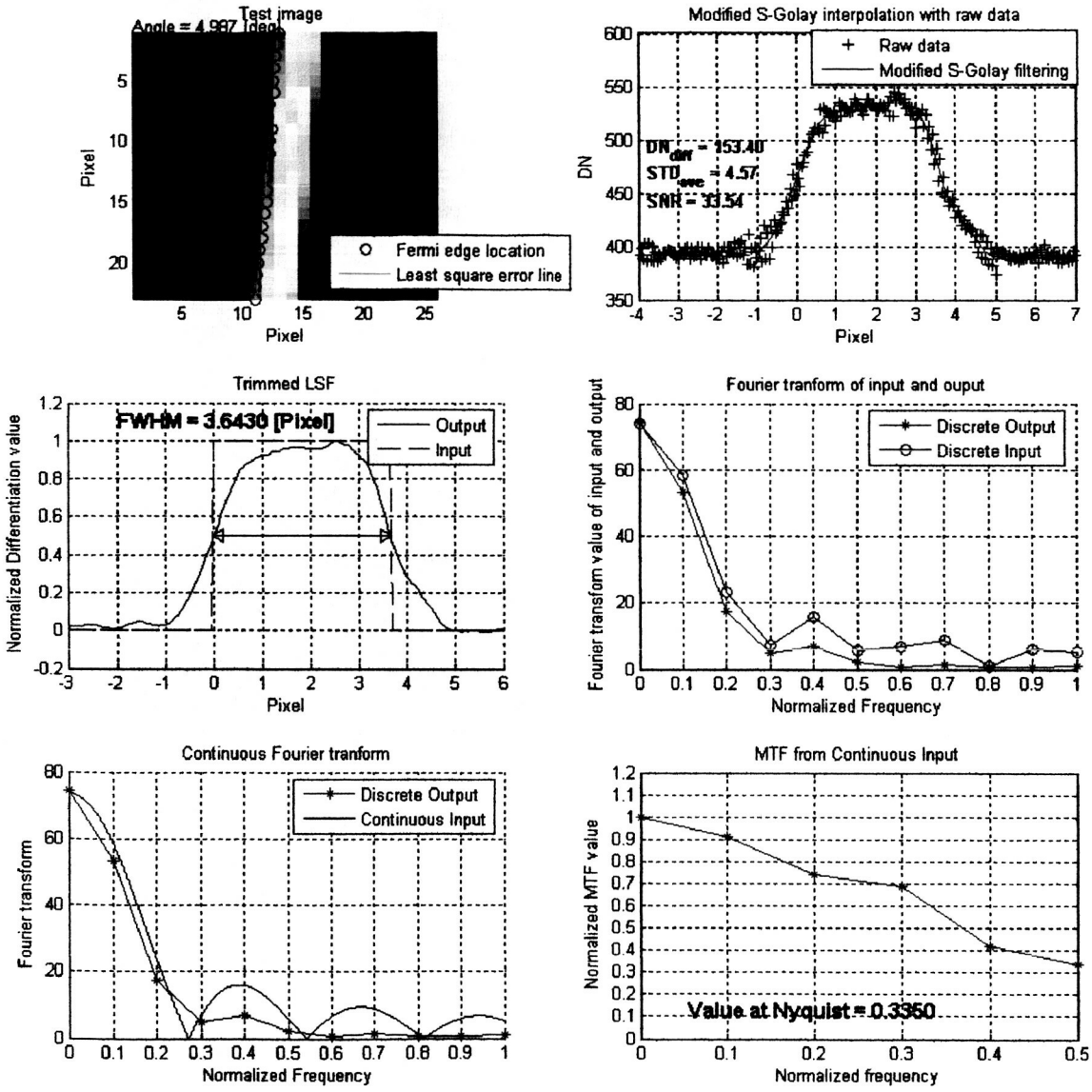

Figure B.9 Quickbird blue tarp target in green band on August 23, 2003 with cubic convolution interpolation.

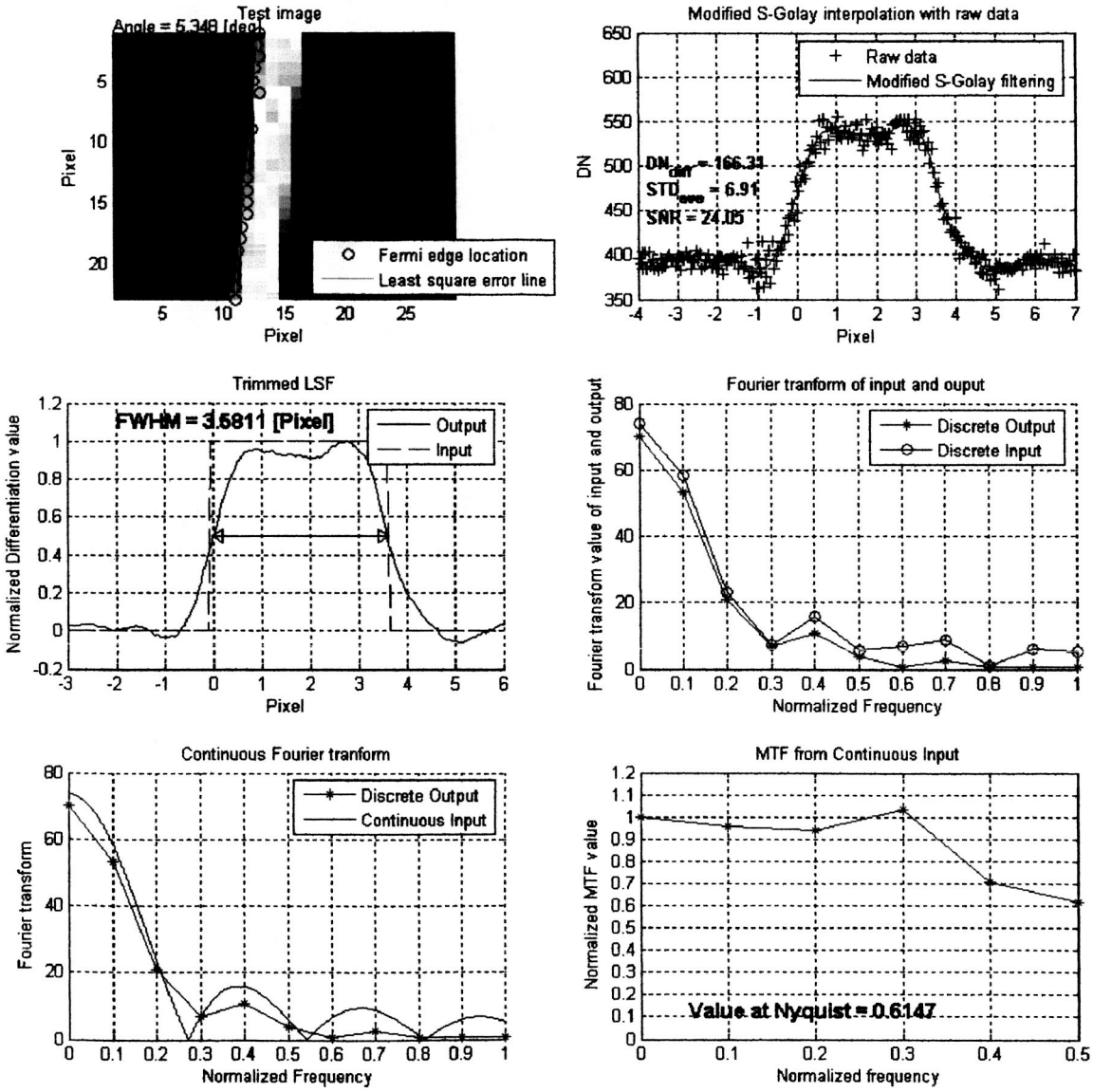

Figure B.10 Quickbird blue tarp target in green band on August 23, 2003 with MTF interpolation.

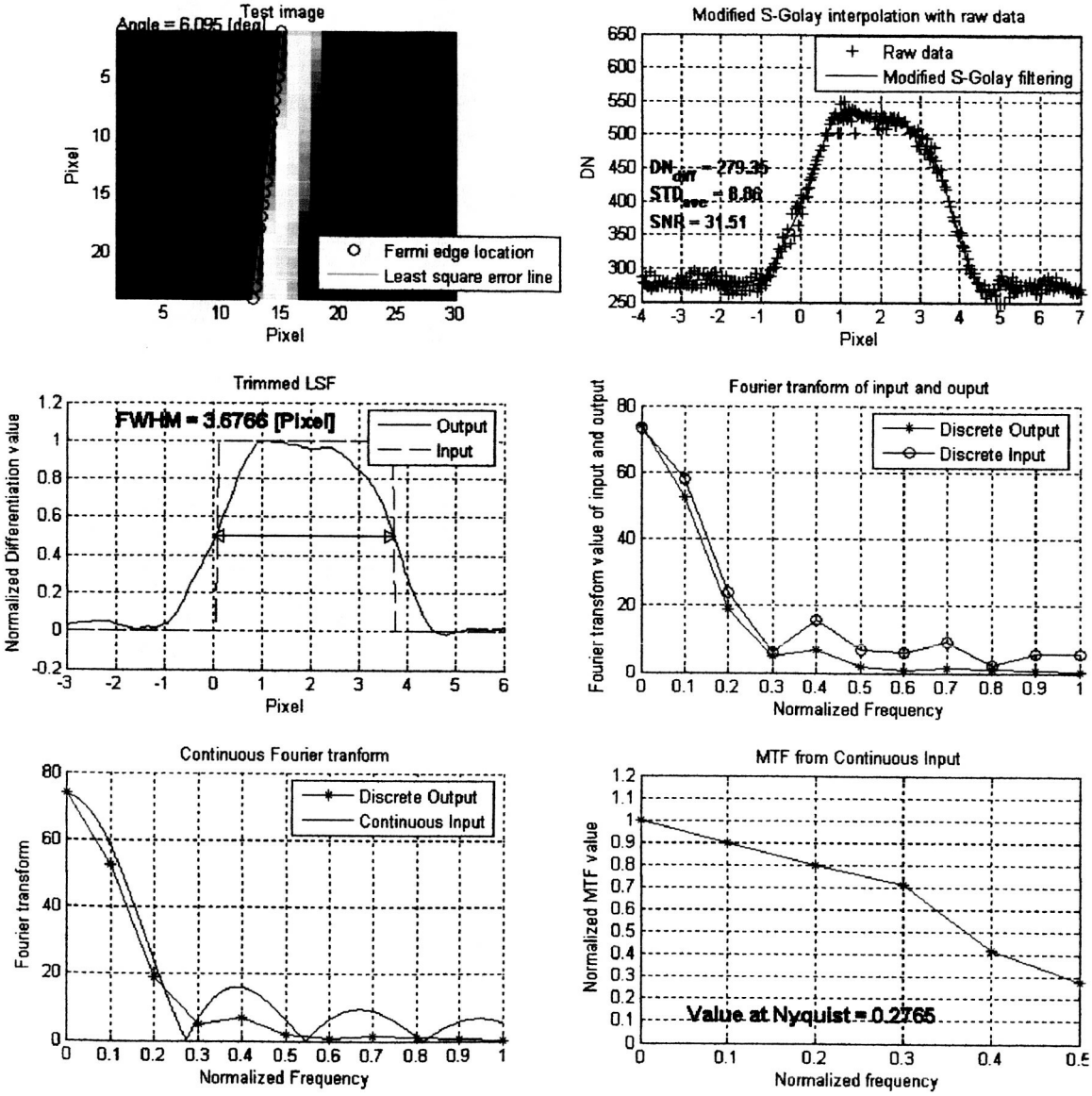

Figure B.11 Quickbird blue tarp target in green band on September 15, 2003 with cubic convolution interpolation.

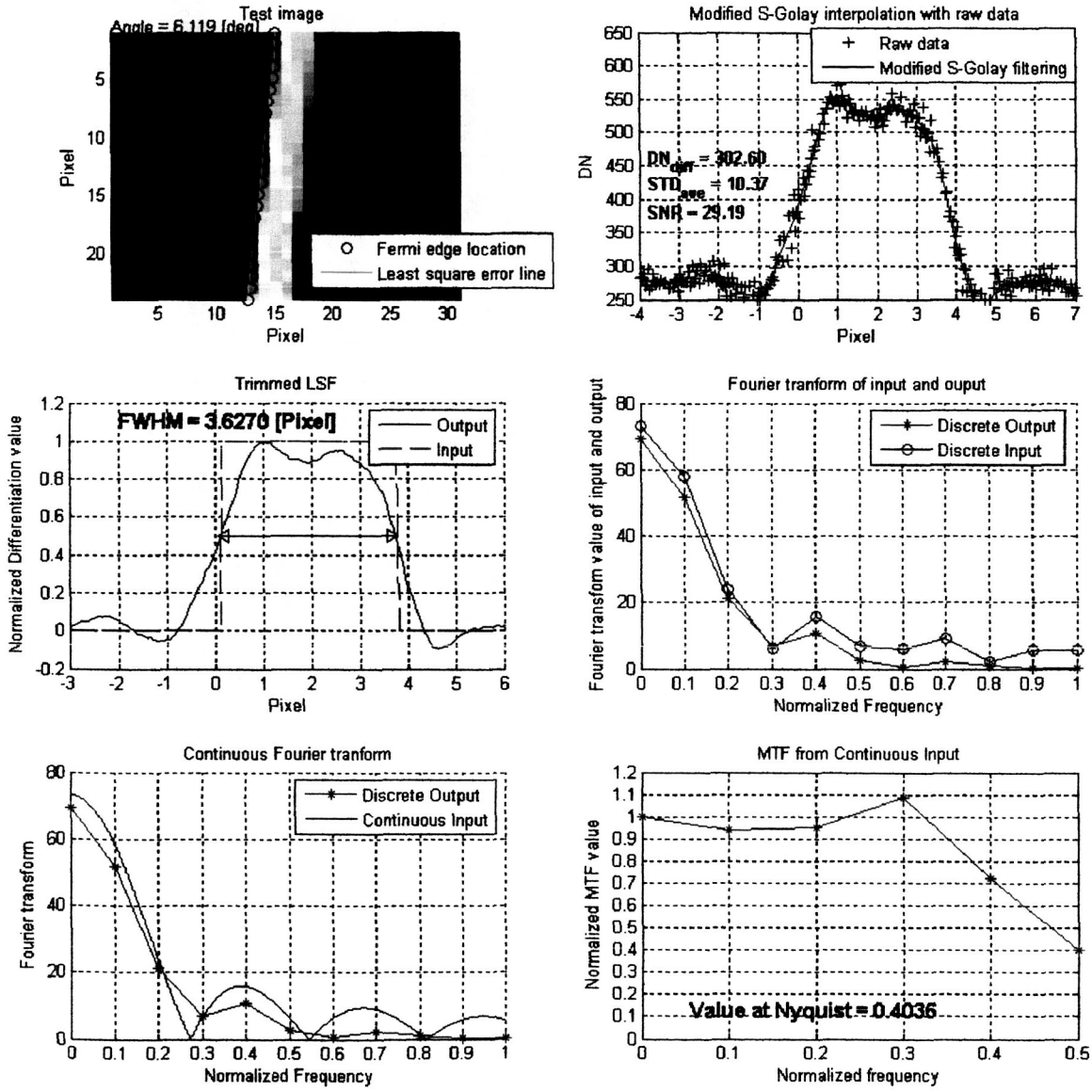

Figure B.12 Quickbird blue tarp target in green band on September 15, 2003 with MTF interpolation.

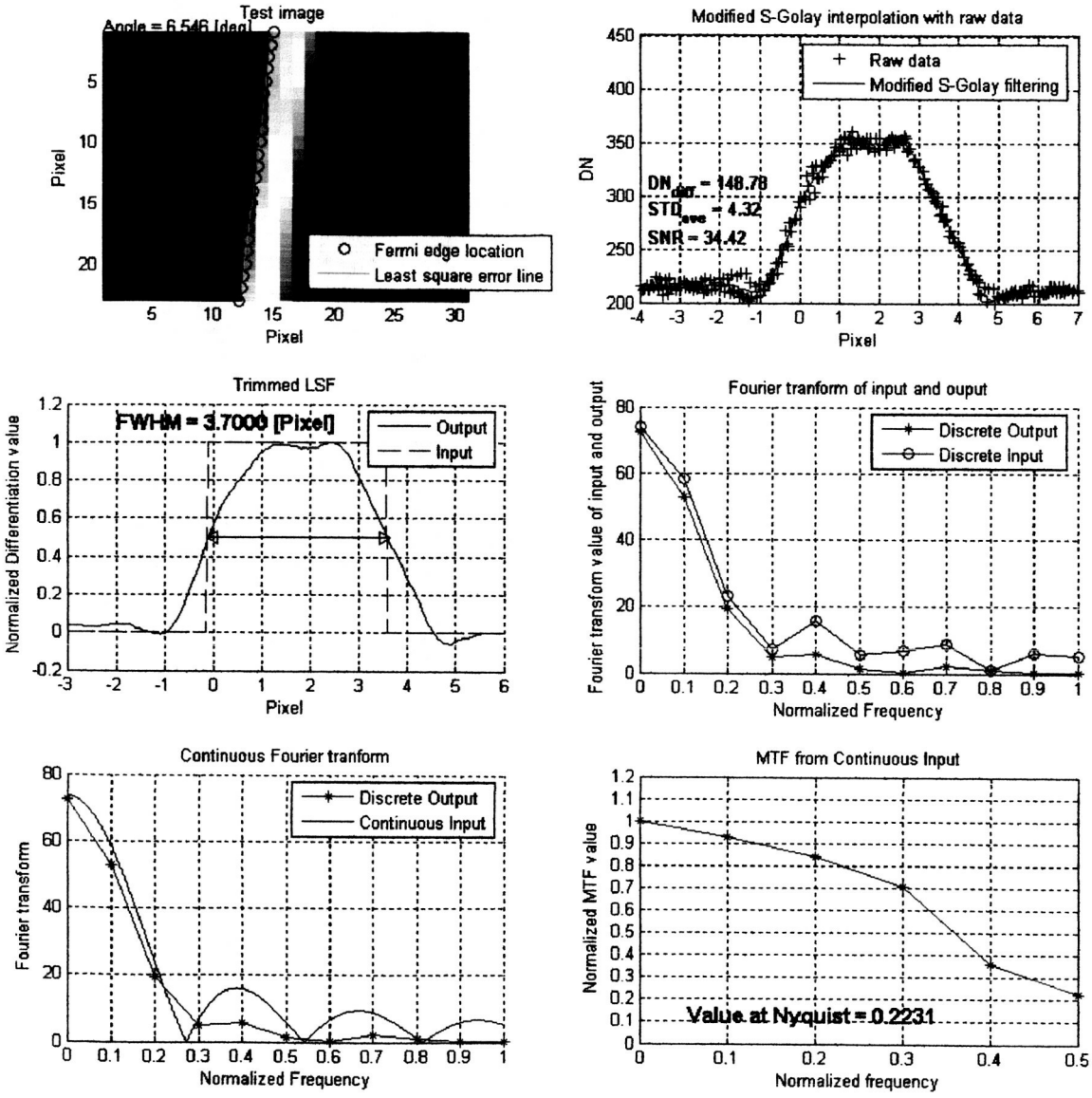

Figure B.13 Quickbird blue tarp target in green band on October 21, 2003 with cubic convolution interpolation.

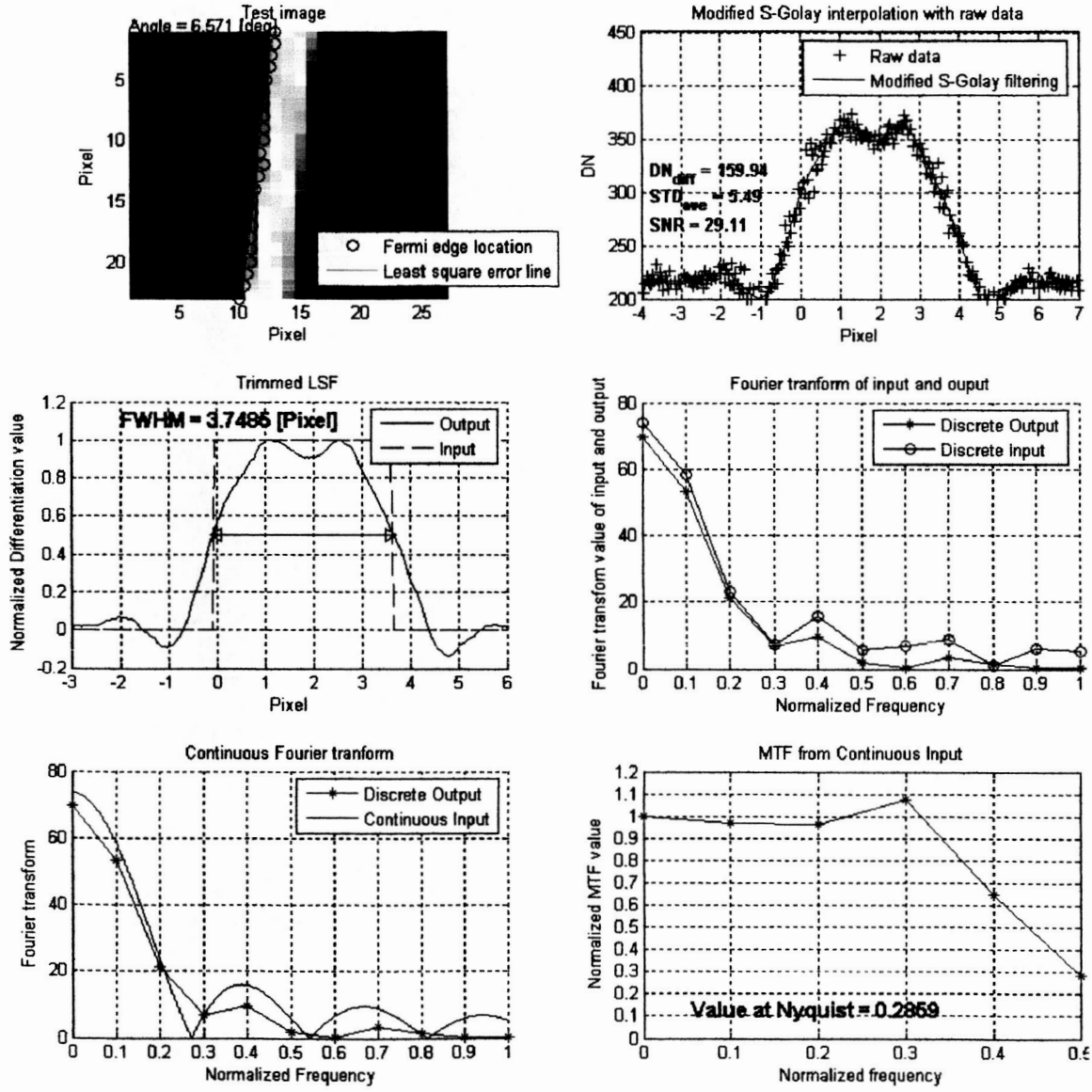

Figure B.14 Quickbird blue tarp target in green band on October 21, 2003 with MTF interpolation.

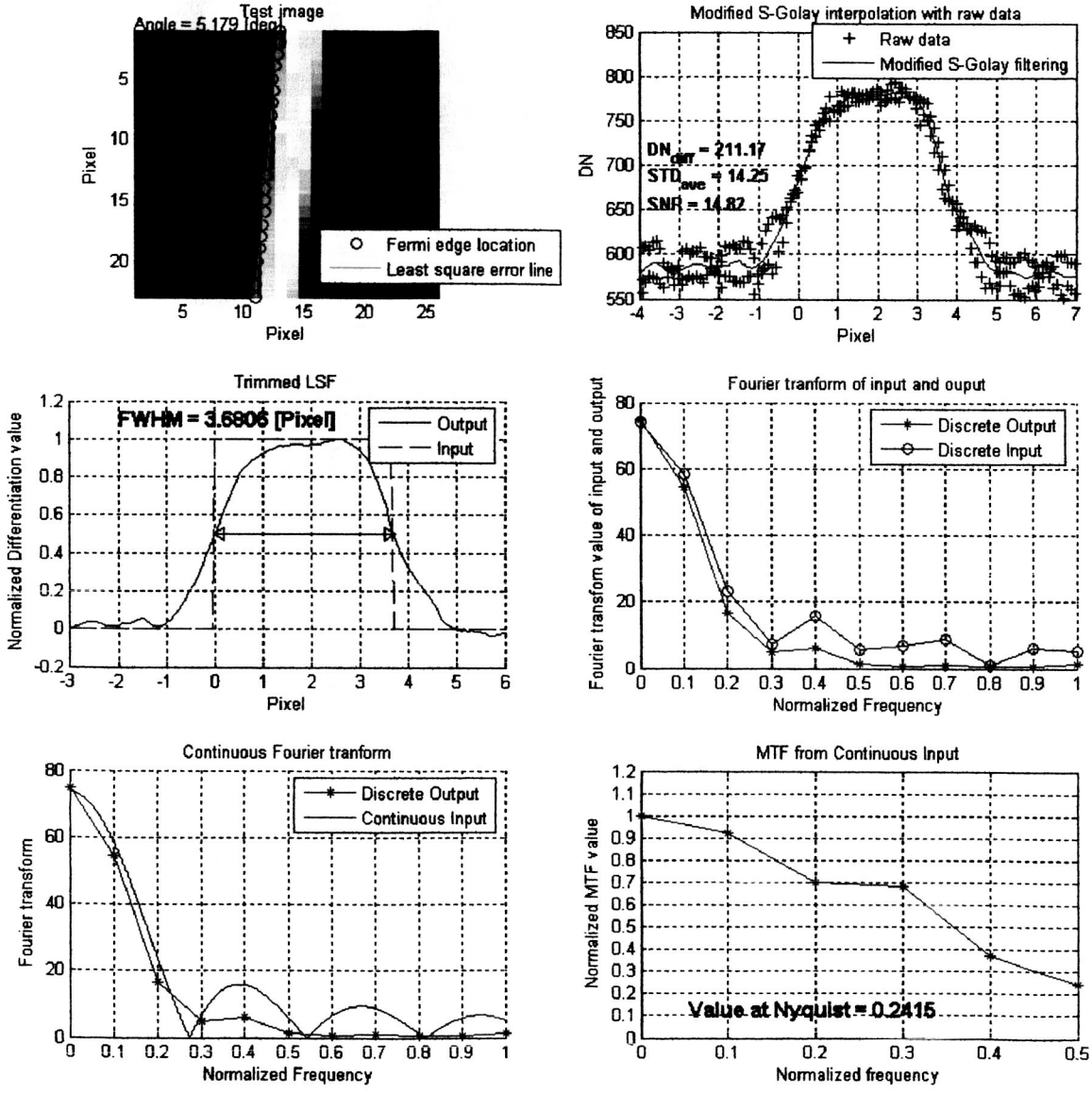

Figure B.15 Quickbird blue tarp target in NIR band on August 23, 2003 with cubic convolution interpolation.

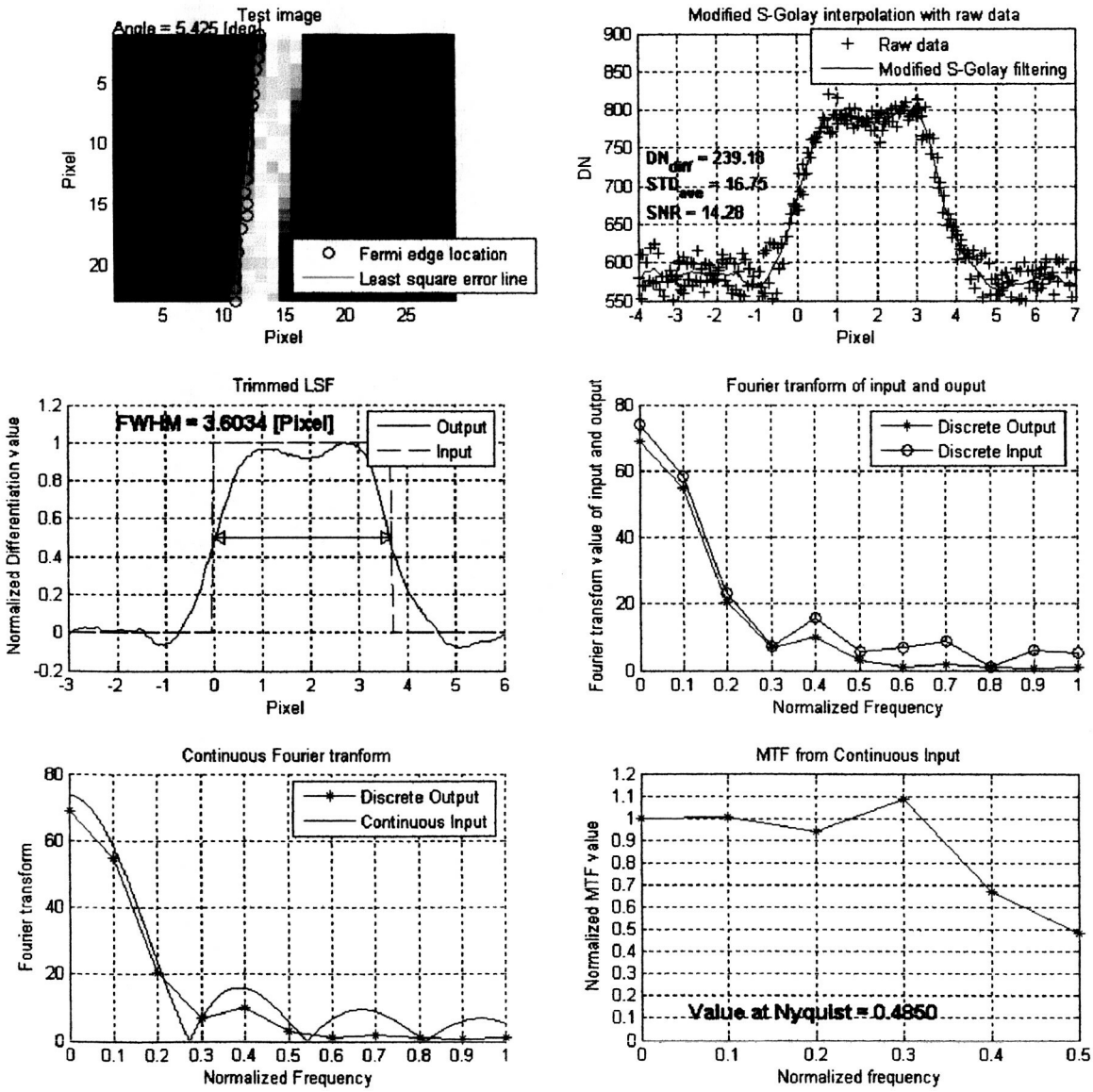

Figure B.16 Quickbird blue tarp target in NIR band on August 23, 2003 with MTF interpolation.

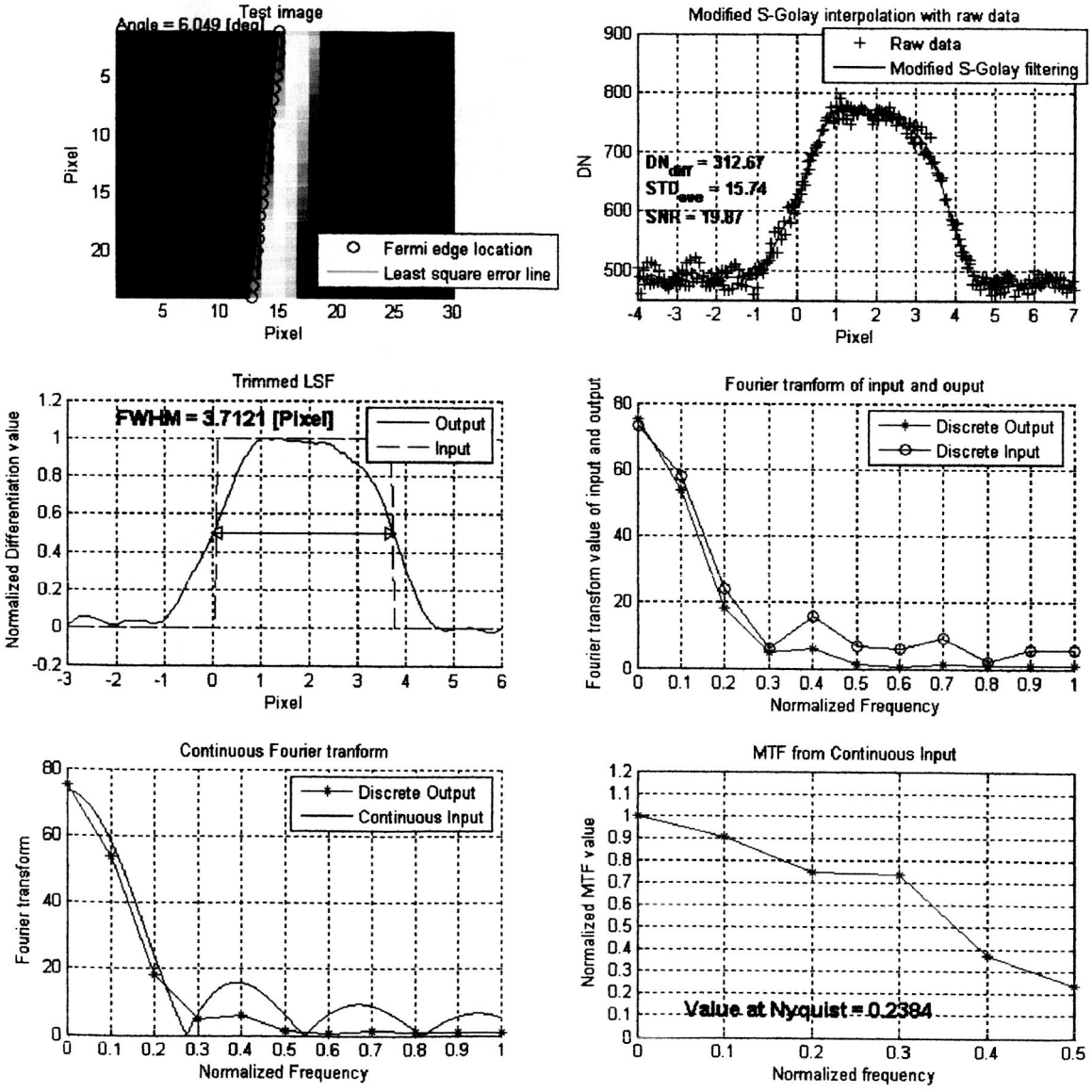

Figure B.17 Quickbird blue tarp target in NIR band on September 15, 2003 with cubic convolution interpolation.

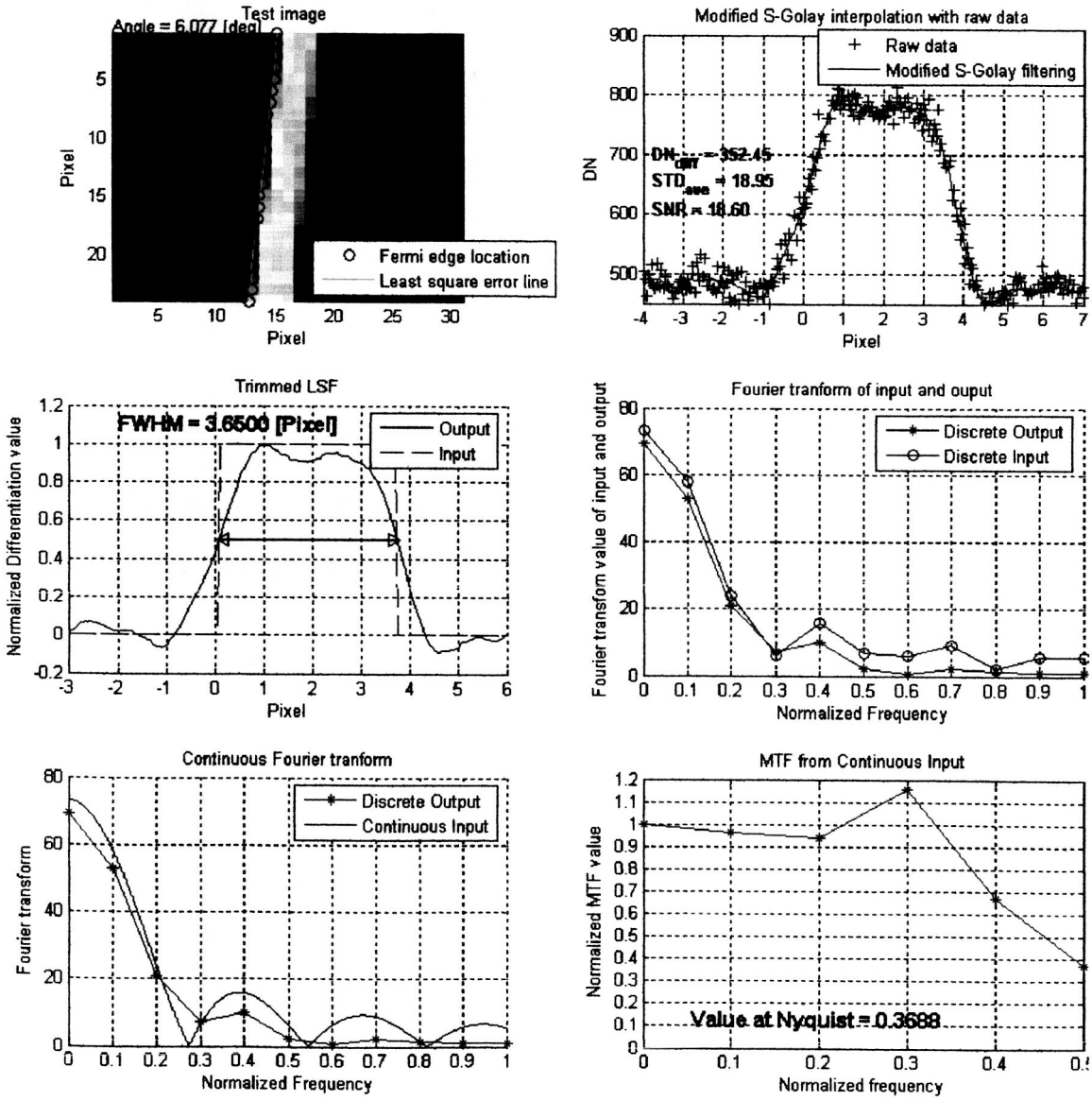

Figure B.18 Quickbird blue tarp target in NIR band on September 15, 2003 with MTF interpolation.

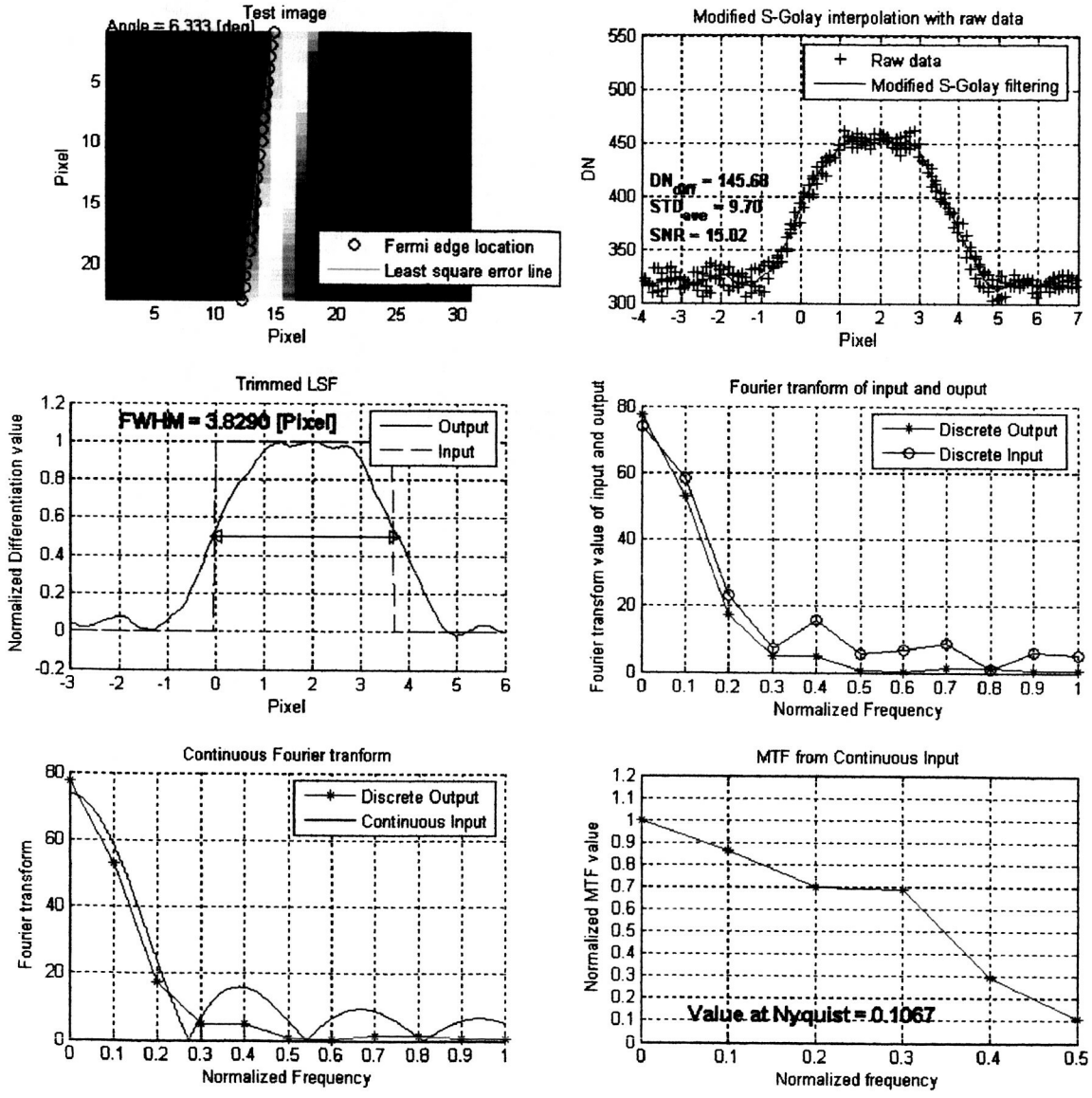

Figure B.19 Quickbird blue tarp target in NIR band on October 21, 2003 with cubic convolution interpolation.

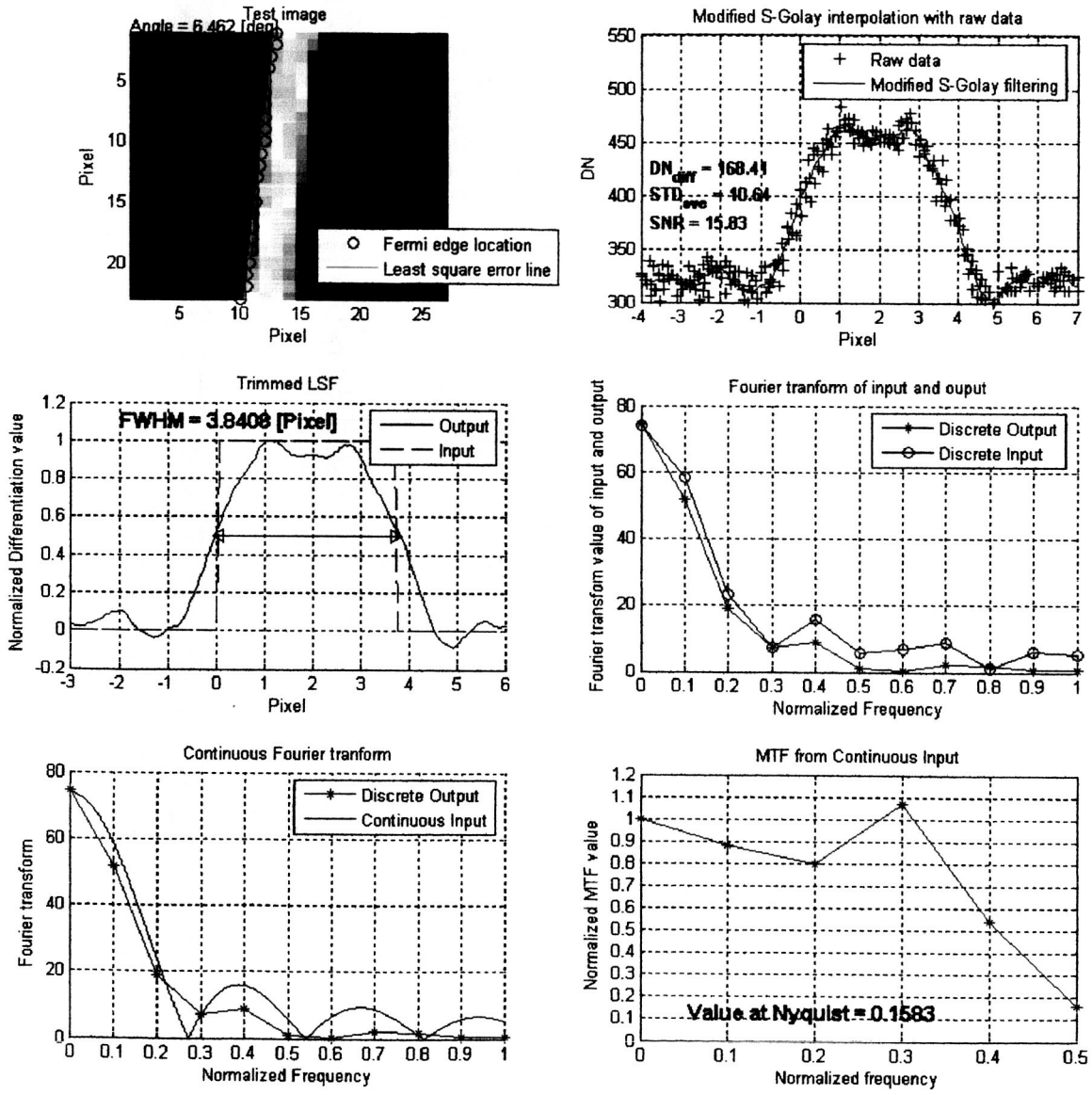

Figure B.20 Quickbird blue tarp target in NIR band on October 21, 2003 with MTF interpolation.

APPENDIX C

Peak Position Estimation of mirror images:

Brookings South Dakota

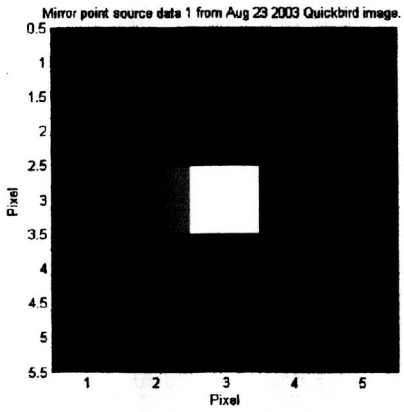

(a) Point source mirror 1

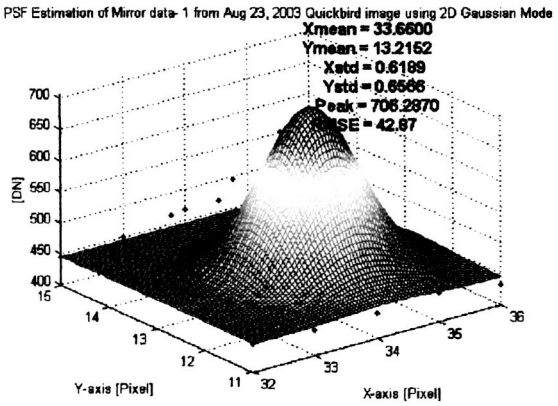

(b) 2-D model and raw data

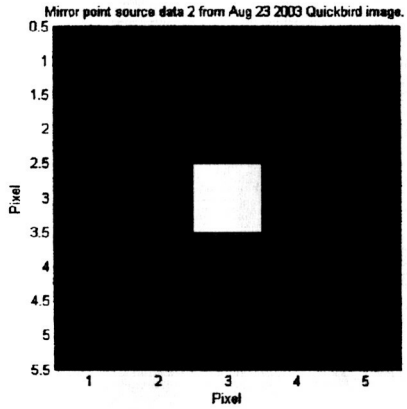

(c) Point source mirror 2

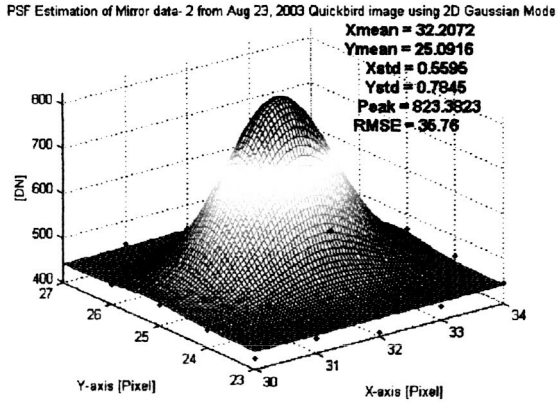

(d) 2-D model and raw data

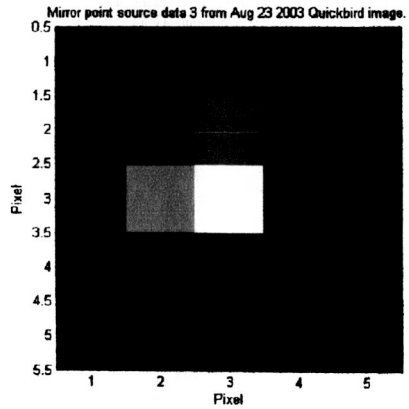

(e) Point source mirror 3

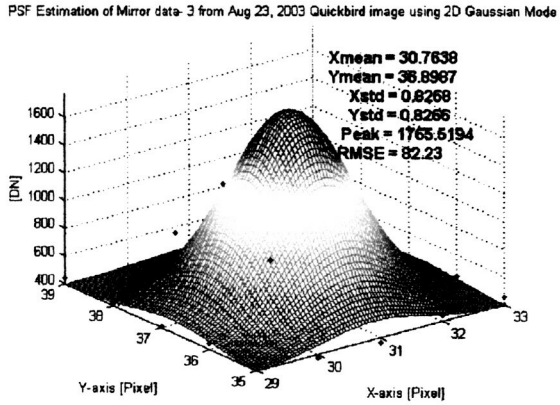

(f) 2-D model and raw data

Figure C.1 August 23, 2003 Quickbird point source images and their peak position estimation using 2-D Gaussian model using mirrors 1, 2, and 3.

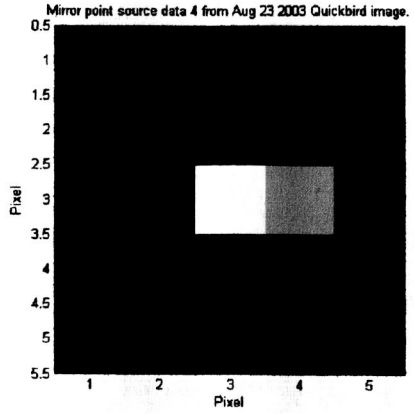

(a) Point source mirror 4

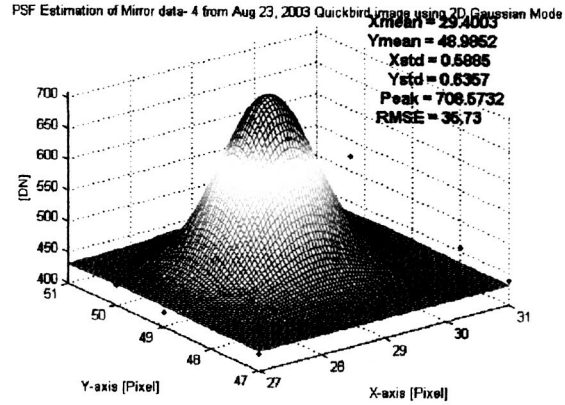

(b) 2-D model and raw data

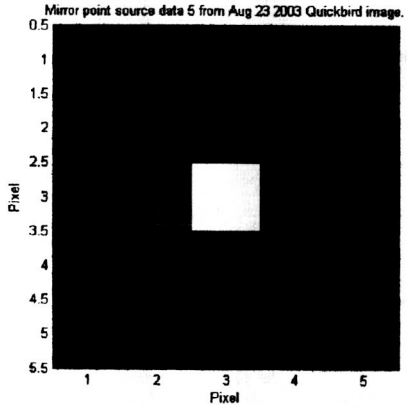

(c) Point source mirror 5

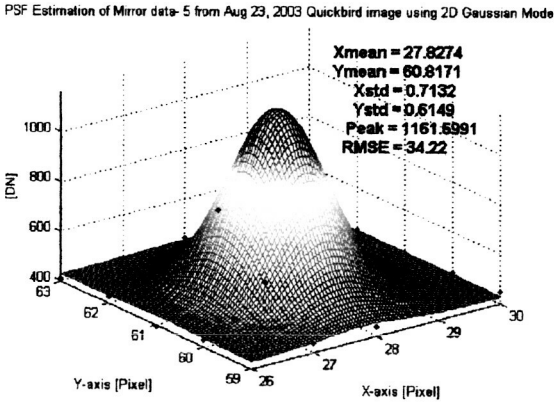

(d) 2-D model and raw data

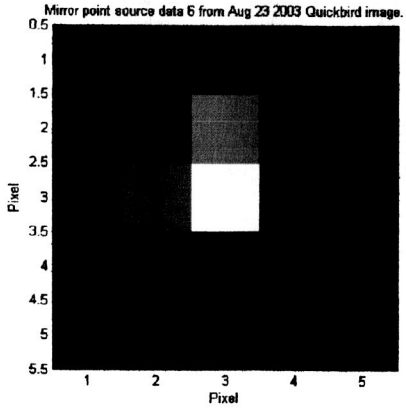

(e) Point source mirror 6

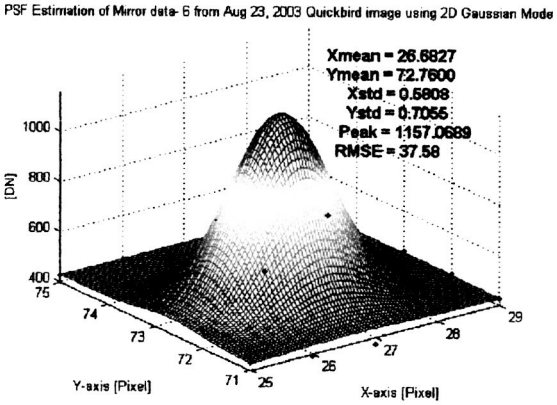

(f) 2-D model and raw data

Figure C.2 August 23, 2003 Quickbird point source images and their peak position estimation using 2-D Gaussian model using mirrors 4, 5, and 6.

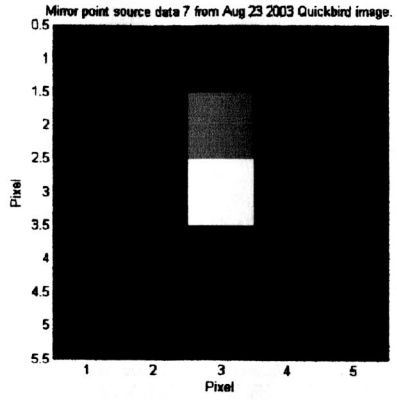

(a) Point source mirror 7

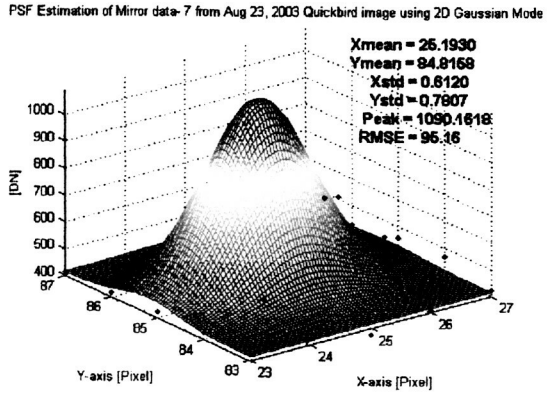

(b) 2-D model and raw data

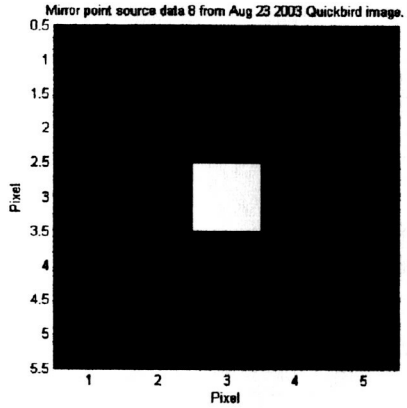

(c) Point source mirror 8

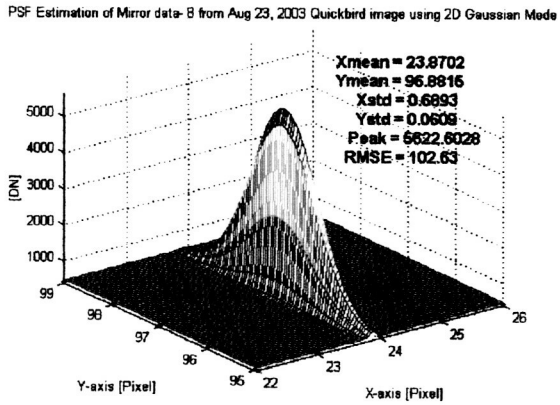

(d) 2-D model and raw data

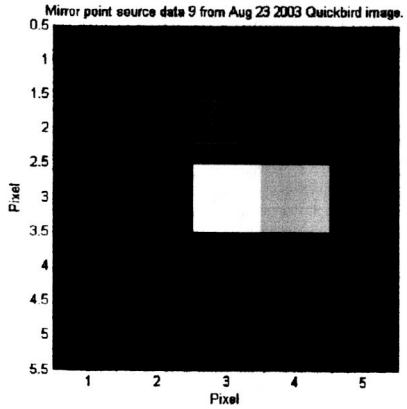

(e) Point source mirror 9

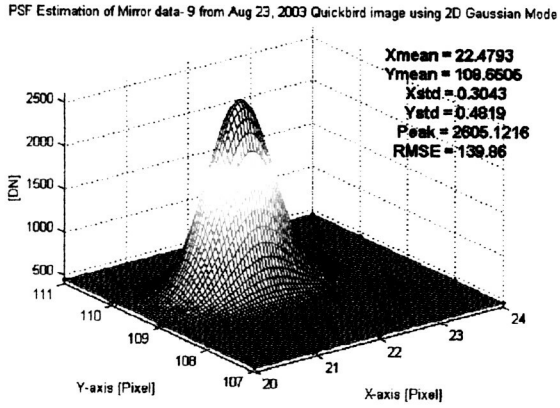

(f) 2-D model and raw data

Figure C.3 August 23, 2003 Quickbird point source images and their peak position estimation using 2-D Gaussian model using mirrors 7, 8, and 9.

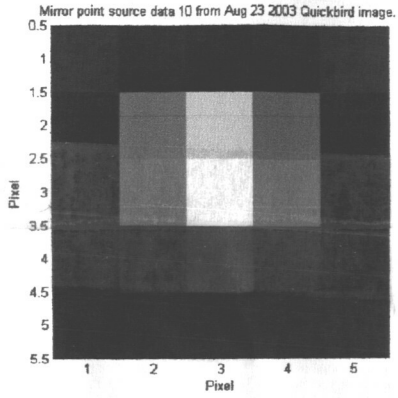

(a) Point source mirror 10

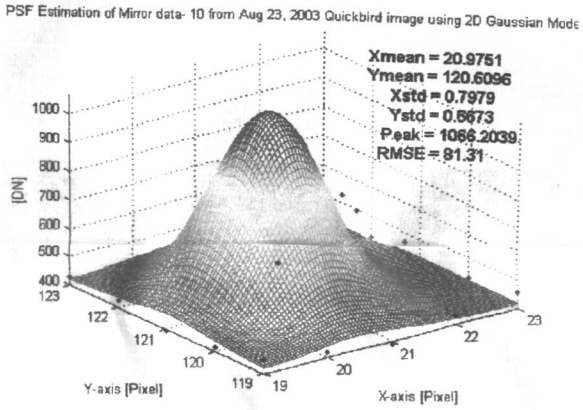

(b) 2-D model and raw data

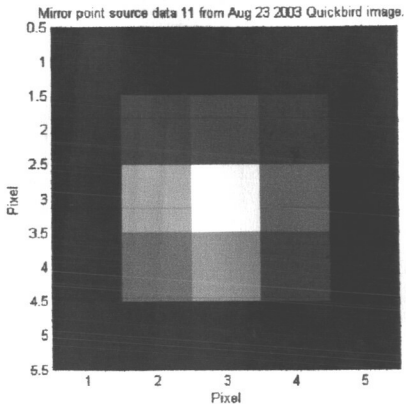

(c) Point source mirror 11

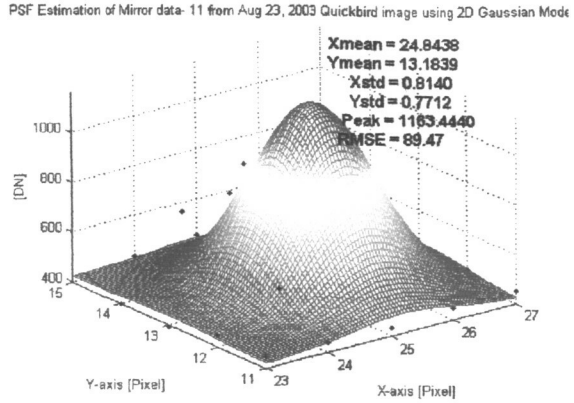

(d) 2-D model and raw data

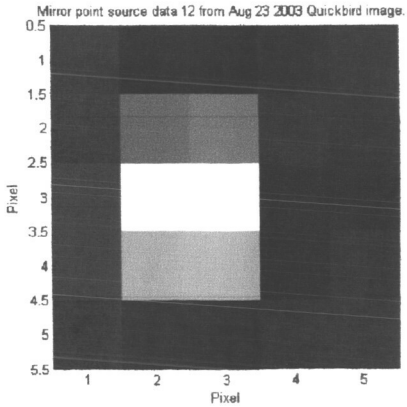

(e) Point source mirror 12

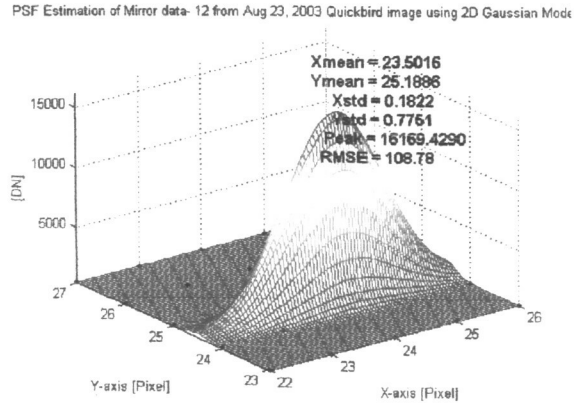

(f) 2-D model and raw data

Figure C.4 August 23, 2003 Quickbird point source images and their peak position estimation using 2-D Gaussian model using mirrors 10, 11, and 12.

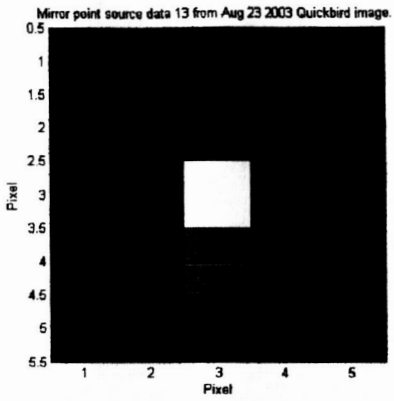

(a) Point source mirror 13

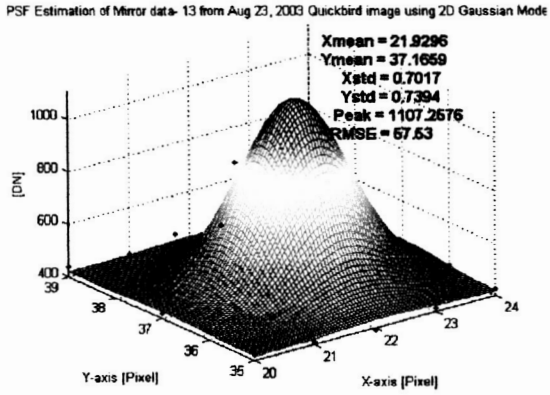

(b) 2-D model and raw data

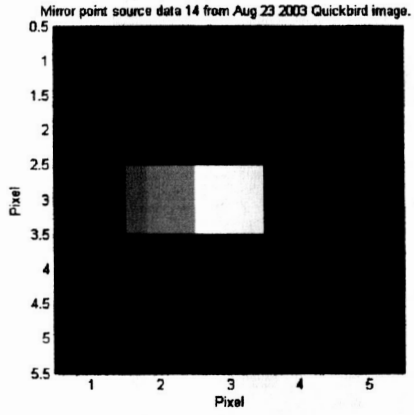

(c) Point source mirror 14

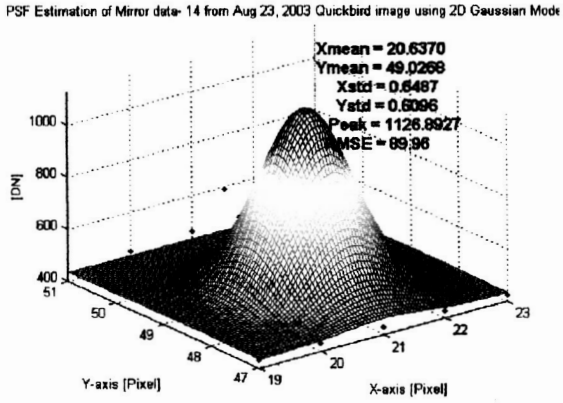

(d) 2-D model and raw data

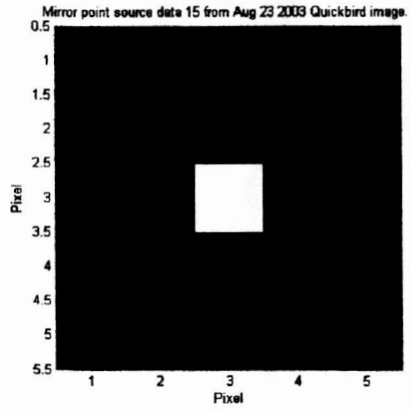

(e) Point source mirror 15

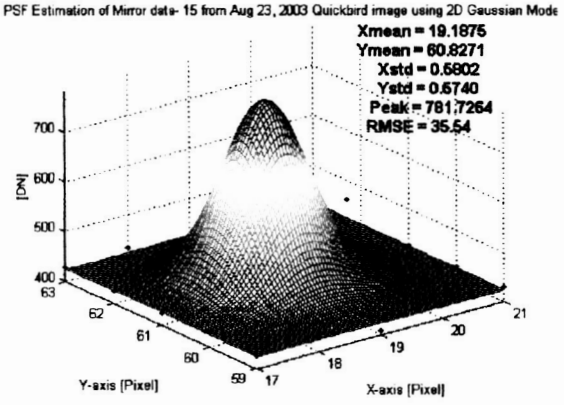

(f) 2-D model and raw data

Figure C.5 August 23, 2003 Quickbird point source images and their peak position estimation using 2-D Gaussian model using mirrors 13, 14, and 15.

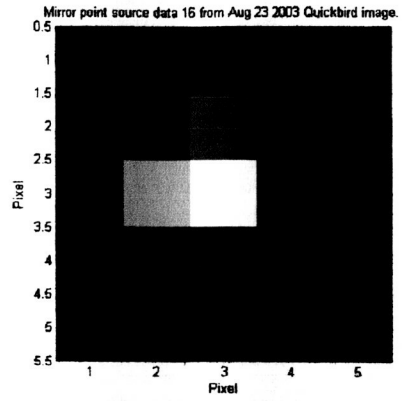

(a) Point source mirror 16

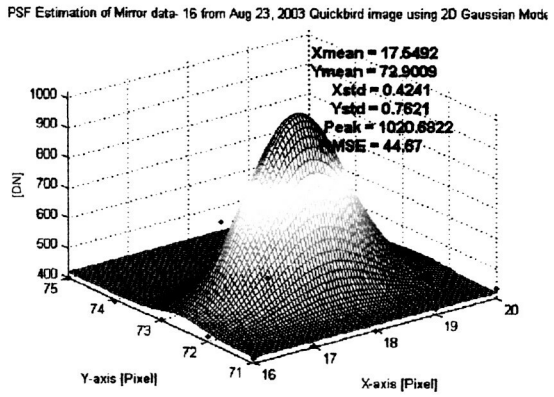

(b) 2-D model and raw data

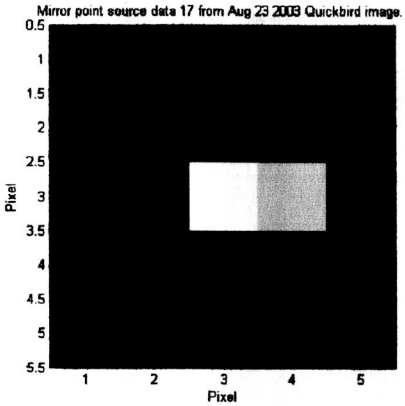

(c) Point source mirror 17

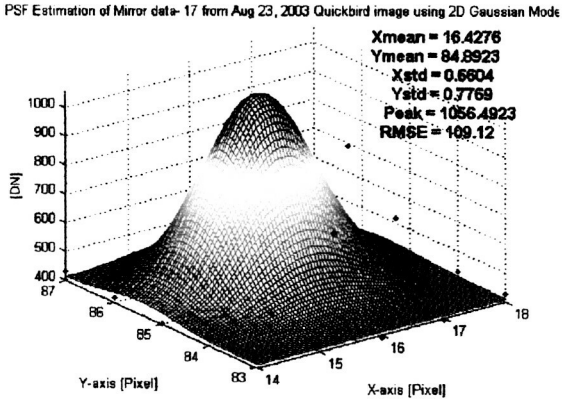

(d) 2-D model and raw data

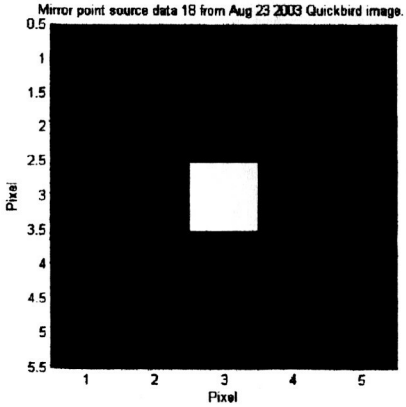

(e) Point source mirror 18

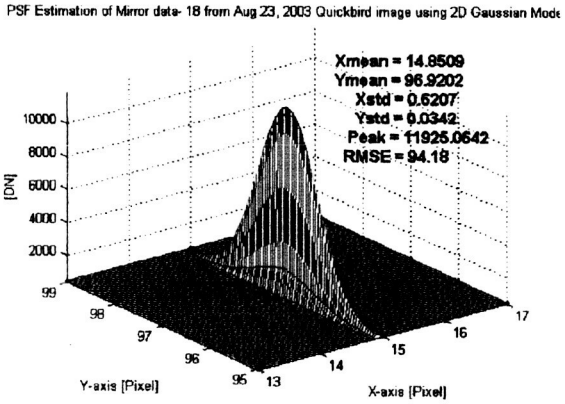

(f) 2-D model and raw data

Figure C.6 August 23, 2003 Quickbird point source images and their peak position estimation using 2-D Gaussian model using mirrors 16, 17, and 18.

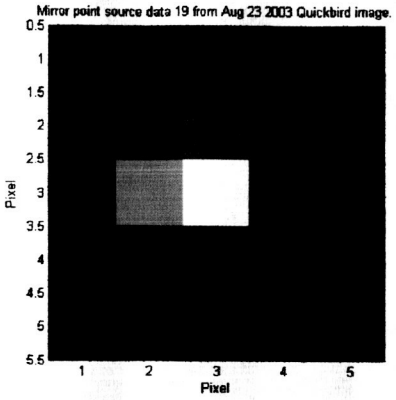

(a) Point source mirror 19

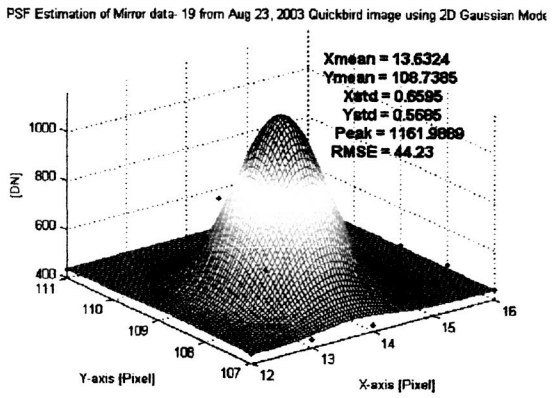

(b) 2-D model and raw data

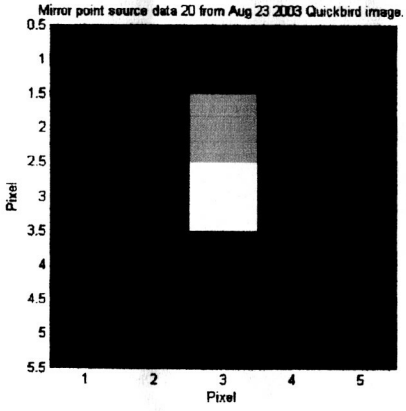

(c) Point source mirror 20

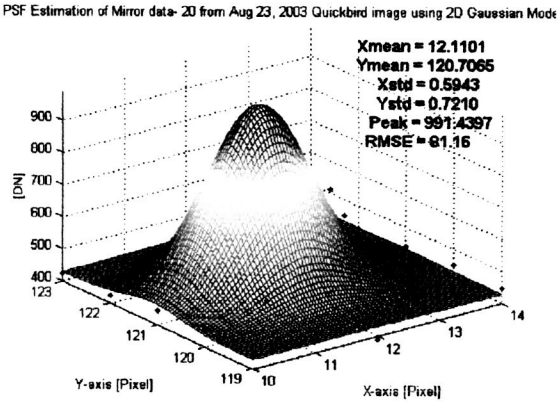

(d) 2-D model and raw data

Figure C.7 August 23, 2003 Quickbird point source images and their peak position estimation using 2-D Gaussian model using mirrors 19 and 20.

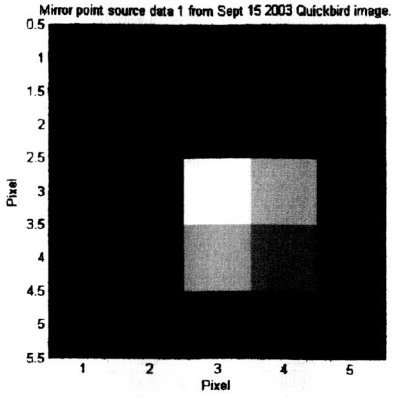

(a) Point source mirror 1

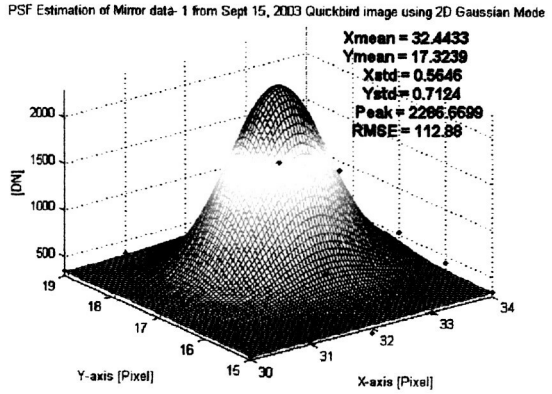

(b) 2-D model and raw data

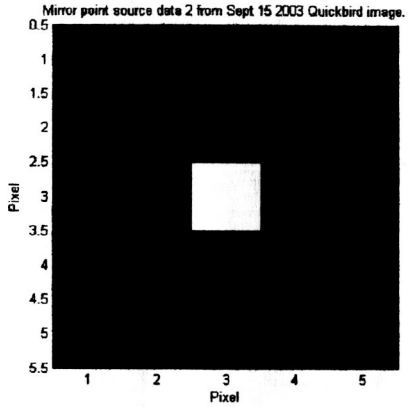

(c) Point source mirror 2

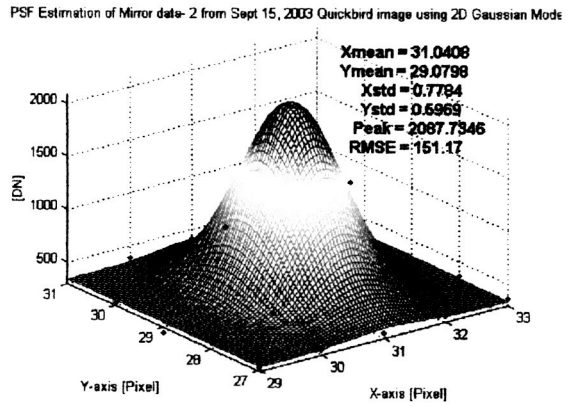

(d) 2-D model and raw data

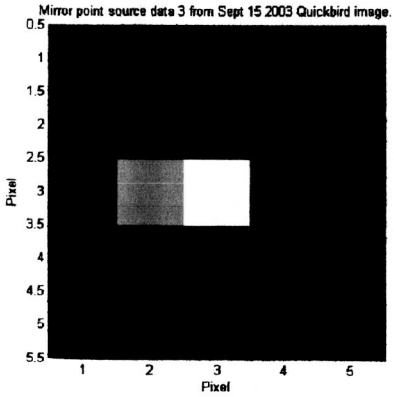

(e) Point source mirror 3

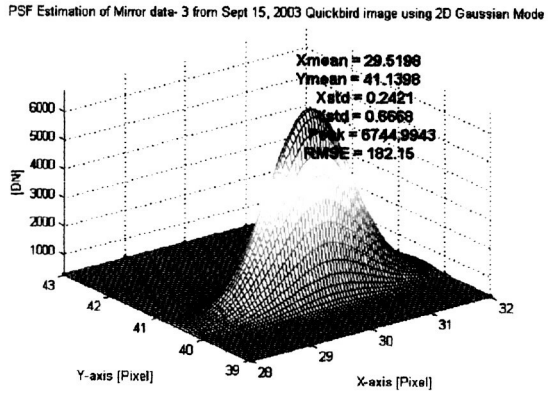

(f) 2-D model and raw data

Figure C.8 Sept 15, 2003 Quickbird point source images and their peak position estimation using 2-D Gaussian model using mirrors 1, 2, and 3.

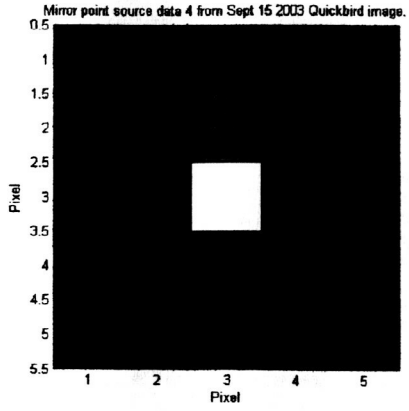

(a) Point source mirror 4

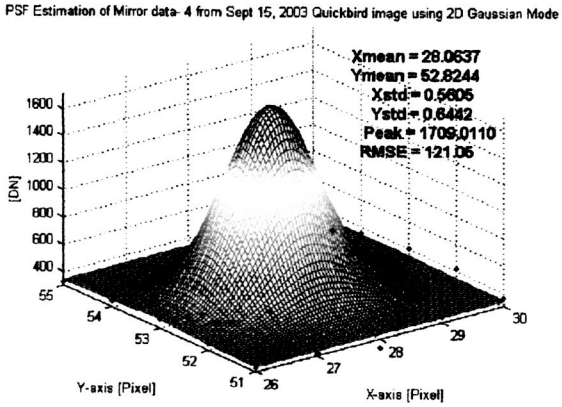

(b) 2-D model and raw data

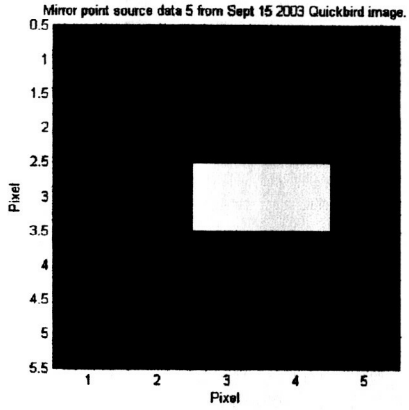

(c) Point source mirror 5

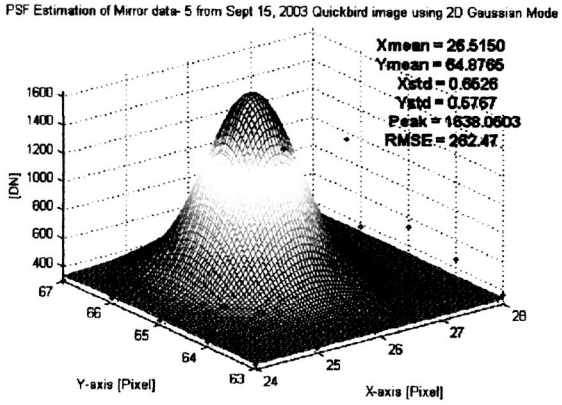

(d) 2-D model and raw data

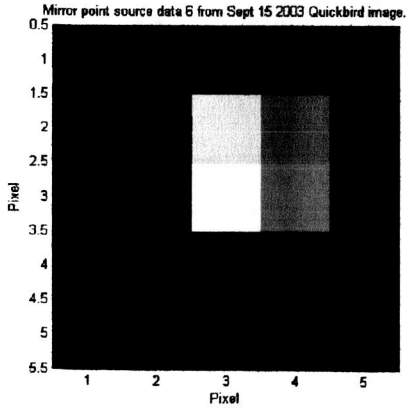

(e) Point source mirror 6

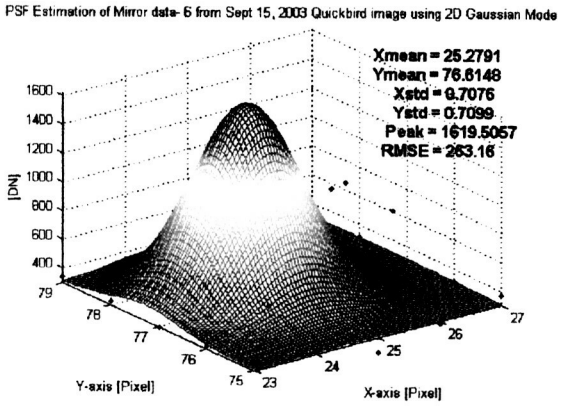

(f) 2-D model and raw data

Figure C.9 September 15, 2003 Quickbird point source images and their peak position estimation using 2-D Gaussian model using mirrors 4, 5 and 6.

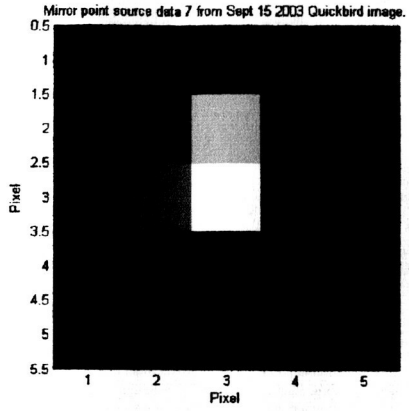

(a) Point source mirror 7

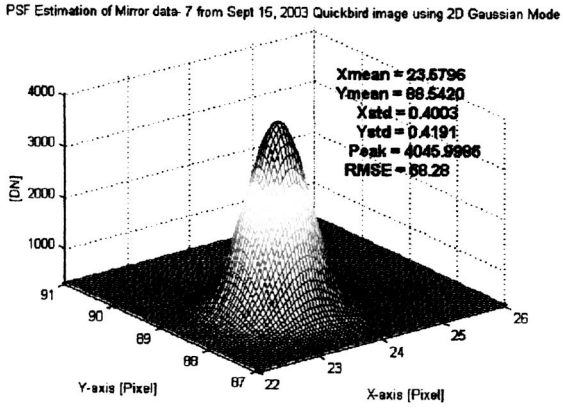

(b) 2-D model and raw data

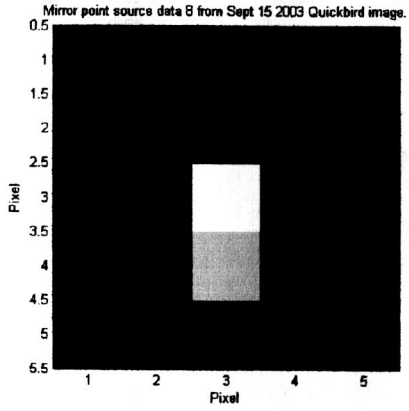

(c) Point source mirror 8

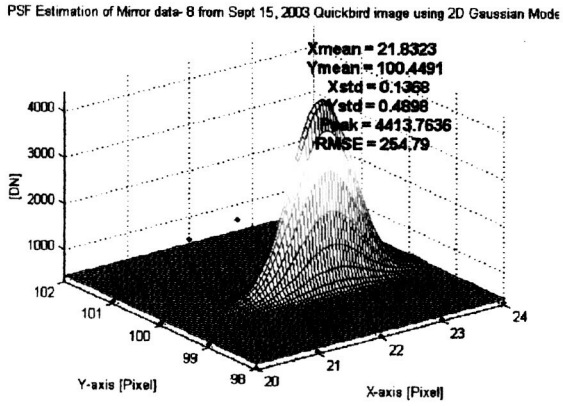

(d) 2-D model and raw data

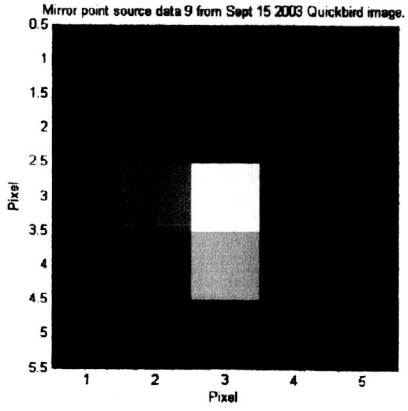

(e) Point source mirror 9

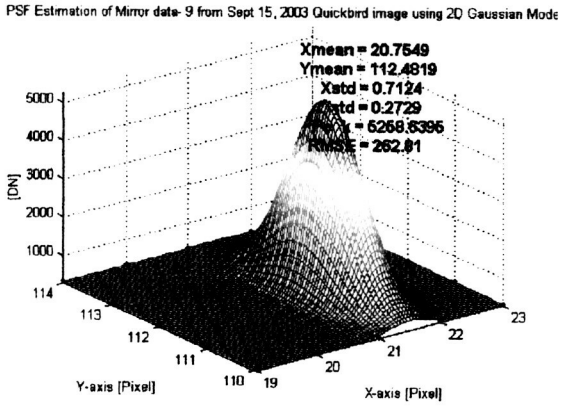

(f) 2-D model and raw data

Figure C.10 September 15, 2003 Quickbird point source images and their peak position estimation using 2-D Gaussian model using mirrors 7, 8, and 9.

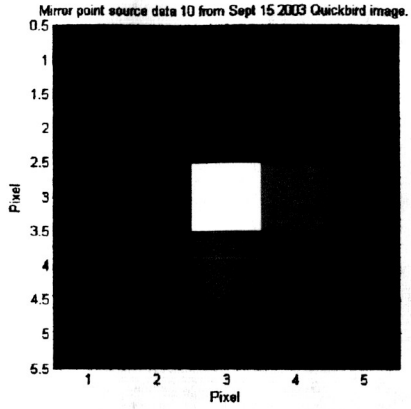

(a) Point source mirror 10

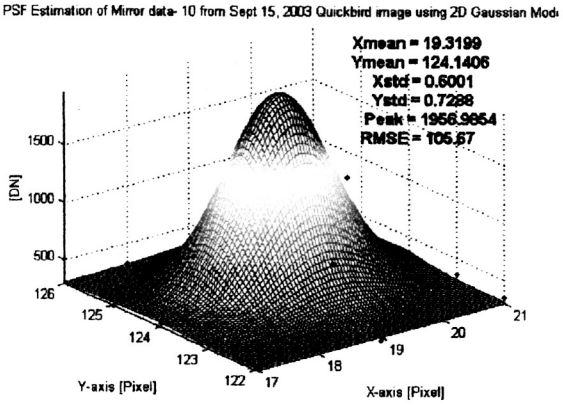

(b) 2-D model and raw data

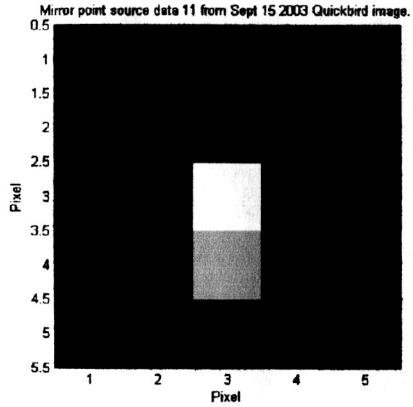

(c) Point source mirror 11

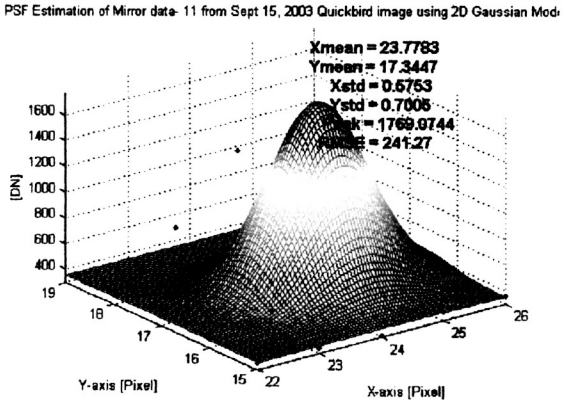

(d) 2-D model and raw data

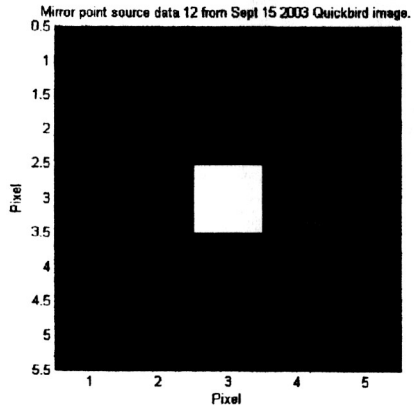

(e) Point source mirror 12

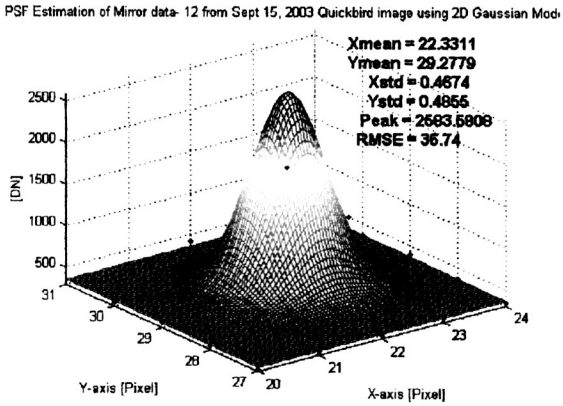

(f) 2-D model and raw data

Figure C.11 September 15, 2003 Quickbird point source images and their peak position estimation using 2-D Gaussian model using mirrors 10, 11, and 12.

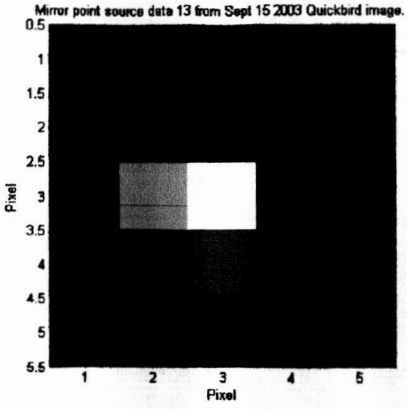

(a) Point source mirror 13

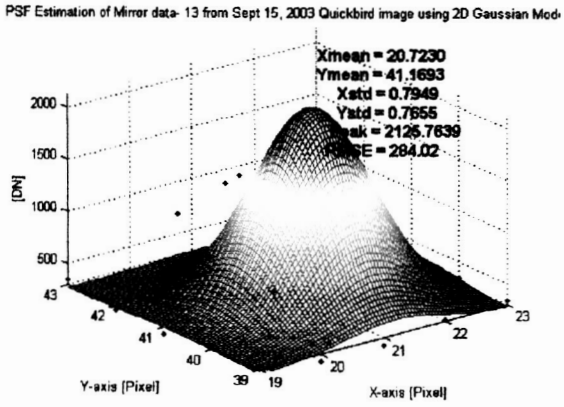

(b) 2-D model and raw data

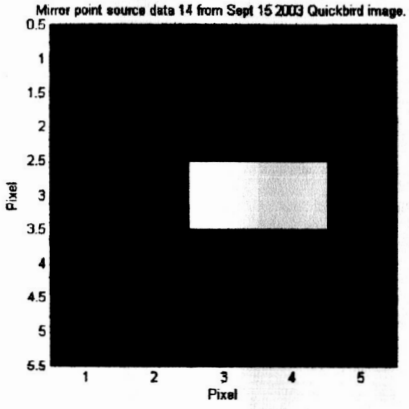

(c) Point source mirror 14

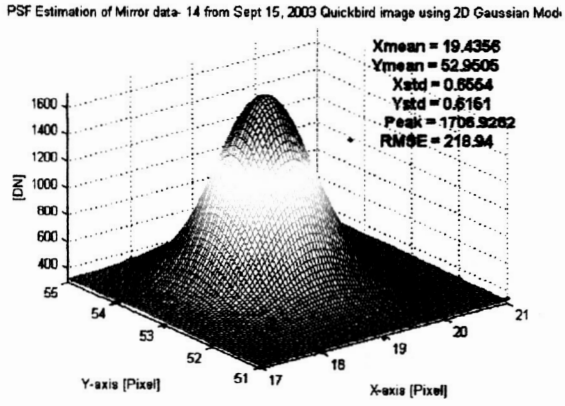

(d) 2-D model and raw data

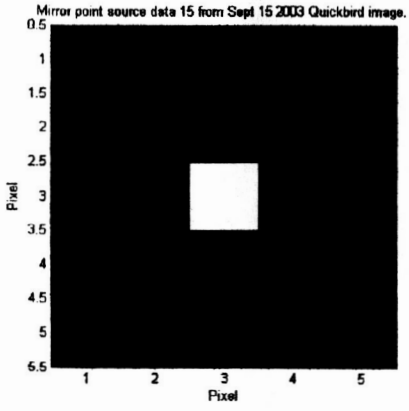

(e) Point source mirror 15

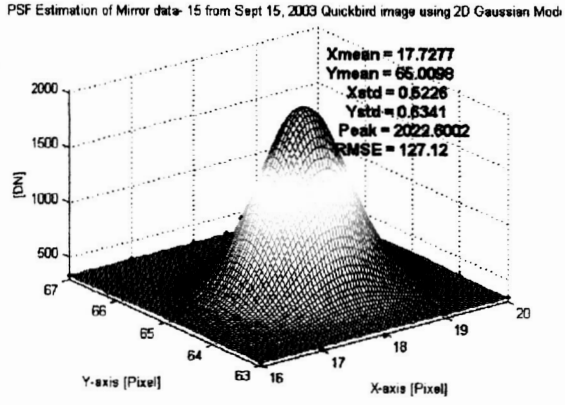

(f) 2-D model and raw data

Figure C.12 September 15, 2003 Quickbird point source images and their peak position estimation using 2-D Gaussian model using mirrors 13, 14, and 15.

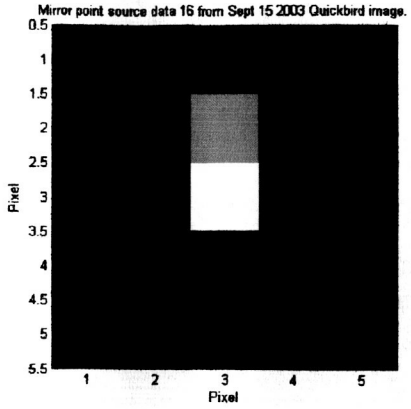

(a) Point source mirror 16

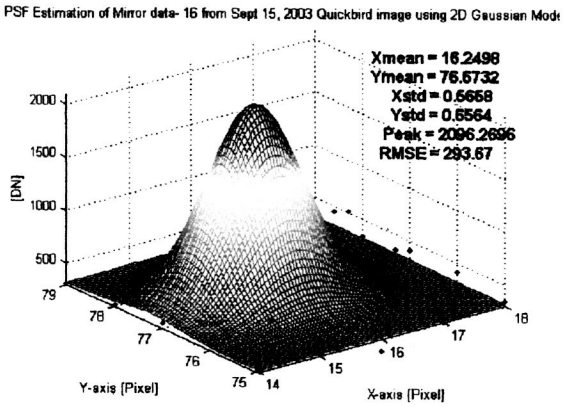

(b) 2-D model and raw data

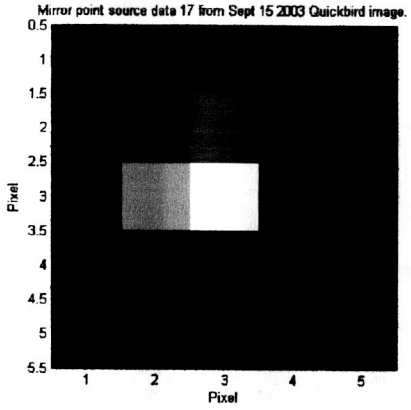

(c) Point source mirror 17

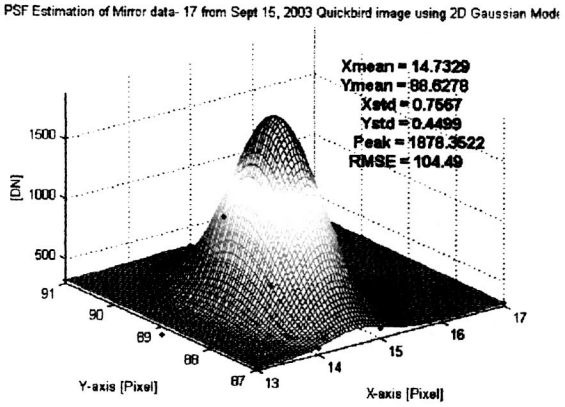

(d) 2-D model and raw data

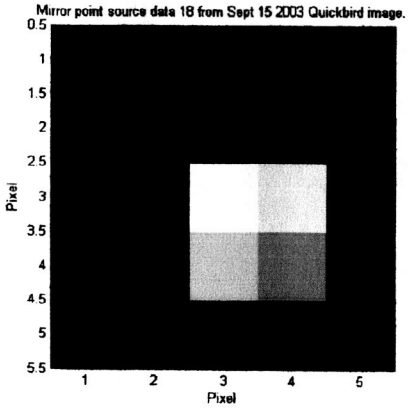

(e) Point source mirror 18

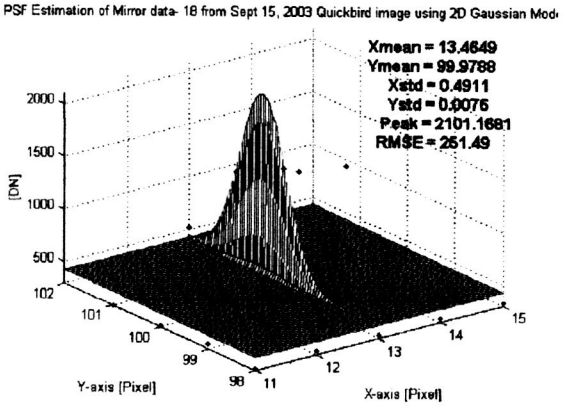

(f) 2-D model and raw data

Figure C.13 September 15, 2003 Quickbird point source images and their peak position estimation using 2-D Gaussian model using mirrors 16, 17, and 18.

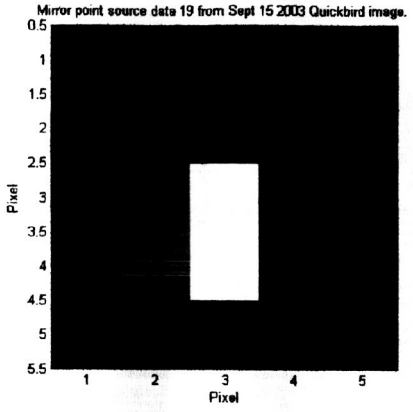

(a) Point source mirror 19

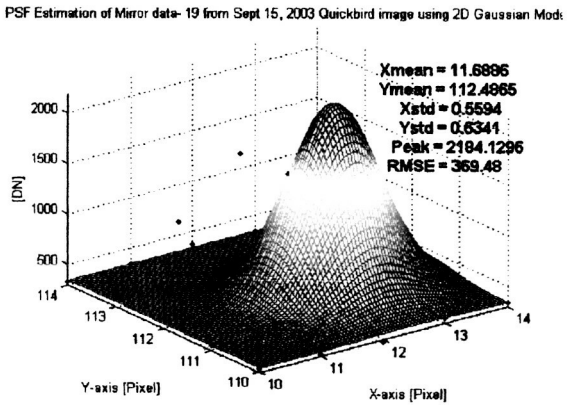

(b) 2-D model and raw data

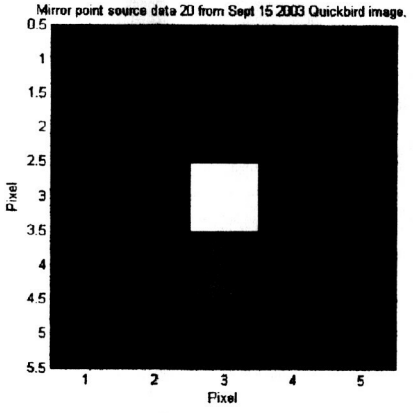

(c) Point source mirror 20

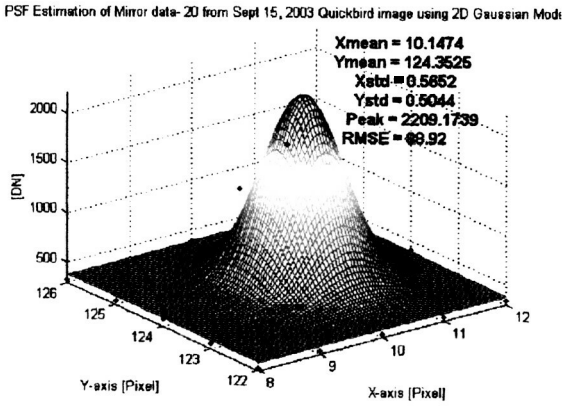

(d) 2-D model and raw data

Figure C.14 September 15, 2003 Quickbird point source images and their peak position estimation using 2-D Gaussian model using mirrors 19 and 20.

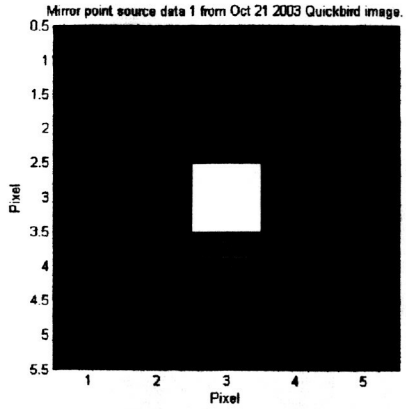

(a) Point source mirror 1

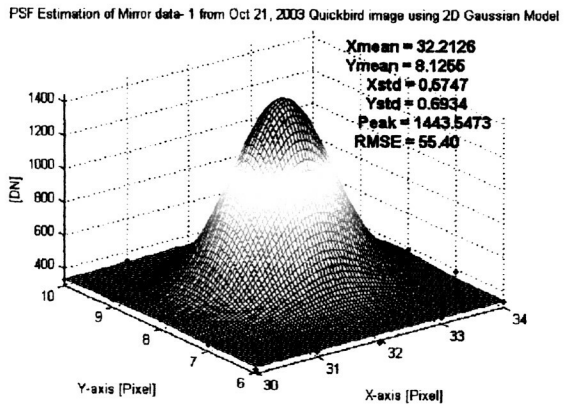

(b) 2-D model and raw data

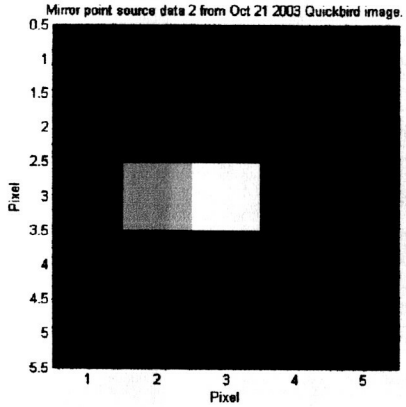

(c) Point source mirror 2

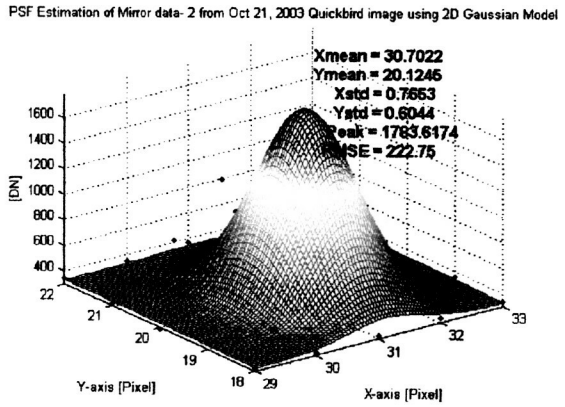

(d) 2-D model and raw data

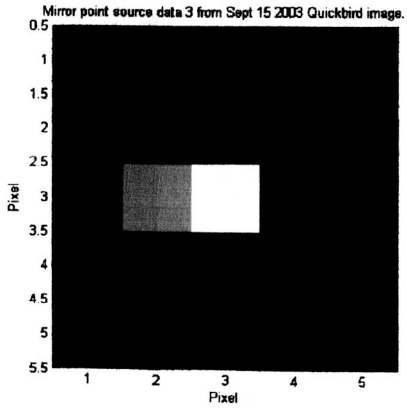

(e) Point source mirror 3

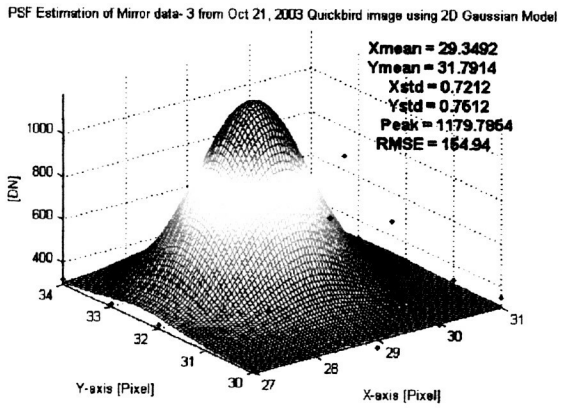

(f) 2-D model and raw data

Figure C.15 October 21, 2003 Quickbird point source images and their peak position estimation using 2-D Gaussian model using mirrors 1, 2, and 3.

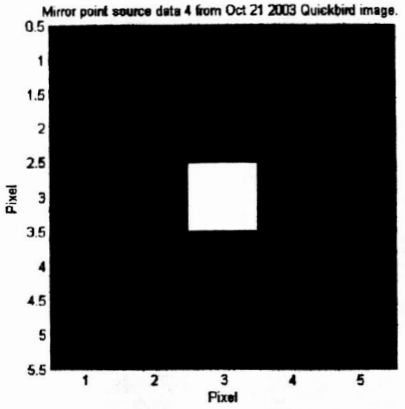

(a) Point source mirror 4

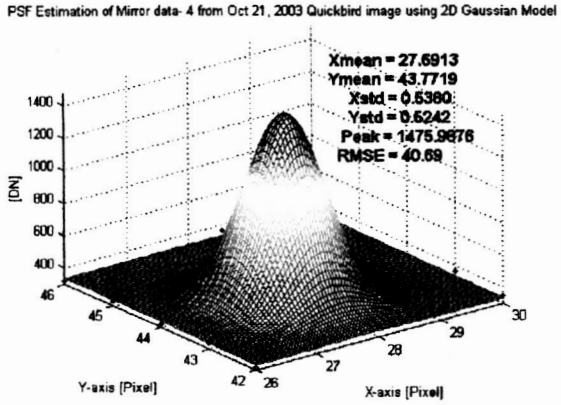

(b) 2-D model and raw data

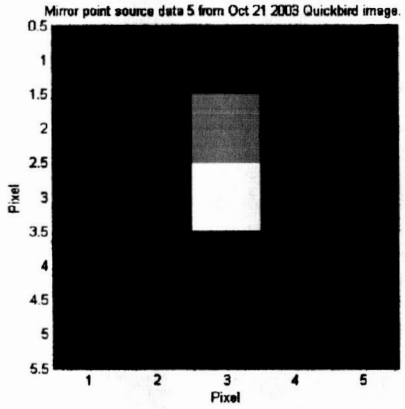

(c) Point source mirror 5

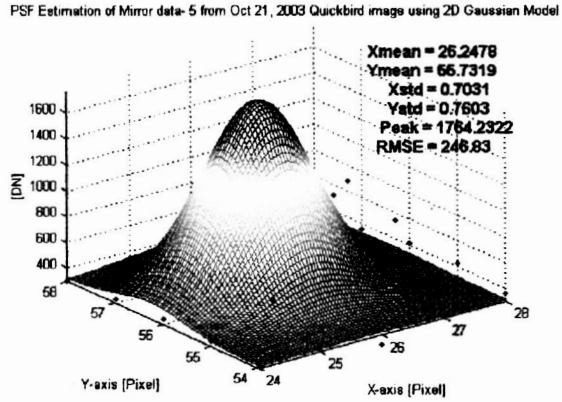

(d) 2-D model and raw data

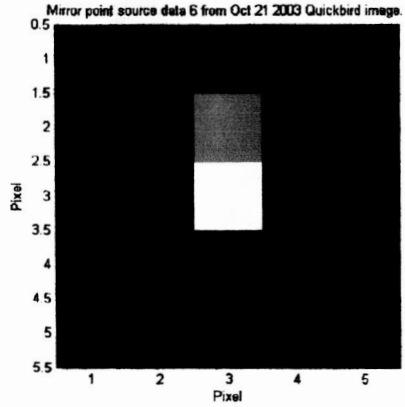

(e) Point source mirror 6

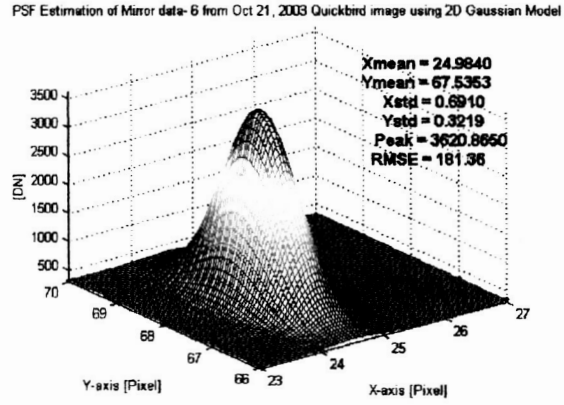

(f) 2-D model and raw data

Figure C.16 October 21, 2003 Quickbird point source images and their peak position estimation using 2-D Gaussian model using mirrors 4, 5, and 6.

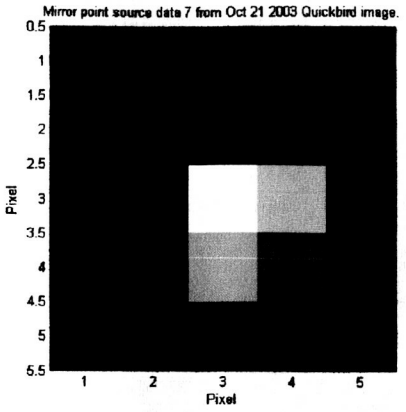

(a) Point source mirror 7

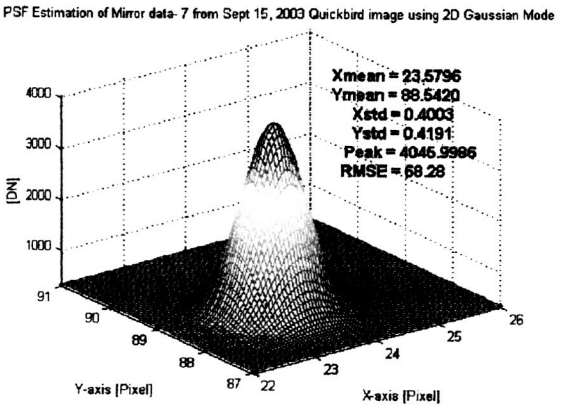

(b) 2-D model and raw data

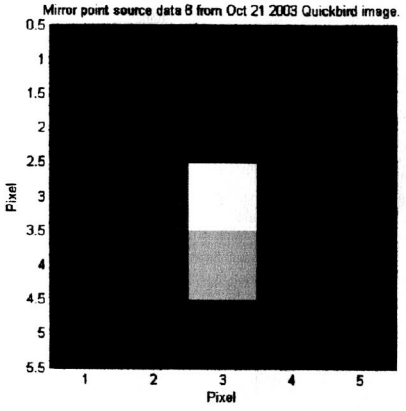

(c) Point source mirror 8

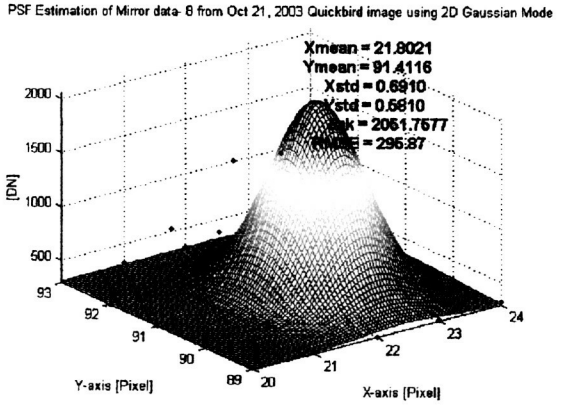

(d) 2-D model and raw data

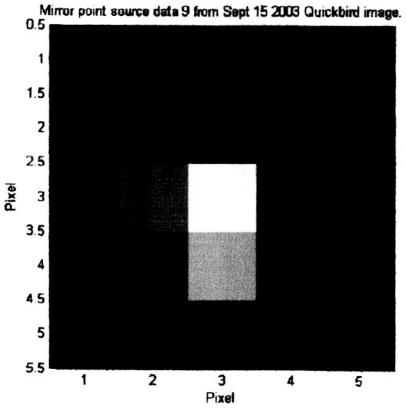

(e) Point source mirror 9

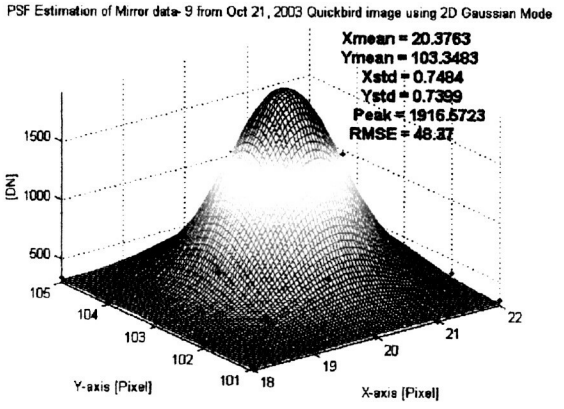

(f) 2-D model and raw data

Figure C.17 October 21, 2003 Quickbird point source images and their peak position estimation using 2-D Gaussian model using mirrors 7, 8, and 9.

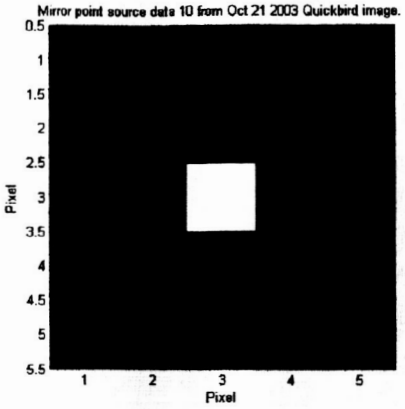

(a) Point source mirror 10

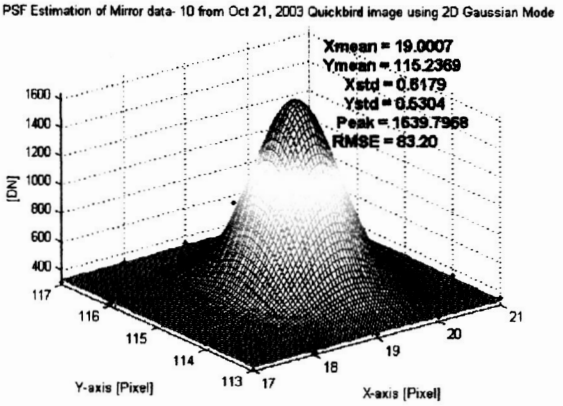

(b) 2-D model and raw data

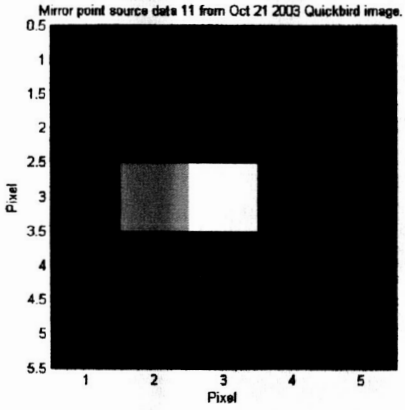

(c) Point source mirror 11

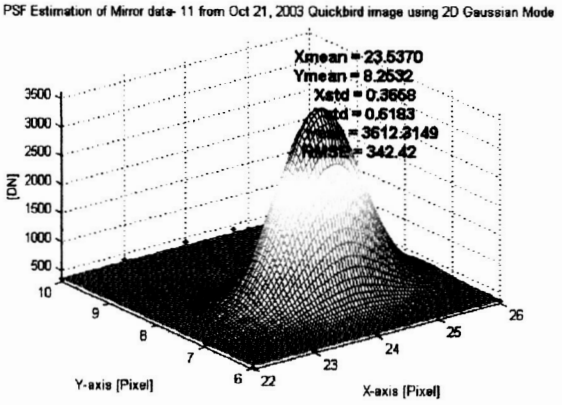

(d) 2-D model and raw data

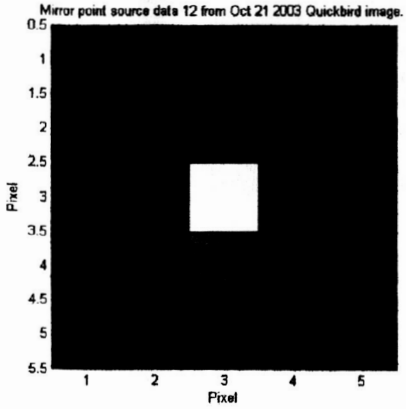

(e) Point source mirror 12

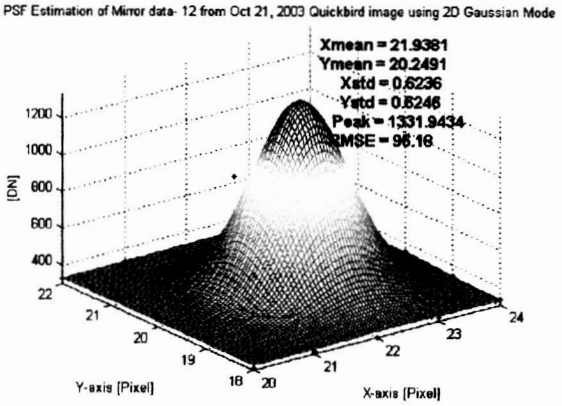

(f) 2-D model and raw data

Figure C.18 October 21, 2003 Quickbird point source images and their peak position estimation using 2-D Gaussian model using mirrors 10, 11, and 12.

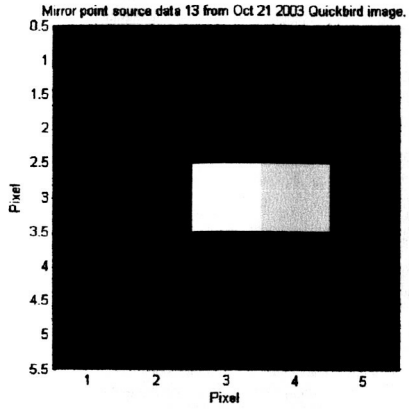

(a) Point source mirror 13

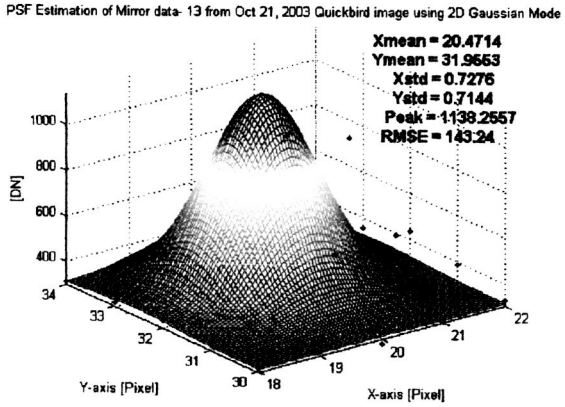

(b) 2-D model and raw data

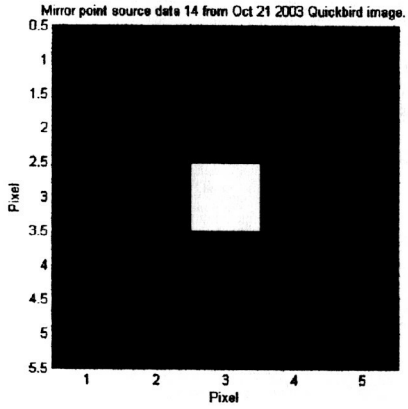

(c) Point source mirror 14

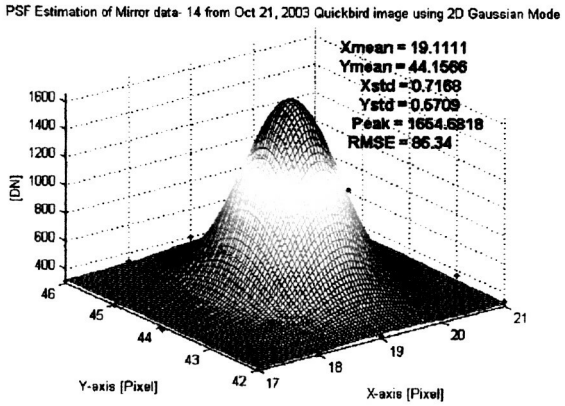

(d) 2-D model and raw data

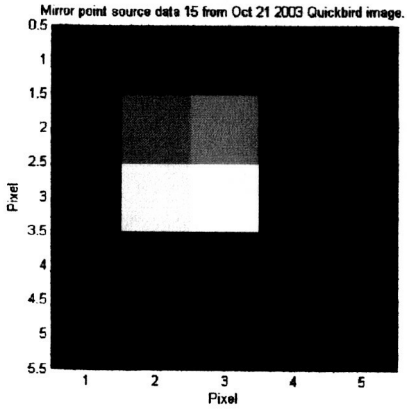

(e) Point source mirror 15

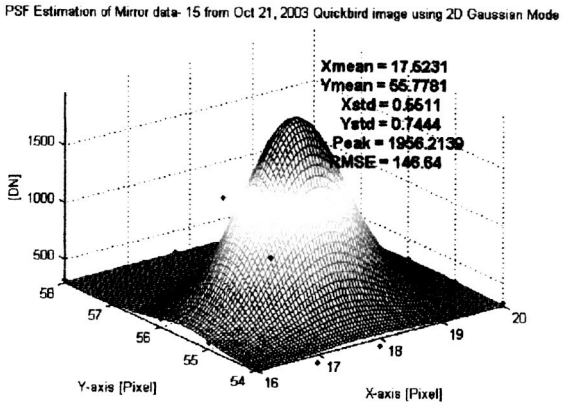

(f) 2-D model and raw data

Figure C.19 October 21, 2003 Quickbird point source images and their peak position estimation using 2-D Gaussian model using mirrors 13, 14, and 15.

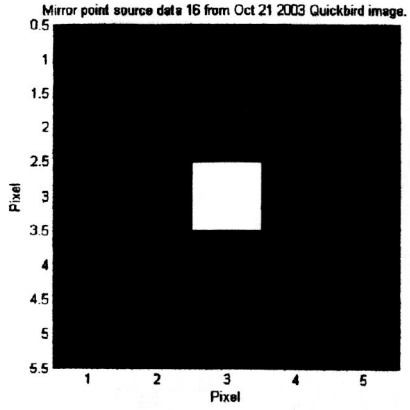

(a) Point source mirror 16

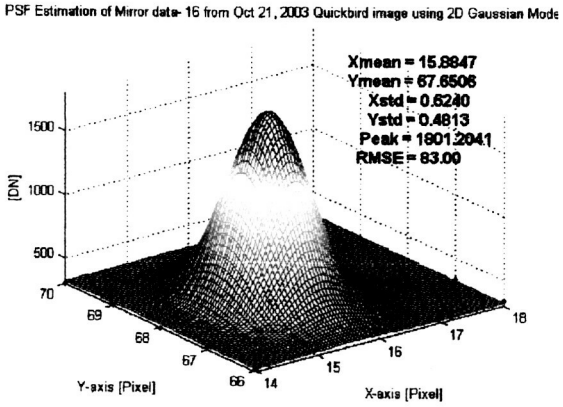

(b) 2-D model and raw data

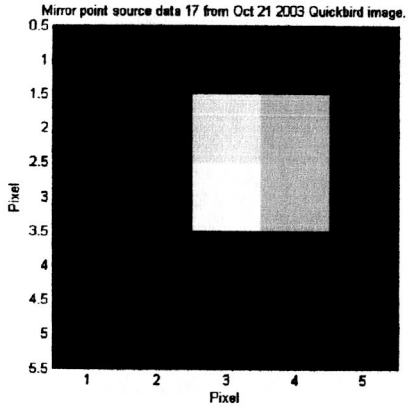

(c) Point source mirror 17

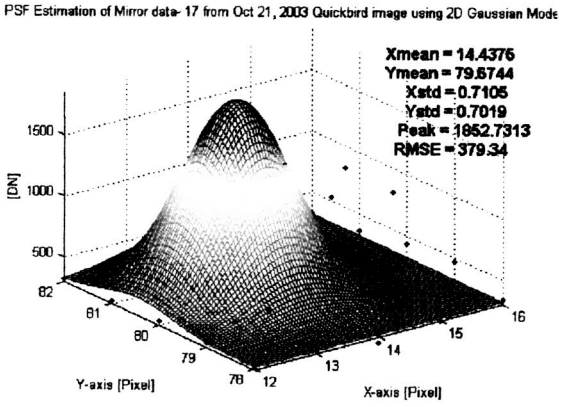

(d) 2-D model and raw data

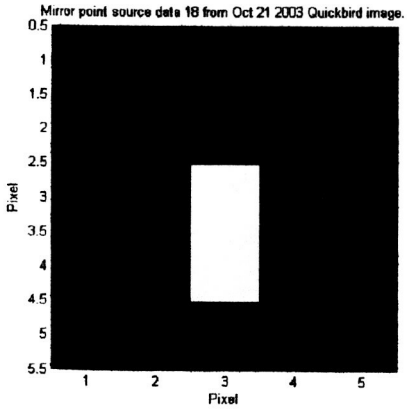

(e) Point source mirror 18

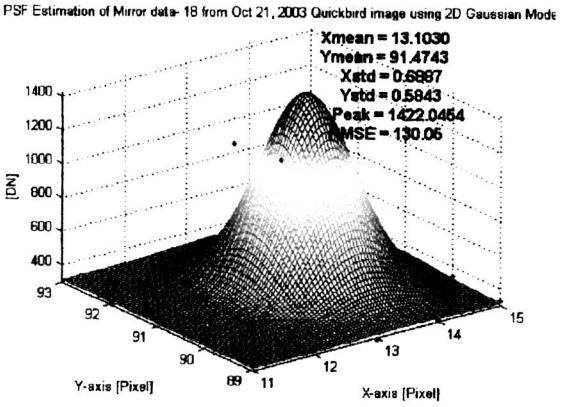

(f) 2-D model and raw data

Figure C20. October 21, 2003 Quickbird point source images and their peak position estimation using 2-D Gaussian model using mirrors 16, 17, and 18.

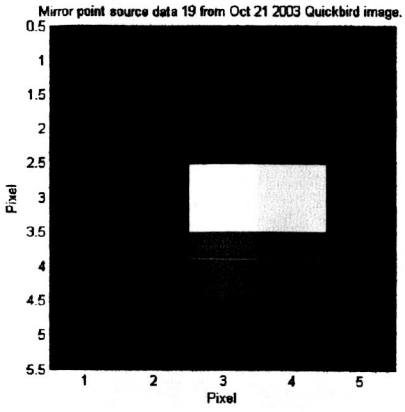

(a) Point source mirror 19

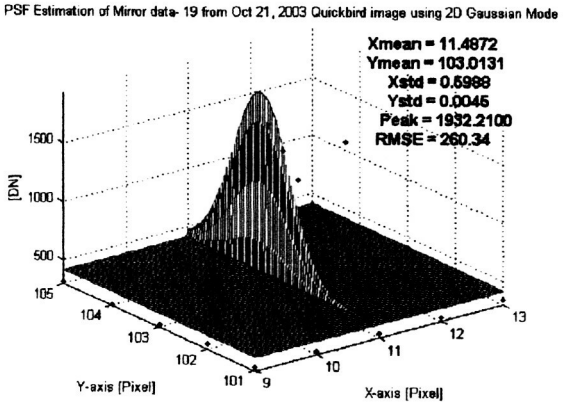

(b) 2-D model and raw data

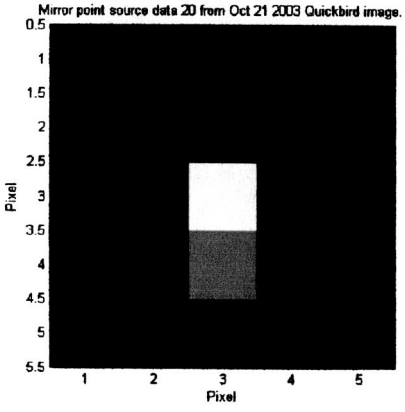

(c) Point source mirror 20

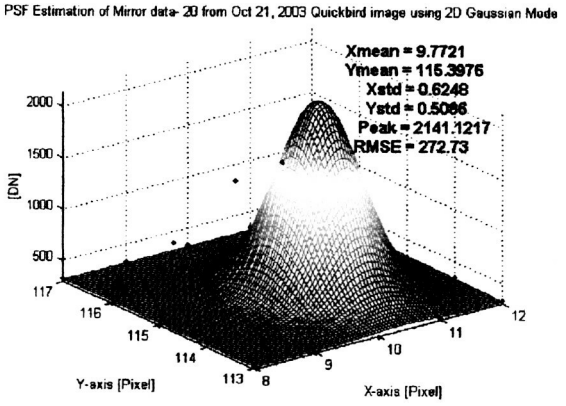

(d) 2-D model and raw data

Figure C.21 October 21, 2003 Quickbird point source images and their peak position estimation using 2-D Gaussian model using mirrors 19 and 20.